ELECTROCHMICAL IMPEDANCE SPECTROSCOPY BIOSENSOR PLATFORM FOR EVALUATION OF BIOFILM

by

Matthew Connor Dusenbery McGlennen

A dissertation submitted in partial fulfillment
of the requirements for the degree

of

Doctor of Philosophy

in

Mechanical Engineering

MONTANA STATE UNIVERSITY
Bozeman, Montana

May 2023

ACKNOWLEDGEMENTS

First and foremost, I would like to thank my advisors, Dr. Stephan Warnat, and Dr. Christine Foreman for their continued support, ideas, problem solving, and benevolence. Their passion for interdisciplinary science is inspiring. Thank you both for allowing me to pursue my own ideas and for your commitment to my professional and personal development throughout my PhD. I would also like to thank my committee members Dr. Cecily Ryan and Dr. Stephen Sofie for accepting the invitation to participate in my PhD work. A special thank you to Dr. Markus Dieser for teaching me, a mechanical engineer, on how to be a microbiologist. I would like to thank the Center for Biofilm Engineering for providing a collaborative multi-disciplinary space to conduct research. Thanks to all the researchers and fellow graduate students who have participated in experiments, troubleshooting, discussions, and camaraderie – Michael Neubauer, Daniel Collins, Haley Kettler, Seth Kane, Jesse Arroyo, Bruce Boles, Madelyn Wilis, Dr. Heidi Smith, Dr. Kristin Brileya, Dr. Andy Lingley, Dr. Joshua Heinemann. I would also like to thank all the undergraduate students that I have had the privilege of mentoring during my time as a graduate student – Ruby Jackson, Lauren Jackson, and Amelia Burda. And most of all, I thank Taylor Boucher for being my best friend and partner in life's adventures.

TABLE OF CONTENTS

TABLE OF CONTENTS CONTINUED

TABLE OF CONTENTS CONTINUED

LIST OF TABLES

LIST OF FIGURES

Figure Page

LIST OF FIGURES CONTINUED

Figure Page

LIST OF FIGURES CONTINUED

Figure Page

ABSTRACT

Microbial biofilms are organized communities of surface-attached microorganisms encased in a self-produced extracellular matrix that pose significant challenges in medicine, the environment, and industry. Biofilms can cause chronic infections, biofouling, and equipment failure, while existing methods for biofilm detection are slow, costly, and labor-intensive. Recently, the use of microfabricated electrochemical impedance spectroscopy (EIS) biosensors has emerged as a promising technique for evaluating biofilm growth in real-time with advantages of small-size, adaptability, low-cost, and high-sensitivity.

In this work, EIS biosensors featuring gold micro-interdigitated electrodes were produced using standard microfabrication techniques. Sensors were integrated into a custom 3D-printable flow cell system, enabling EIS measurements and confocal laser scanning microscopy (CLSM) imaging simultaneously. Green fluorescently labeled *Pseudomonas aeruginosa* PA01, a model biofilm forming bacteria, was introduced into flow chambers and subsequent growth was monitored by EIS, CLSM, and biomass enumeration. Using the system, biofilm growth, dispersal, and the effects of cell-signaling suppression were evaluated. The sensors were also tested in an oil-water emulsion and field-tested on an alpine snow-patch and pond.

Improved stability of EIS measurements was achieved by coating the sensors' counter and reference electrodes with an electrically conductive polymer. Biofilm growth was successfully detected using EIS biosensors at an optimized single-frequency, with average decreases in impedance of ~22% by 24 hours. Likewise, biofilm dispersal via chemical treatments were successfully detected with average increases in impedance of ~14% over the ensuing 12 hours. When cells were exposed to a quorum sensing inhibition agent, impedance did not decrease for 18 hours. Impedance changes due to biofilm growth, dispersal, and effects of quorum sensing inhibition were validated by CLSM images and biofilm enumeration. Similarly, in an oil-water emulsion the biosensors successfully detected biofilm growth, dispersal, and effects of quorum sensing inhibition. In an alpine field-test, samples containing varying concentrations of microbes could be detected using the EIS biosensors.

This work demonstrates that EIS biosensors are a promising tool for real-time monitoring of biofilm dynamics in a variety of aqueous environments. Overall, EIS biosensing holds great potential for *in situ* and real-time data regarding biofilm colonization that is not possible with existing techniques.

INTRODUCTION

Motivation

Microfabricated biosensors offer great potential for scientific and engineering innovations, and they have found widespread applications in various fields such as medicine, industry, and environmental conservation. The benefits of these sensors are vast and compelling, including their compact size, cost-effectiveness, high sensitivity, versatility, and ability to provide real-time data. Additionally, these biosensors can be customized and designed to work in diverse settings, enabling them to collect data from otherwise unreachable areas. With their miniaturization, they can be integrated into various devices and systems, allowing for continuous monitoring and analysis.

Among the many types of sensors, microfabricated electrochemical impedance spectroscopy (EIS) sensors are gaining adoption due to their numerous advantages, including simple design, low-cost fabrication, and adaptability to a wide variety of detection targets. EIS is an informative method of characterizing materials that can be used to analyze bulk and interfacial properties of liquids, solids, or gasses (Lvovich, 2012; Vadhva et al., 2021). When the technique of EIS is applied to microfabricated sensors and is used to measure biological or chemical reactions, the resulting devices are termed EIS biosensors. EIS biosensors are non-invasive, sensitive, and cost-effective devices, which makes them preferable tools for rapid and portable *in situ* or point-of-care detection (Cesewski and Johnson, 2020). EIS biosensors are also label-free, meaning they do not require any tagging/labeling agents which can affect the activity of the targets of interest (Mazzaracchio et al., 2019; Queiros et al., 2013). The affinity of EIS biosensors can be enhanced by adding ligands (*e.g.,* DNA, RNA, antibodies, or peptides) to the sensor surface, which

allows conversion of bio-recognition events such as antibody-antigen, substrate-enzyme, or whole cell binding, into meaningful signals (Trunzo and Hong, 2020). EIS biosensors are suitable for various applications in areas such as medical diagnostics and environmental monitoring, as they can detect trace amounts of target molecules.

Given that microorganisms are abundant in many aqueous environments, EIS biosensors could be deployed for their detection. Microorganisms in aqueous environments form biofilms, which are defined as proliferating communities of microbes attached to surfaces, embedded within a self-produced extracellular polymeric substance (EPS) matrix (Hall-Stoodley et al., 2004). In nature, the vast majority of microorganisms exist as biofilms (Mazza, 2016). Analysis of biofilms can be particularly difficult due to their tendency to develop in inaccessible locations and their constantly evolving nature. Biofilms often exist in polymicrobial communities that interact with each other in intricate ways (Roy et al., 2018). Depending on microbial species, environmental conditions, and nutrient availability, biofilm structure, and composition can vary. Combined, these factors make the study of biofilm challenging. An inexpensive microfabricated EIS biosensor that could accurately and promptly detect biofilm contamination in real-time would be highly desirable in a range of industrial and scientific contexts.

Although EIS biosensors show promise in studying biofilm, challenges remain to fully realize their capabilities and establish the technology as a reliable tool for biofilm research. EIS signals must be correctly interpreted in the context of the testing conditions. For instance, EIS biosensor signals are influenced by fluid types, environmental conditions, and types of organisms present (Sopoušek et al., 2021). Standardized procedures for EIS biosensing need to be established to ensure consistent and reproducible results across different studies and applications. The research

presented in this dissertation aims to address some of the gaps by improving design and integration, exploring the limits, and expanding on the capabilities of EIS biosensors. Ultimately, these advances will lead to better adoption of microfabricated biosensors into mainstream analysis of biofilm.

Dissertation Outline

Chapter 1: Introduction. An overview of biofilm physiology is provided. This is followed by a discussion of microfabricated systems for characterizing biofilms, electrochemical impedance spectroscopy, the importance of electrochemical interfaces for biosensing, the effects of biofilm on electrochemical interfaces, and micro-interdigitated electrodes for biofilm detection. Key research gaps and research objectives are presented. The main body of this dissertation (Chapter 2-5), address the outlined objectives.

Chapter 2: "Effects of *Escherichia coli* K12 Biofilm on Sensor Thin Film Materials" published in the Journal of The Institute of Electrical and Electronics Engineers Sensors, 2019. In this study, the long-term effects of biofilm formation on the properties of aluminum (metallic thin-film material) and a-Si_xN_y:H (dielectric thin-film material) are evaluated. Material degradation caused by *Escherichia coli* K12 biofilm growth is determined by electrical sheet resistance measurements (collinear four-point-probe) and Fourier-transform infrared spectroscopy (FTIR) absorption spectra over a time period of 7 weeks. The results suggest that sensor materials (e.g., gold, polycrystalline silicon, and nickel) should be investigated to determine their susceptibility to microbially influenced corrosion, and encapsulation with a-Si_xN_y:H can minimize degradation.

From this study, the corrosive nature of biofilm is evident which underscores the need for corrosive resistant, reliable, sensor design in future studies.

Chapter 3: “Using Electrochemical Impedance Spectroscopy to Study Biofilm Growth in a 3D Printed Flow Cell System”, published in the Journal Biosensors and Bioelectronics: X, March 2023. This work demonstrates that microfabricated sensors modified with PPy:PSS coatings enable highly stable time-resolved EIS measurements under both abiotic (free of microbes) conditions and when subjected to *Pseudomonas aeruginosa* biofilm growth. Electrochemical impedance data from sensors integrated into a novel 3D-printed flow cell corroborates distinct biofilm growth stages that is confirmed using confocal laser scanning microscopy (CLSM).

Given the success of the sensor in monitoring biofilm growth, the subsequent logical progression is to evaluate the sensor's efficacy in detecting biofilm dispersal maneuvers.

Chapter 4: “Application of Impedance Sensor for Assessing Biofilm Control in Real Time”, prepared for submission to the Journal of Industrial Microbiology and Biotechnology, April, 2023. In this study, real-time impedance measurements of biofilm growth under flow conditions were made possible through a custom flow cell system equipped with integrated sensors, proving to be effective at assessing the growth and dispersal (using either chlorine or biocide) of *P. aeruginosa* biofilm in growth medium and an oil-water emulsion. Additionally, the sensors successfully detect delayed biofilm growth in the presence of a bacterial quorum sensing inhibitor.

To broaden the potential uses of the sensor, the next logical step is to assess its effectiveness in other fluid environments containing microorganisms.

Chapter 5: “Microsensors in Icy Environments to Detect Microbial Activities”, published in the Journal of Microelectromechanical Systems, 2020. In this study, data is presented on the use of microfabricated EIS sensors for the detection of microbes in both laboratory and field-based

liquid, semi-solid, and icy environments. The results demonstrate that samples that vary in phase (solid vs. liquid), temperature, and microbial concentration generate discrete impedance spectra in laboratory conditions and subsequently in an environmental field-test.

Chapter 6: Conclusions and future direction of EIS biosensing for biofilm monitoring. This chapter highlights the key findings and conclusions of this work. Remaining challenges, and possible future directions of this technology are discussed.

Background

The following sections provide essential background about biofilm physiology, and the current analytical methods used to investigate biofilms. This is followed by sections that elucidate the concepts of electrochemistry, electrochemical impedance spectroscopy (EIS), and EIS biosensing, which are crucial to understanding the operation of this sensor technology.

Biofilms

A biofilm is a cooperative aggregate of microorganisms associated with a surface, enclosed in self-produced extracellular polymeric substance (EPS) composed of polysaccharides, proteins, lipids, and extracellular DNA (Azeredo et al., 2016; Lappin-Scott and Costerton, 1989; Wimpenny et al., 2000). It is estimated that up to 80% of all microbial biomass exists as biofilm (Bar-On and Milo, 2019). Biofilm-forming microorganisms attach to surfaces, communicate with each other in a coordinated manner, and carry out regulated processes leading to maturation. Cell-to-cell communication occurs via signaling molecules called autoinducers in a process referred to as quorum sensing (QS), which allows cells to sense and respond to population density and regulate gene expression (Davies et al., 1998). Biofilms maintain a protected mode of growth that allows

them to survive for long durations with minimal nutrients and endure in high-stress conditions or harsh environments (Costerton et al., 1999).

Biofilm contamination is a ubiquitous problem in many aqueous environments. For instance, industry contamination of precision machining and grinding fluids causes premature degradation of fluids and workplace pathogenic exposure (Simpson et al., 2003). In the medical field, biofilms form on surgical implants and indwelling catheters, leading to infections and detrimental health effects (Lisoń et al., 2022). In environmental settings, biofilms contaminate municipal water supplies or pipe networks, potentially leading to widespread illness (Wingender and Flemming, 2011). Collectively, the economic cost of biofilm related problems worldwide is in excess of $5 trillion a year (Cámara et al., 2022).

The success of removing biofilm is greatest when targeting microorganims at certain life stages. For example, during the early stages of biofilm development, free-floating cells are more susceptible to antimicrobials and biocides (Gu et al., 2019). However, mature biofilms exhibit high resistance to antimicrobials making treatment more difficult (Davies, 2003; Hall-Stoodley et al., 2004). This resistance is possibly due to the microbes being encased and protected by EPS. This barrier acts to deter physical removal and provides enhanced resilience against chemical disruption by blocking the diffusion of antimicrobials into the bulk of the biofilm (Stewart, 2003). Once surfaces and fluids are contaminated with biofilm decontamination is difficult, even after meticulous cleaning, since even a few residual cells can quickly repopulate the system. The problem is further exacerbated as biofilms often reside in hard-to-reach locations.

Currently, techniques that are available to measure biofilm formation and growth generally require time for culture and/or involve labor-intensive handling steps (Pantanella et al., 2013).

Harvested sessile bacteria can be enumerated using colony-forming unit plate-counts and staining methods, like crystal violet (CV), safranin, or trypan blue (Christensen et al., 1982; Pitts et al., 2003). The reproducibility can vary based on the skill and training of the operator. Biofilms can be analyzed with quantitative Polymerase Chain Reaction (qPCR), various microscopy techniques (e.g., epifluorescence and confocal laser scanning microscopy (CLSM), transmission electron microscopy (TEM), or scanning electron microscopy (SEM) (Hassan et al., 2011; Peeters et al., 2008; Thurnheer et al., 2004). However, these techniques are either labor-intensive, expensive, or require labeling, and generally are destructive to the biofilm providing only a single time point for each sample. Furthermore, different techniques are deployed for different biofilm types, making comparability and consistency challenging across studies. As a result, there is a lack of consensus on how best to evaluate biofilms (Azeredo et al., 2016).

Pseudomonas aeruginosa is a model biofilm forming organism (Hall-stoodley et al., 2004) and has been the focus of intense study because of its prominent role in disease and widespread environmental presence. The ability of *P. aeruginosa* to readily form biofilms, hinders eradication (Moradali et al., 2017). *P. aeruginosa* grows readily in many diverse environments and is an especially virulent opportunistic infection when normal immune defenses are disabled. For instance, patients with cystic fibrosis whose airways become colonized with *P. aeruginosa,* develop chronic infections that are almost impossible to eradicate (Killough et al., 2022; Tuon et al., 2022;). *P. aeruginosa* also is a major pathogen in burns and other chronic wounds, on implanted biomaterials such as knees, hips, or valves, and within hospital surfaces and water supplies (Breathnach et al., 2012).

P. aeruginosa is especially difficult to eradicate because it is naturally resistant to many antibiotics. According to the world health organization (WHO), *P. aeruginosa* is recognized as a priority pathogen for new antibiotic development since number of multidrug-resistant strains are increasing (World Heath, 2017).

Pseudomonas is a common genus of bacteria found in industry, such as in metalworking fluids (MWFs) which are complex mixtures of chemicals used as cooling and lubricating agents in a variety of machining processes (Saha and Donofrio 2012). The quality of MWFs is degraded by microbial contaminates which not only pose potential workplace health concerns, such as dermatitis or hypersensitivity pneumonitis, but may also lead to premature deterioration of the costly fluid (Koch, 2023).

For the above reasons *P. aeruginosa* is chosen as a model biofilm producing bacteria for development of an EIS biosensor. The research aim is to use EIS to detect all stages of *P. aeruginosa* biofilm development including initial attachment, proliferation, and mature biofilm production.

Microfabricated Systems for Real-time Biofilm Detection

In the past decade, microfabricated systems have expanded into the field of microbiology and have been increasingly used to evaluate/detect biofilm (Tiozzo-Lyon et al., 2023). Microfabricated system design has brought about advantages such as manufacturing precision, ability to control feature size, potential for high reproducibility, ease of modification for specific applications, and low-cost for large quantity fabrication (Baracu and Dinu Gugoasa, 2021). Consequently, microfabrication has advantages that can be applied for the creation accurate biofilm detection devices.

Broadly, microfabricated detection systems can be categorized as having optical, mechanical, or electrochemical transduction mechanisms. Each technique has strengths and weaknesses for evaluating biological phenomenon including biofilm monitoring (Subramanian et al., 2019). Briefly, optical systems detect changes in light properties, such as intensity, wavelength, polarization, or phase shift, and turn the signal into a measurable quantity, such as voltage, current, or frequency (Zhang et al., 2011). However, optical systems are susceptible to interference from non-biofilm components and are unsuitable for opaque fluids. Mechanical microsystems operate by physically measuring the change of mechanical properties such as mass, stiffness, or viscoelasticity, translating the change into a signal (Chalklen et al., 2020). Mechanical sensors are limited by susceptibility to ambient noise and vibrations. These limitations can lead to inaccurate measurements making mechanical sensors less suitable for biofilm analysis, especially in industrial locations where vibrations may be encountered. Electrochemical sensors detect changes in electric potential, charge buildup, or current resulting from chemical reactions between the analyte and electrodes (Grieshaber et al., 2008). These changes are then converted into a signal that can be utilized. Electrochemical sensors offer several advantages, including immunity to ambient vibrations, non-invasive analysis with high sensitivity and selectivity, real-time response, suitability for use in various fluid types (including opaque fluids), and low power consumption.

Electrochemical sensors can be classified into three categories: amperometric, potentiometric, and impedimetric (EIS). Amperometric sensors require an electrical current and often require the addition of redox mediators which are intermediate electron carriers or reservoirs that allow reversible charge transfer through the electrode/electrolyte interface (Zhang et al.,

2022). Potentiometric sensors require auxiliary reference electrodes to obtain valid data complicating the design and operation (Zdrachek and Bakker, 2019).

In contrast, EIS measurements use a sinusoidal electrical perturbation, which has less impact on the electrochemical system compared to amperometric measurements, where the applied potential could alter the system. Additionally, EIS sensors do not require the addition redox mediators (Dorledo de Faria et al., 2019). Lastly, EIS measurements can be carried out over a broad range of applied frequencies, enabling collection of additional electrochemical data that encompasses both the system's surface and bulk properties. Collectively, these advantages make EIS a desirable technique for studying biofilms.

Electrochemical Impedance Spectroscopy (EIS)

EIS is a technique in which a sine wave voltage or current is applied to an electrochemical system, and the corresponding current or voltage is measured (Figure 1.1a). Fundamentally, impedance measures the opposition of electrical flow in an alternating current (AC) system. The quotient of the time dependent voltage to the time dependent current is termed impedance (Figure 1.1b; Lvovich, 2012). EIS is used in a wide range of application because of the informative outputs it provides. Examples where EIS is applied include the characterization of fuel cell reactions, the development of coating materials, the evaluation of battery performance, and the monitoring of metal and alloy corrosion (Lasia, 2014; Wang et al., 2021).

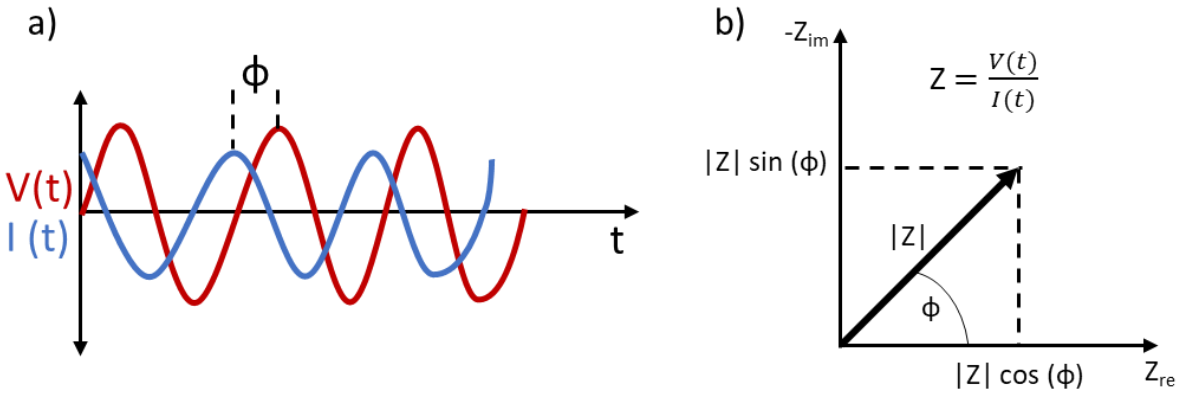

Figure 1.1: Schematic representation of EIS. a) The ratio of the potential (V) to the current (I) is the impedance (|Z|), and the phase shift difference between the voltage and current (ϕ). b) The magnitude of impedance can be represented in both real (Z_{re}) and imaginary (Z_{im}) parts and are related mathematically with the phase lag.

EIS measurements are carried out in either potentiostatic (sine wave voltage) or galvanostatic (sine wave current) conditions. Several conditions must be satisfied to obtain valid EIS data. First, the measured impedance must be causal, meaning that the impedance response must come only from the applied perturbation. Second, to ensure no alterations to the electrochemical system under test, and to ensure the measurements are "pseudo-linear", the electrical perturbations in EIS measurements are kept small (*i.e.*, ≤50 mV or ≤100 μA). Third, while the measurement is taking place, the system remains stable.

In the process of performing an EIS measurement, the impedance is measured at various perturbation frequencies, typically ranging from 0.1 Hz to 1 MHz. This procedure produces an impedance spectrum, which is a graphical representation of the system's impedance as a function of applied frequency. By examining this spectrum, insights into the electrical characteristics of the system are obtained (Vivier and Orazem, 2022).

Impedance extends from the concepts of Ohm's law, which describes the relationship between voltage and current passing through a resistor, shown in equation 1.1:

$$V = IR \tag{1.1}$$

In an alternating current (AC) system, impedance is represented as Z, as shown in equation 1.2:

$$V = I\boldsymbol{Z} \tag{1.2}$$

However, in a standard EIS experiment applying a sinusoidal voltage to a material or system, the resulting current response can be expressed as a sinusoidal function with the same frequency, but with a phase shift and possibly a different amplitude, as shown in equation 1.3:

$$\boldsymbol{Z} = \frac{V(t)}{I(t)} = \frac{|V|sin(\omega t)}{|I|\sin(\omega t + \phi)} \tag{1.3}$$

where t is time, ω is the applied angular frequency in radian s^{-1} related to frequency, f, in Hz by $\omega=2\pi f$, and ϕ is the phase shift difference between the voltage and current. Using Euler's identity, which simplifies and converts trigonometric functions into exponential functions in polar coordinates, equation 1.3 is converted to equation 1.4:

$$\boldsymbol{Z} = \frac{|V|e^{j\omega t}}{|I|e^{j\omega t+\omega}} \tag{1.4}$$

where j is the complex imaginary square root of -1. Impedance spectroscopy measurements are typically presented in the Cartesian complex plane, where the complex impedance is divided into its real and imaginary components, as shown in equation 1.5:

$$\boldsymbol{Z} = Z_{re} + jZ_{im} \tag{1.5}$$

where Z_{re} is the real part of impedance, and Z_{im} is the imaginary part of impedance. The impedance of an ideal resistor, R, is purely real, as described in Equation 1.6:

$$Z_{re} = R \tag{1.6}$$

whereas both inductors and capacitors have purely imaginary impedance and contribute to the imaginary portion of impedance, as described in Equation 1.7:

$$Z_{im} = X_L - X_C \tag{1.7}$$

where X_L is the reactive inductance, and X_C is the reactive capacitance. Impedance of both inductors and capacitors varies with frequency. The reactive inductance of an inductor increases with the applied angular frequency as shown in Equation 1.8:

$$X_L = j\omega L \tag{1.8}$$

where L is the inductance. Furthermore, the impedance of a capacitor decreases as the applied frequency increases, as shown in Equation 1.9:

$$X_C = \frac{-1}{j\omega C} \tag{1.9}$$

where C is the capacitance. The overall impedance of a system is often expressed as the magnitude of impedance using equation 1.10:

$$|Z| = \sqrt{(Z_{re})^2 + (Z_{im})^2} = \sqrt{R^2 + (X_L - X_C)^2} \tag{1.10}$$

where |Z| is the magnitude, or modulus of impedance. Finally, the phase angle shift difference between the voltage and current is represented in Equation 1.11:

$$\phi = \tan^{-1}\frac{Z_{re}}{Z_{im}} = \tan^{-1}\frac{X}{R} \tag{1.11}$$

Since EIS involves complex numbers, there are two common ways to represent impedance spectra. The first method involves plotting either the magnitude of impedance (|Z|), or the calculated phase angle shift (ϕ) with respect to the applied frequency. This is called a Bode plot (Fig 1.2a). The second method involves plotting real components of impedance (Z_{re}) against the imaginary components of impedance (Z_{im}) across the impedance spectrum. This is called a Nyquist plot (Figures 1.2b and 1.2c).

One approach to elucidate impedance spectra is by fitting impedance data to electrochemical equivalent circuits (EECs) (Furst and Francis, 2019). EECs are used to fit measured EIS spectra with known circuit elements such as resistors (R), constant phase elements (CPEs), capacitors (C), and Warburg elements (W) combined in either parallel or series (Furst and Francis, 2019). Each of the circuit elements represent unique electrochemical components in an electrochemical system. The Randle's circuit is frequently used to represent electrode-electrolyte systems because it provides a simple and effective way to model the complex electrochemical processes that occur at the electrode-electrolyte interface (MacDonald and Andreas, 2014). The circuit is composed of R_s (solution resistance), C_{DL} (double layer capacitance), R_{CT} (charge transfer resistance), and W (Warburg element). In a Randal's circuit (Figure 1.2b), resistance of the bulk electrolyte solution is R_s. The C_{DL} is the capacitance that arises from the separation of charges that occurs at the interface, due to the adsorption of ions or molecules on the electrode surface. The R_{CT} is the resistance to the electrochemical reaction occurring at the electrode surface. Lastly, W represents the diffusion of ions in the electrolyte solution (Bahadır and Sezgintürk, 2016).

Impedance measurements can be categorized into two types based on their surface characteristics and how measurements are taken (Zhang et al., 2022). The differences are defined by the charge transfer capability, which can be either faradic or non-faradaic. In electrochemical faradic systems, charge is transferred across an interface (Figure 1.2b). Faradic impedance systems allow charge to transfer through the electrode surface and often incorporate a redox mediator that can undergo cyclical oxidation and reduction with the electrode. Moreover, a Direct Current (DC) offset is sometimes required. Non-faradic measurements do not allow charge to transfer through

the electrode surface, meaning that the electrode behaves as a pure insulator. No redox-active molecule is required with this type of measurement.

The Randal's circuit assumes a faradaic electrochemical system but can be modified to account for non-faradaic circumstances. If there are no redox-active molecules present, the electrode cannot facilitate charge transfer, resulting in the replacement of both R_{CT} and W elements with R_{LEAK} (Figure 1.2c). This parameter represents the ohmic losses that occur within the system.

Non-faradaic systems are advantageous for remote sensing applications since they do not require the addition of redox mediators, which could alter the system under test. As discussed in the following section, the use of an EIS biosensor is designed to operate under non-faradaic conditions, but biofilm potentially contributes redox mediators resulting in signals from both faradaic and non-faradaic processes (Bellin et al., 2014; Bellin et al., 2016).

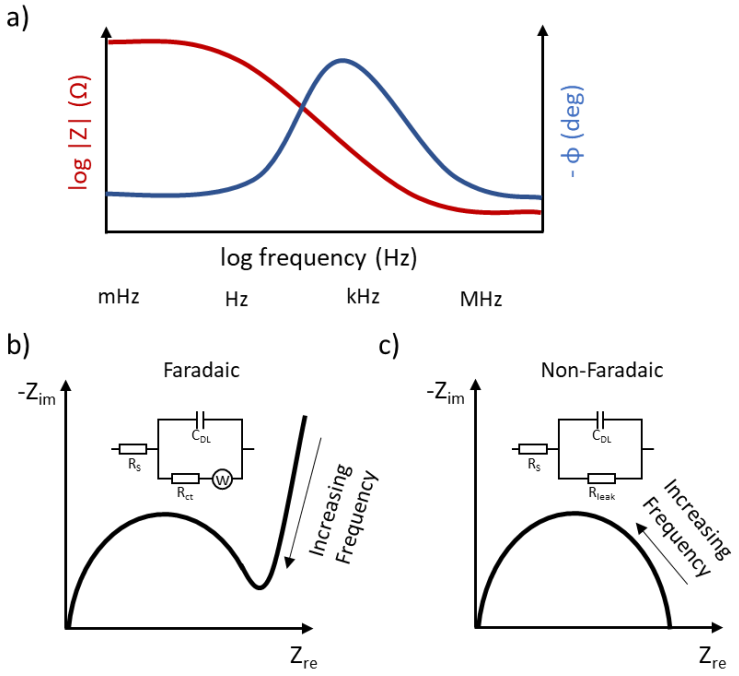

Figure 1.2: Graphical representation of EIS spectra: a) Bode plot of impedance, b) Nyquist plot and Randle's equivalent circuit for faradaic impedance, c) Nyquist plot and modified Randle's equivalent circuit for non-faradaic impedance.

Importance of the Electrochemical Interface for Aqueous Electrochemical Biosensing

The electrochemical double layer (EDL) is an important concept in electrochemistry and in understanding how EIS biosensors operate. The EDL occurs at the interface between a solid electrode and a liquid electrolyte and is formed when electrons from the electrode surface interact with ions in the surrounding electrolyte solution (Kosri et al., 2022). In the commonly cited Gouy–Chapman–Stern (GCS) EDL model (Kosri et al., 2022), the electrochemical interface is divided into five regions (Fig 1.3a). The first layer is the electrode itself, where the applied current or electrical potential dictates the surface charge. The second layer, called the inner Helmholtz plane, consists of species specifically adsorbed on the electrode surface, such as reactants and solvent molecules (Dunwell et al., 2018). Just beyond the inner Helmholtz plane is the outer Helmholtz plane, which consists of stationary solvent ions and molecules with opposite charges to the electrodes drawn to the electrode by electrostatic forces (Wu, 2022). Beyond the outer Helmholtz plane is the diffuse layer consisting of ions of both signs distributed in the electrolyte solution (Wu, 2022). Lastly, the bulk layer is composed of the electrolyte solution beyond the influence of the electrode's charge. Taken together, these components describe the charge distribution in an electrochemical system.

The potential difference across the EDL is known as the electrode potential, which is defined as the difference between the electrochemical potential of the electrode and that of the bulk electrolyte (Brown et al., 1999; Markovic, 2013). The magnitude of the electrode potential is influenced by the nature of the electrode, the electrolyte composition, temperature, and the presence of other ions or molecules at the electrode surface (Dunwell et al., 2018). The magnitude of electrode portential decay in a double layer is shown in Figure 1.3b.

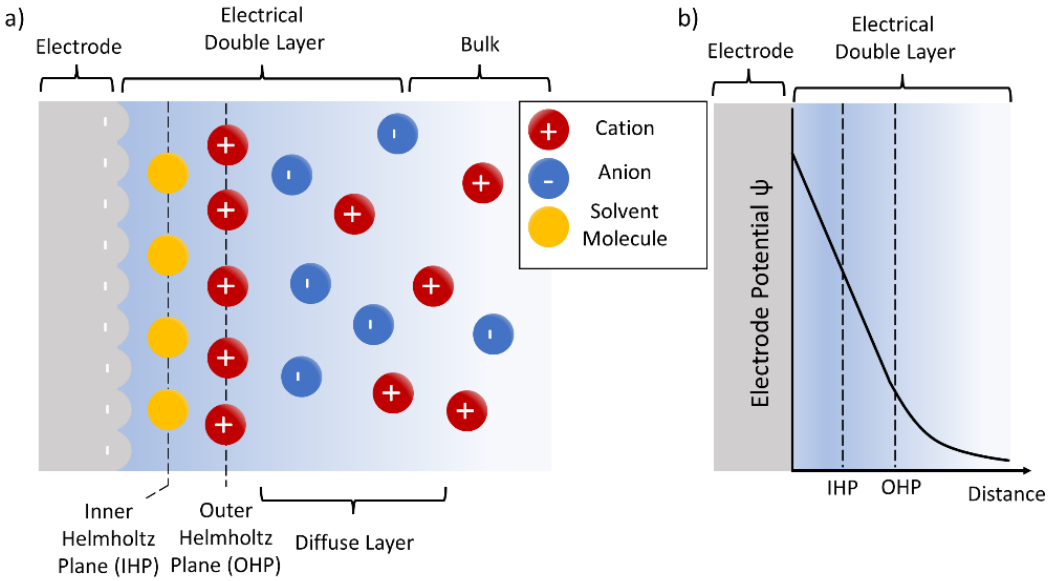

Figure 1.3 a) Schematic of the electrochemical double layer and its components, b) the electrode potential as a function of distance from the electrode surface.

A biosensor electrode in contact with a target liquid analyte forms a capacitive double-layer between the electrode surface and the bulk fluid of the analyte, and collectively comprise the electrochemical system. During an electrochemical biosensing event, biochemical reactions in the system, occurring near the electrode, alter the charge distribution and can be detected. Specifically, when target molecules interact with the biosensor electrode, changes to charge distribution in the double layer and/or changes in relative permittivity occur. These changes can be detected with impedance measurements (Bahadır and Sezgintürk, 2016).

This research focuses on impedimetric biosensing, but it should be noted that electrochemical biosensors also include potentiometric and amperometric sensors, which measure either changes in electrode potential, or current responses due to biochemical reactions, respectively.

Effects of Biofilm on Electrochemical Systems

When an EIS biosensor is deployed in a fluid seeded with microorganisms, microbial growth and EPS production are initiated, leading to biofilm development. The biofilm (*e.g.*, microorganisms, EPS matrix, and nutrients), and the surrounding liquid can collectively be considered an electrochemical system (Wang et al., 2009). Growth, attachment, or detachment of biofilm on the sensor can correspond with distinct changes to the electrochemical signals (Marsili et al., 2010; van Duuren et al., 2017). Detecting biofilm with EIS biosensors is based on the principle that both the electrochemical interface and bulk properties of an aqueous system change when a biofilm proliferates. It is unclear what causes the electrochemical changes, but several mechanisms have been proposed. For instance, electrochemically active biofilms such as *Pseudomonas aeruginosa* produce at least four redox-active molecules, such as phenazines, including pyocyanin (PYO), phenazine-1-carboxamide (PCN), 5-methylphenazine-1-carboxylic acid (5-MCA), and phenazine-1-carboxylic acid (PCA), all of which have strong redox activity (Bellin et al., 2016, Qiao et al., 2015). These substances can increase the concentration of charge carriers near the electrode interface, and/or become integrated into the biofilm matrix, creating conductive pathways for electron transfer which influence impedance spectra. EPS components such as polysaccharides, proteins and extracellular DNA may also alter the electron transfer characteristics in biofilms (Gula et al., 2020; Li et al., 2016; Malvankar et al., 2011; Tan et al., 2019; Wang et al., 2022). Another possible mechanism by which biofilms might generate changes in electrochemical properties is through the extension of electrically conductive pili or nanowires, which extend from the surface of some bacteria and could facilitate electron transfer to an electrode (Malvankar and Lovley, 2014; Maruthupandy et al., 2015). Additionally, bacterial metabolism involves the conversion of large organic compounds (*i.e.*, carbohydrates and sugars) into organic

acids and carbon dioxide, releasing the ionic metabolites into the medium which could also alter conductivity (Brosel-Oliu et al., 2019a).

Figures 1.4B-4E are schematic representations of the electrochemical processes that can affect the electrochemical properties of a biofilm including attachment of cells to the substrate (Figure 1.4B), the production of EPS matrix (Figure 1.4C), presence of metabolically active planktonic cells (Figure 1.4D), and secretion of proteins, macromolecules, and redox metabolites onto the electrode surface (Figure 1.4E).

EECs can be used to model electrochemical processes that occur when a sensor is deployed in biofilm, depicted in Figure 1.4A. As previously described, the Randle's circuit is frequently used to represent electrode-electrolyte systems, but when applied to EIS biosensors, modifications to the circuit components should be considered. To take into consideration the non-idealities at the electrochemical interface, a CPE_{DL} is often implemented (Figure 1.4A). The system resistance including electrical connection and the resistance of the thin film electrodes is modeled as $R_{connection}$. The system's overall capacitance including parasitic losses and the baseline empty cell capacitance is modeled as $C_{geometry}$. Several additional equivalent circuit models for characterizing biofilm formation have been considered. For instance, bacteria and biofilm matrix characteristics have been modeled with resistance and capacitance elements in both parallel and series configurations (Dominguez-Benetton et al., 2012; Furst and Francis, 2019; Kim et al., 2012; Kumar et al., 2023; Paredes, J. et al., 2014; Paredes et al., 2013; Subramanian et al., 2019; Zheng et al., 2013). Eventually EEC fitting may lead to a deeper understanding of the various biofilm processes.

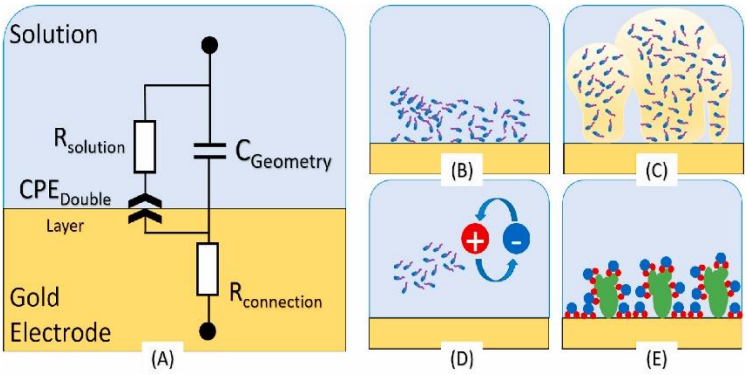

Figure 1.4: (A) Equivalent complex circuit model of an electrode-electrolyte electrochemical impedimetric cell containing microorganisms and biofilm. Bacteria contribute to different mechanisms at the interface and bulk solution in an electrochemical cell. (B) bacteria in close contact with the surface contributing to the double-layer capacitance. (C) extracellular polymeric substance (EPS) production contributing to the double-layer capacitance. (D) planktonic growth contributing to the bulk solution resistance. (E) proteins and macromolecules adsorption onto the electrode surface contribute to changes in the double-layer capacitance (Image Credit: Matt McGlennen, CBE. Figure used with permission from Elsevier, Vélez Justiniano et al., (2023)).

µIDEs for Biological Recognition

This study focuses on the utilization of micro interdigitated electrodes (µIDEs), a specific type of EIS biosensor, which is a microfabricated electrode design with a unique structure consisting of a patterned array of "fingers", usually between 1-50 µm that are separated by small gaps, usually between 1-50 µm (Dizon and Orazem, 2020). The length and spacing of the electrodes can be individualized depending on the application of interest. Figure 1.5 illustrates the structure of the µIDEs. µIDEs operate under conventional two-electrode system configurations and have been used for sensing biological samples via impedance (Gomez et al., 2002; Radke and Alocilja, 2004; Yang et al., 2004). A significant advantage of µIDEs in biological applications is the maximized sensitivity achieved by the increased surface area in contact with the media under test (Ibrahim et al., 2013). The narrow gap between electrodes increases the signal-to-noise ratio (Kosri et al., 2022). In addition, µIDEs are easily fabricated at a low-cost, do not require a reference

electrode, and have a small footprint making them ideal for high-throughput manufacturing (Brosel-Oliu et al., 2019a; Maduraiveeran et al., 2018).

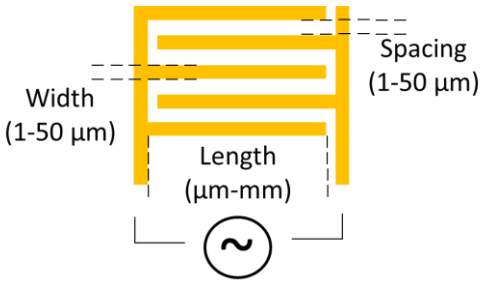

Figure 1.5: Graphical representation of a µIDE

The use of µIDEs for EIS biochemical sensing applications has gained interest in recent years. In the last two decades, µIDEs have been used to detect planktonic cells (Kim et al., 2012; Mallén-Alberdi et al., 2016; Tang et al., 2011; Xu et al., 2020) and to monitor biofilm formation (Estrada-Leypon et al., 2015; Liu et al., 2018; Paredes, J. et al., 2014; Paredes, Jacobo et al., 2014; Paredes et al., 2012, 2013; Subramanian et al., 2017). For instance, Yang was able to discern *Salmonella Typhimurium* concentrations down to 10^6 colony-forming units (CFUs) ml^{-1} with a simple µIDE setup (Yang, 2008) and could also detect foodborne pathogens using the same device (Yang and Bashir, 2008). Brosel-Oliu et al., developed a novel label-free µIDE biosensor functionalized with DNA aptamers that could detect *Escherichia coli* O157:H7 with a detection limit down to around 10^2 cfu ml^{-1}. Moreover, no response of the sensor was registered in the presence of other bacterial strains (*E. coli* K12, *Salmonella typhimurium*, *Staphylococcus aureus*), confirming the selectivity (Brosel-Oliu et al., 2019b; Brosel-Oliu et al., 2018). Lastly, Paredes et al., showed that µIDEs on silicon substrates were an accurate and dependable way to detect *Staphylococcus aureus* biofilms in aqueous media (Paredes et al., 2012).

Comparison of past studies using EIS biosensors for detecting biofilm is limited by high variation between experimental setups, and methods of data analysis leading to discordant results (Table 1.1).

Table 1.1 Summary of reports using EIS μIDE sensors for biofilm detection

Target Organism(s)	**Reactor Type; Fluid Conditions**	**Duration; Measurement Interval**	**Electrode modification**	**Abiotic control?**	**Confirmational technique**	**Statistical Analysis**	**Ref (year)**
Candida albincans, Strep sanguinis, Step mutans	Well-plates; Static	48 hrs; 15 min	NR	Yes	NR	NR	Abrantes et al. (2020)
Pseudomonas aeruginosa PA01 and PAET1, *Staph aureus* MRSA	Microfluidic; Flow	85 hrs; 12 hr	NR	NR	CLSM and Biofilm Enumeration	Yes, pearson's correlation test	Blanco-Cabra et al. (2021)
Pseudomonas aeruginosa and *Stenotrophomonas maltophilia*	Microfluidic; Flow	3 days; <10 min	NR	Yes	Epifluoresence and Crystal Violet	Yes, pearson's correlation test	Bruchmann et al. (2015)
Pseudomonas aeruginosa ATCC14454	Well-plates; Static	168 hrs; 24 min	NR	Yes	Crystal violet staining and SEM	NR	Chabowski et al. (2017)
Staph aureus	Microfluidic; Flow	24 hrs; 10 min	NR	NR	Optical and SEM	NR	Estada-Leypon et al. (2015)
E. coli	Simulated Catheter; Flow	24 hr; 30 min	NR	Yes	CFU Enumeration and Optical Absorbance	Yes, Endpoint T-test	Huiszoon (2019, 2021)
Pseudomonas aeruginosa PA01	NR	1 hr; 2 min	NR	Yes	SEM	NR	Kim et al. (2012)
E. coli, Salmonella	PDMS* Wells; Static	48hrs; 3hrs	NR	NR	NR	NR	Liu et al. (2018)
Staph epidermidis	Well-plates, CDCBGR, Petri Dish; Varies	25 hrs; 30min	NR	No	Optical	NR	Parades et al. (2012, 2013, 2014a 2014b)
E. coli K12	Microfluidic; Flow	60 hrs; 10-15 min	NR	Yes	Epifluoresence	NR	Subramanian et al. (2017)
Pseudomonas aeruginosa PA14 and mutants	Well-plates; Static	72 hrs; 5 min	NR	Yes	CLSM	NR	Van Duuren et al. (2017)
Pseudomonas aeruginosa PA01	Microfluidic; Flow	36-72 hrs; 30 min	Yes; PPy:PSS coating	Yes	CLSM and Biofilm Enumeration	Yes, T-test	McGlennen et al. (This Study)

NR= Not Reported

*PDMS=Polydimethylsiloxane

CDCBGR= CDC Bioflm Growth Reactor

SEM = Scanning Electron Microscopy

CLSM = Confocal Laser Scanning Microscopy

CV = Crystal Violet Staining

As evident in the literature, a variety of biofilm forming microorganisms have been evaluated by EIS, which may explain the discrepancy in impedance measurements, possibly due to difference in the electrochemical properties of different biofilms. A variety of experimental formats (*i.e.*, static vs. continuous flow, batch vs. flow reactor), and sensor electrode geometries may also influence results. Most studies utilized bare gold electrodes, which are known to experience sensor drift. The duration of testing ranges from as little as 1 hr to 168 hrs. Many do not report on abiotic controls or lack the statistical assessment of differences in signals over time. Lastly, correlation of impedance data to standard biofilm techniques, such as CLSM imaging is often absent. Acknowledging the limitations in previous endeavors to implement EIS biosensing for biofilm monitoring, the research undertaken in this dissertation endeavors to mitigate these shortcomings and contribute to the advancement of the field.

Knowledge Gaps

There are significant deficits in the understanding of EIS biosensing for *in situ* monitoring of biofilms which need further study. One critical area that requires exploration is the reliability of sensors over extended periods of exposure to microbial contamination. Microbial colonization on surfaces has been shown to cause corrosion and material degradation, which can also occur on a sensor surface leading to compromised reliability and shortened lifespan, in a process called microbially influenced corrosion (MIC) (Beech and Sunner, 2004; McGlennen et al., 2019). The impacts of microbial fouling on microfabricated sensors must be understood further to optimize designs and coatings, and to minimize the effects of MIC.

Although highly sensitive, EIS biosensors are susceptible to sensor drift, which refers to the gradual deviation of a sensor's output from its expected value or baseline over time (Roberts

and Sombers, 2018). Sensor drift can occur even in the absence of biologic material, causing shifts in the EIS spectra over time. This drift results from changes in the physical and chemical properties of the sensing elements, such as from surface imperfections or defects in the electrode structures resulting in non-uniform current distribution or alterations in the local electrochemical environment. Overall, minimizing drift in EIS sensors requires careful consideration of the sensor's design, fabrication, operation, and appropriate attention to signal processing and data analysis techniques. Further study is required to discern and reduce the impacts of sensor drift.

An additional overlooked component of EIS biosensing studies is that majority of testing has been conducted under static conditions (no-flowrate) that might not reflect the realities of most naturally occurring biofilms. Opportunities to deploy a sensor in an actual fluid-flow environment would be a notable advancement in biofilm monitoring and research.

Ultimately, the usefulness of an EIS biosensor lies in its ability to be used in a practical, real-world scenario to evaluate biofilm control and generate dependable data that can be utilized to take appropriate actions. This goal is especially challenging since biofilms flourish in harsh environments that are often difficult to access. An assessment on the capabilities of EIS biosensors applied in a real-world or simulated environment would drive the advancement of this innovative technology.

Research Goals, Hypotheses, and Objectives

Broadly, this work aims to develop and evaluate the use of microfabricated sensors as a novel methodology for real-time characterization of biological phenomenon. Specifically, this work aims to evaluate liquid environments that support microbial contamination and biofilm growth. **The overarching goal** of this work is to develop a highly-sensitive microfabricated sensor

and platform for *in situ* microbial analysis of biofilm-forming bacteria. The **central hypothesis** is that microfabricated EIS biosensors can reliably monitor biofilm *in situ*. To test this hypothesis, an optimized EIS biosensor is designed and fabricated, and a platform to validate sensor data is developed. Using a model biofilm-forming bacterial strain, the sensor is tested against biofilm growth, suppression, and dispersal in a variety of fluids.

To support this overarching goal of developing a microfabricated sensor system, four objectives are considered:

Objective 1: Investigating and mitigating the negative effects of biofilm on commonly used sensor materials. This objective aims to evaluate the severity of degradation of commonly used sensor thin film materials due to abiotic and biofilm-induced corrosion. The study seeks to quantify how microfabricated thin films degrade over time in a standard biofilm growth reactor, assess changes to the thin films' material properties, and consider potential solutions for improving sensor design.

To address this objective, material degradation caused by *Escherichia coli* K12 biofilm growth is determined by monitoring changes to electrical sheet resistance measurements (collinear four-point-probe) and Fourier-transform infrared spectroscopy (FTIR) absorption spectra over a time period of 7 weeks. Aluminum (metallic thin-film material) corroded significantly, whereas a-Si_xN_y:H (dielectric thin-film material) remained unaffected by MIC. It is concluded that to mitigate the negative effects of biofilm induced corrosion on sensors, an encapsulation material such as a-Si_xN_y:H can be utilized to protect the underlying conductive sensor material, and thus improve sensor durability. This objective is investigated in Chapter 2. Once the corrosive nature of biofilm is characterized, the next task is to develop corrosive resistant, reliable, sensor design.

Objective 2: Optimizing/enhancing a novel sensor design and developing an integrated platform to evaluate planktonic and biofilm growth under continuous flow conditions. This objective aims to improve sensor design by enhancing measurement stability and reducing sensor drift. An additional aim is to design a custom biofilm growth reactor flow cell system which integrates microfabricated sensors with CLSM imaging, a standard biofilm microscopy technique.

To address this objective, unmodified microfabricated sensors are evaluated under abiotic conditions resulting in unpredictable drift. Sensors modified with PPy:PSS coatings mitigate drift and result in highly stable time-resolved EIS measurements. An optimal PPy:PSS coating thickness is selected. A novel 3D-printed flow cell system that integrates sensors and enables real-time EIS measurements with simultaneous CLSM imaging during biofilm growth is designed. Furthermore, the system operates under continuous flow conditions, mimicking naturally occurring biofilm. It is concluded that during biofilm growth, this system successfully links continuous EIS data with CLSM imaging and will serve as the experimental platform for subsequent objectives. These aims are investigated in Chapter 3. Given the successful development of a continuous flow platform with seamless CLSM and EIS integration, the subsequent logical progression is to evaluate the sensor's responses to biofilm growth.

Objective 3: Understanding the relationship between biofilm development and sensor responses by correlating EIS data with a standard biofilm microscopy technique. This objective aims at collecting sensor signals throughout the stages of biofilm development. Using the flow cell system, EIS data is captured, and correlated with qualitative and quantitative CLSM assessments of biofilm.

To address this objective, real-time impedance measurements of biofilm growth under flow conditions were carried out using the novel 3D-printed flow cell system developed in objective 2. *Pseudomonas aeruginosa* PA01 served as the model biofilm-forming bacteria. Simultaneous EIS and CLSM were collected during biofilm growth from planktonic cell attachment through maturation. It is concluded that EIS microsensor data collection, in parallel with CLSM visualization, can reproducibly detect increasing levels of biofilm development. This objective is investigated in Chapter 3. Given the success of the sensor platform in correlating biofilm growth to EIS and CLSM, the subsequent logical progression is to evaluate the sensor's efficacy in detecting biofilm dispersal maneuvers.

Objective 4: Demonstrating the utility of EIS biosensors during biofilm dispersal and suppression. The aim of this objective is to test the utility of the biosensors to monitor biofilm control interventions. Within this aim, sensors are tested during biofilm removal treatments with commercially available disinfectants. Additionally, sensors are tested to assess the effects of cell-signaling inhibition on biofilm.

To address this objective, the novel 3D-printed flow cell system developed in objective 2 is used to monitor biofilm responses to antimicrobial treatments and a bacterial cell signaling suppressive agent. It is concluded that EIS microsensor data collection, in parallel with CLSM visualization, can reproducibly detect biofilm dispersal and suppression of cell signaling. This objective is investigated in Chapter 4. Given the success at detecting growth and dispersal in standard growth solution, the next logical step is to assess its utility in other biofilm relevant fluid environments.

Objective 5: Demonstrating the utility of EIS biosensors in an industrial fluid and in a natural setting. This objective aims at expanding the utility of the sensors outside of the laboratory. One aim is to test the sensors in an industrially relevant fluid prone to biofilm contamination. Sensors are tested for their ability to detect growth, dispersal, and inhibition in this fluid. A second aim involves testing the sensors to detect microbes in nature, specifically on a snow-patch and in an alpine pond.

To address the first part of this objective, the novel 3D-printed flow cell system developed in objective 2 is used to monitor biofilm growth, dispersal, and suppression responses in an industrially relevant oil-water emulsion fluid. It is concluded that in an oil-water emulsion, EIS microsensor data collection can reproducibly detect biofilm dispersal and suppression of cell signaling. To address the second part of this objective, a field-test of the sensor is conducted in an icy environment. It is concluded that under icy condition in a field test, EIS microsensors can differentiate varying concentrations of microbes. This objective is investigated in Chapters 4 and 5.

MATERIALS

Contribution of Authors and Co-Authors

Manuscript in Chapter 2

Author: Matthew McGlennen

Contributions: Investigation, Conceptualization, Methodology, Formal analysis, Data curation, Writing – original draft.

Co-Author: Markus Dieser

Contributions: Conceptualization, Formal analysis, Writing – review & editing.

Co-Author: Christine M. Foreman

Contributions: Conceptualization, Supervision, Funding acquisition, Writing – review & editing.

Co-Author: Stephan Warnat

Contributions: Conceptualization, Supervision, Funding acquisition, Writing – review & editing.

Manuscript Information

Matthew McGlennen, Markus Dieser, Christine M. Foreman, Stephan Warnat

2019 IEEE Sensors

Status of Manuscript:
____ Prepared for submission to a peer-reviewed journal
____ Officially submitted to a peer-reviewed journal
____ Accepted by a peer-reviewed journal
_x_ Published in a peer-reviewed journal

Publisher: IEEE
Published: Jan 14, 2020
DOI:10.1109/SENSORS43011.2019.8956741

Abstract

Micro-fabricated sensors enable the study of chemical and physical dynamics in aqueous environments such as rivers, lakes or oceans at low cost. Sensors must work reliably in these environments, which include both biological and chemical challenges. However, sensor thin films have not been studied in detail for aqueous applications, and more specifically how biotic interactions may change sensor material properties. In this study, the long-term effects of biofilm formation on the properties of aluminum (electric conductor) and a-Si_xN_y:H (insulating material) were investigated. Material degradation caused by *Escherichia coli* K12 biofilm growth was determined by electrical sheet resistance measurements (collinear four-point-probe) and Fourier-transform infrared spectroscopy (FTIR) absorption spectra over a time period of 7 weeks. Changes of the surface topography were tested using scanning electron microscopy (SEM) and white light interferometry. Aluminum was found to be heavily degraded at three weeks, whereas a-Si_xN_y:H was inert during the entire investigation period. As differences between thin film sensor materials are evident, more detailed investigations including a broader range of materials should be explored.

Introduction

Biofilms form on many types of substrata, including natural and engineered surfaces. When conditions allow, bacterial cells colonize surfaces and become embedded in extracellular polymeric substance (EPS) (Azeredo et al., 2017). Within minutes of substrate submersion in aqueous environments, microbial growth and EPS production are initiated, leading to the development of biofilm (Videla & Herrera, 2005). Biofilms can inhibit the performance of sensors used in studying the dynamics of aqueous environments. Microbial activity leading to deterioration

of surfaces containing biofilm is termed bio-corrosion or microbially influenced corrosion (MIC) (Beech and Sunner, 2004). For instance, *Pseudomonas aeruginosa*, a bacterial strain that forms corrosive biofilms (Li et al., 2016), has been shown to alter surface and material properties of nickel-copper and nickel-zinc thin films (San et al., 2014). *Escherichia coli* has been shown to accelerate corrosion in marine like environments on aluminum alloys (Pratikno & Titah, 2017), likely due to the secretion of metabolic organic acids (Ashton et al., 1973).

Surface micromachined sensors are based on the deposition of metallic and insulating materials. An inert interface between the active sensor surface and the aqueous media is required for reliable operation (Warnat et al., 2015). TiN and SiN have been reported to be inert in aqueous media, and still allow fully functional device operation. However, bio-corrosion/degradation of these materials has yet to be determined. Moreover, mechanisms to protect electrically conductive materials from environmental effects, and to improve sensor material reliability awaits investigation. Table 2.1 summarizes previous work on material and sensor reliability in aqueous environments. The present study examines the effects of biofilm growth on the material properties of two thin film materials. The focus was given to electronic conductivity, surface morphology, and bulk stoichiometric properties, and how they change as a function of exposure to biofilms.

Materials and Methods

Sample preparation

Samples of aluminum were deposited using physical vapor deposition (PVD) with thermal evaporation using Modu-Lab PVD. Amorphous silicon nitride with incorporated hydrogen (a-Si_xN_y:H) was deposited using PECVD with a chuck temperature of 100ºC. This low deposition temperature allows a-Si_xN_y:H to be used as an inert encapsulation layer for most electrically

conductive materials, comparable to the use of aluminum herein. Higher deposition temperatures could cause chemical reactions between the material and the substrate (Sedky et al., 2001). Also, lower deposition temperatures increase the hydrogen concentration in the a-Si_xN_y:H film through the use of NH_3 and SiH_4 reaction gasses. As an extreme example, non-stoichiometric a-Si_xN_y:H films made from PECVD were studied for their ability to be used as an encapsulation layer for sensor applications in aqueous media by studying long term reliability under exposure to biofilm. PECVD a-Si_xN_y:H films were deposited at the Utah Nanofabrication Facility. Samples were cleaved from the wafers and characterized prior to experimentation (see material characterization).

Table 2.1: Previous work on material and sensor reliability in aqueous environments

Subject	**Methods**	**Results**	**Ref**
Atomic layer deposition (ALD) post-processing of Al_20_3 and TiO_2 to encapsulate poly multi-user MEMS processing systems (PolyMUMPs) devices for aqueous environments	Thermal actuation in aqueous media/seawater, and displacement measurements	Performance of MEMS structures enhanced with ALD coating for long term use	(Warnat et al., 2015)
Dissolution kinetics of e-beam, low-pressure chemical vapor deposition (LPCVD) and plasma-enhanced chemical vapor deposition (PECVD) SiO_2 and a-Si_xN_y:H thin films in aqueous media	AFM, ellipsometry, and resistance changes	Combination encapsulation layers demonstrate increased electronic device lifetime	(Kang et al., 2014)
Biocorrosion of Al 6063 by *E. coli* in seawater	Corrosion rates, and microscopy	*E. coli* accelerates aqueous corrosion rates	(Pratikno and Titah, 2017)
MIC of Ni-Zn and Ni-Cu thin films from *P. aeruginosa*	SEM, polarization, and EIS	*P. aeruginosa* increased corrosion of Ni-Cu alloy but protected Ni-Zn	(San et al., 2014)

Culture Conditions and Biofilm Reactors

Center for disease control (CDC) biofilm reactors (Biosurface Technologies, Bozeman, MT) were used to grow biofilm following standardized methods (Goeres et al., 2005). Reactors were autoclaved for 30 min. Each reactor contained 350 mL of 1X tryptic soy broth (TSB; BD Bacto) media. Aluminum and a-Si_xN_y:H coated wafers were cut into approximately 1x1 cm samples, and sterilized in a 30% hydrogen peroxide bath for 10 min, followed by 30 min in 70% ethanol. Sample wafers were then glued with a drop of silicone adhesive to polycarbonate sample holders, mounted to CDC reactor rods, and allowed to cure for 24 hours. To ensure sample wafers and rods were thoroughly sterilized, and to guarantee abiotic conditions for control experiments, final sterilization of the CDC reactor rod assemblies involved exposure to UV light (254 nm) for two hours. All steps were performed inside a biosafety cabinet. Samples were prepared in triplicates per time point.

E.coli K12 was grown in TSB at 37°C while shaking at 125 rpm for 16 h, following standard methods (Sezonov et al., 2007). Subsequently, CDC reactors filled with 350 mL of autoclaved 1X TSB media were inoculated with 2 ml of bacterial enrichment. Inoculated reactors were run for 24 hours in batch mode at 22 °C on a stir plate at 125 rpm, followed by continuous flow operation of a 1:10 dilution of the TSB medium at a flow rate of 2 ml/min for 7 weeks (Figure 2.1). Abiotic control reactors were included using the same CDC reactor setup filled with either autoclaved deionized water (DI) or 1:10 diluted TSB media both operated in batch mode for 7 weeks. Triplicate sample wafers were collected at the beginning and 3, 5, and 7 weeks of operation. At each time point, sample wafers were removed from the polycarbonate sample holder with a sterile razor blade and transferred into 50 ml Falcon tubes containing 5 ml of 1X phosphate buffer saline solution (PBS). Sample wafers were placed into 50 ml Falcon tubes filled with 4.5g/L Tween

80 in 1X Dulbecco's phosphate-buffered saline (DPBS; Thermo Fisher), 5 ml of lab grade acetone, and 5 ml of isopropanol to remove biofilms. Sample wafers were sonicated at 60 W for 10 min at 22 °C, followed by a deionized water rinse. After biofilm removal, the samples were air-dried and stored in sterile Petri dishes at 22 °C until further analyses.

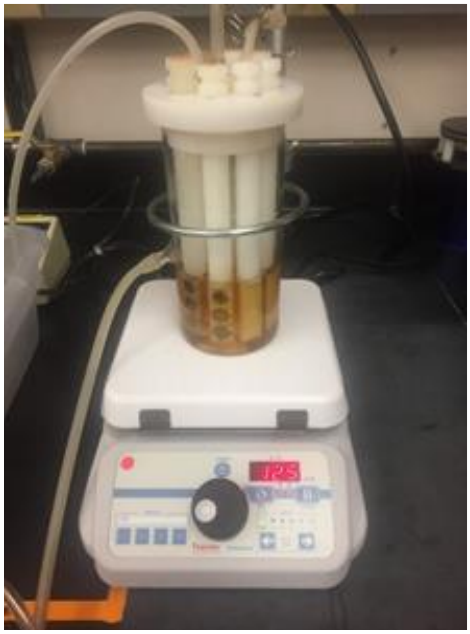

Figure 2.1: CDC biofilm reactor containing *E. coli* K12 biofilm growing on aluminum and silicon nitride substrate samples.

Materials Characterization

Techniques used to determine changes of the coated aluminum wafers included collinear four-point-probe sheet resistance measurement with a Keithley 2450 SourceMeter, scanning electron microscopy (SEM; Integrated Auger nanoprobe based on Physical Electronics 710), and energy-dispersive x-ray analysis (EDX; Bruker X-Flash 6I10). Wafers coated with a-Si_xN_y:H were analyzed with Fourier transform infrared spectroscopy (FTIR) attenuated total reflectance absorbance (Thermo Fischer Scientific Nicolet iS10 with a Harrick VariGATR ATR attachment) as well as with Filmetrics Profilm 3D white light interferometry.

Results

Collinear four-point-probe sheet resistance measurements of the aluminum sample wafers demonstrated a statistically significant increase in the sheet resistance after exposure to biofilm over the 7-week period (one way ANOVA: $F(3, 236)=1185.3$, $P<0.001$; Figure 2.2). At each time point investigated, an increase in sheet resistance was noticed, likely due to the corrosion of the film. Abiotic control studies show only slight increases in sheet resistance and showed no visual signs of degradation. Due to the high resistance and instability, a-Si_xN_y:H sheet resistance values are not reported.

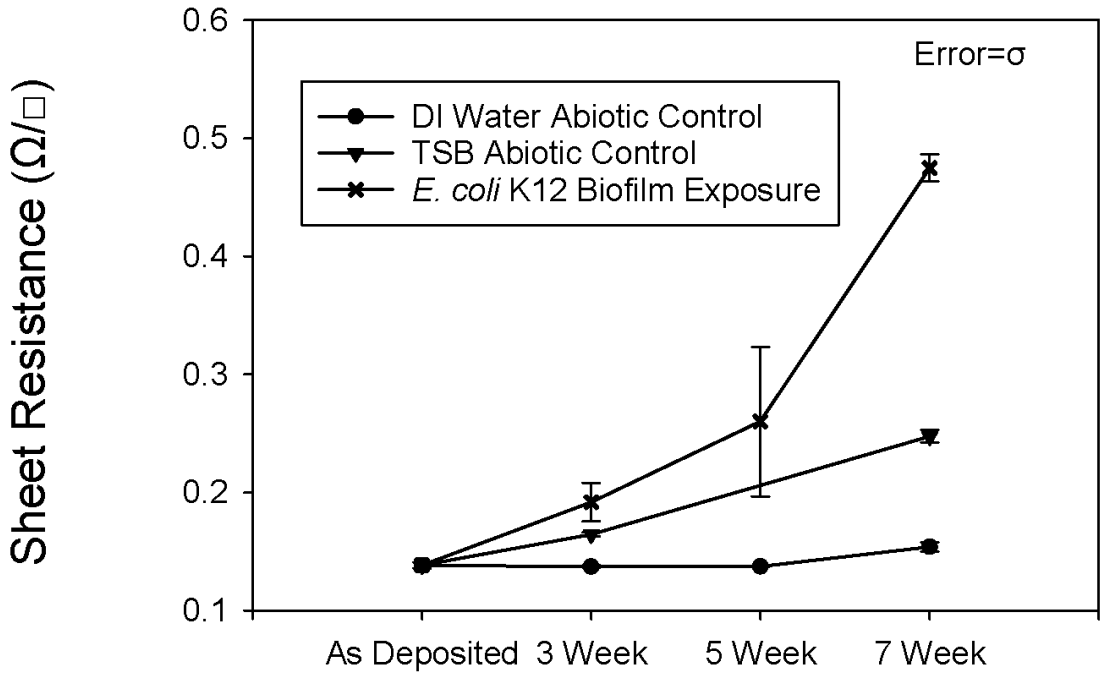

Figure 2.2: Collinear four-point-probe sheet resistance of aluminum thin film measured at time intervals of 0, 3, 5, and 7 weeks in CDC biofilm reactor.

Apparent differences were observed between aluminum and a-Si_xN_y:H coated samples exposed to *E. coli* biofilm. The original microstructure of the aluminum thin film (i.e., at the beginning of the experiment) was imaged using SEM (Figure 2.3a) and shows evidence of hillock formation on the surface (Bordo and Rubahn, 2012). After three weeks of exposure to biofilm, topographical features such as crevices and pits were abundant on the aluminum surface (Figure 2.3b). By week 7 much of the aluminum thin film was removed (Figure 2.3d) with only small amounts of aluminum remaining. EDX analysis confirmed the corrosion of aluminum film, showing the exposed underlying silicon substrate within a pit (Figure 2.3c).

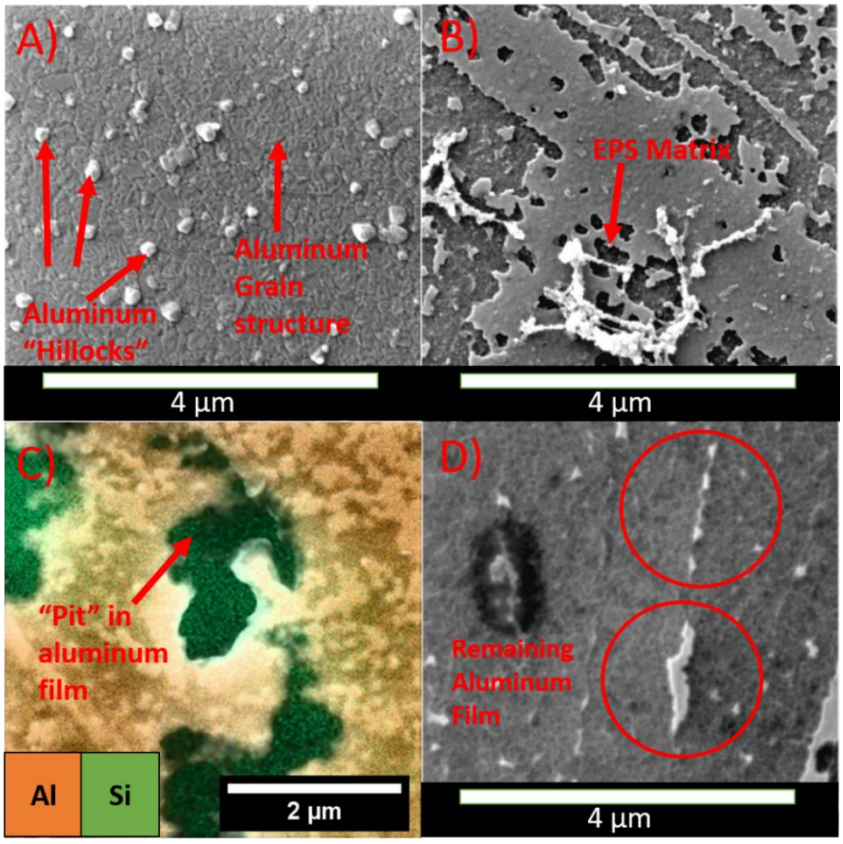

Figure 2.3: SEM images of aluminum PVD thin film surface a) as deposited showing aluminum hillocks on surface b) after 3 weeks in CDC biofilm reactor c) EDX analysis map of aluminum thin film surface after 3 weeks in biofilm reactor revealing underlying silicon substrate and d) SEM image of aluminum surface after 7 weeks in CDC biofilm reactor.

To study bulk structural changes on the a-Si_xN_y:H samples, FTIR absorption spectra were measured over 500 to 3500 cm^{-1} (Figure 2.4). Spectra show both symmetric and antisymmetric Si-N stretching modes in all samples, regardless of the duration of exposure to biofilm. Relative absorbances remained the same throughout the specified time intervals and suggested no significant change in the film stoichiometry. These results suggest that a-Si_xN_y:H is a promising material for encapsulating active sensor structures in aqueous media.

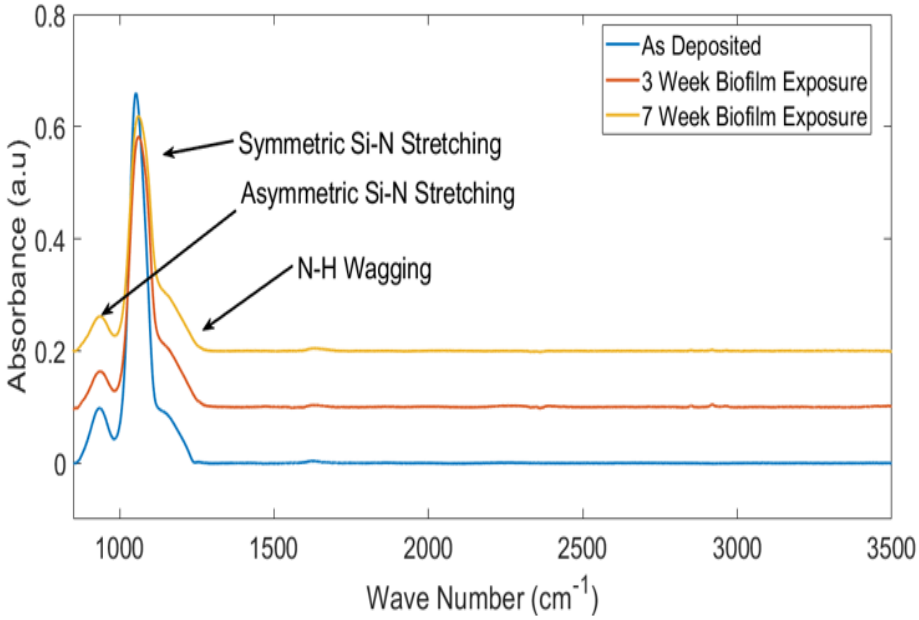

Figure 2.4: FTIR spectra of a-Si_xN_y:H thin films, measured at timepoints of 0, 3, and 7 weeks.

White light interferometry data was collected on wafer samples from an as-deposited a-Si_xN_y:H, and 7 weeks biofilm exposed sample (Figure 2.5). Area maps of sample surfaces were collected and show surface morphology and average roughness values. The as-deposited a-Si_xN_y:H sample had an average roughness of 2.2 nm while the 7-week exposed sample had an average roughness of 2.3 nm. No visual differences were noticed between samples, further

suggesting that a-Si_xN_y:H is a promising encapsulation material to protect metallic thin films used for aqueous sensing.

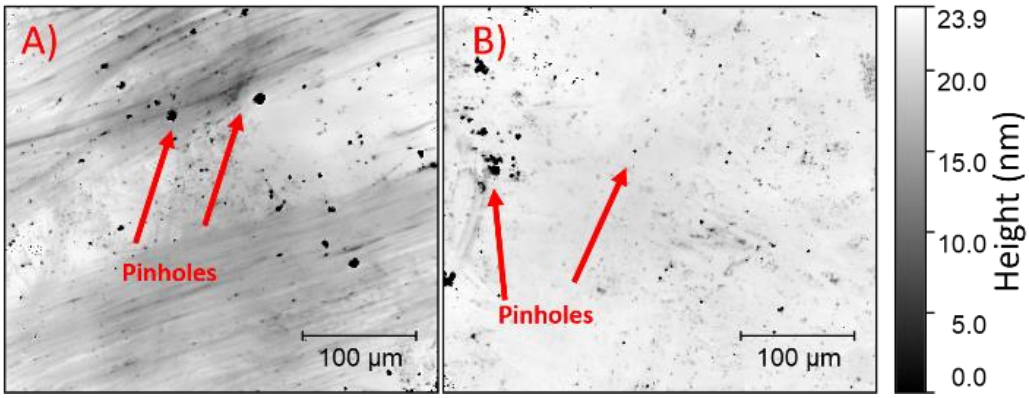

Figure 2.5: White light interferometry image of A) as deposited a-Si_xN_y:H thin film and B) after exposure to biofilm for 7 weeks.

Conclusion

Biofilm adhesion and growth affects material properties when attached to surfaces and allowed to propagate. In aqueous environments biofilm formation occurs on a wide variety of substrates and can lead to biofouling (Lappin‐Scott and Costerton, 1989). Conductive materials are very susceptible to corrosive biofilms and precautions should be made to mitigate damage that can occur due to prolonged exposure in aqueous environments. In the present study, biofilm adhesion and growth was shown to impact aluminum thin films. Aluminum thin films used in aqueous environments showed an apparent increase in sheet resistance, suggesting that they are not reliable for use in aqueous environments by themselves. Therefore, a protective barrier should be considered. Conversely, low deposition temperature a-Si_xN_y:H coatings remained inert throughout the course of the experiment. The results show that this coating has the potential to protect conductive sensor materials from fouling and biological damage. These results suggest that

other sensor materials (*e.g.*, gold, polycrystalline silicon, and nickel) should be investigated to determine their susceptibility to microbially influenced corrosion, and the ability of a-Si_xN_y:H to encapsulate the materials to minimize material degradation. Future work should focus on higher resolution time-series investigations to determine when the materials are no longer viable for optimal sensor performance.

USING ELECTROCHEMICAL IMPEDANCE SPECTROSCOPY TO STUDY BIOFILM IN A 3D PRINTED FLOW CELL SYSTEM

Contribution of Authors and Co-Authors

Manuscript in Chapter 3

Author: Matthew McGlennen

Contributions: Investigation, Conceptualization, Methodology, Formal analysis, Data curation, Writing – original draft.

Co-Author: Markus Dieser

Contributions: Conceptualization, Formal analysis, Writing – review & editing.

Co-Author: Christine M. Foreman

Contributions: Conceptualization, Supervision, Funding acquisition, Writing – review & editing.

Co-Author: Stephan Warnat

Contributions: Conceptualization, Supervision, Funding acquisition, Writing – review & editing.

Manuscript Information

Matthew McGlennen, Markus Dieser, Christine M. Foreman, Stephan Warnat

Biosensors and Bioelectronics: X

Status of Manuscript:
____ Prepared for submission to a peer-reviewed journal
____ Officially submitted to a peer-reviewed journal
____ Accepted by a peer-reviewed journal
_x_ Published in a peer-reviewed journal

Publisher: Elsevier
Published: March 5, 2023
DOI: https://doi.org/10.1016/j.biosx.2023.100326

Abstract

Biofilm contamination is a widespread issue that can occur anywhere when organisms attach to surfaces in the presence of water. In industrial environments, formation of biofilms can lead to component failure, material degradation, and biofouling or spoilage, which collectively come with significant economic costs. Microfabricated electrochemical impedance spectroscopy (EIS) sensors have emerged as a promising tool for monitoring biofilm as EIS sensors capture information about biofilm growth autonomously in real-time; however, sensors suffer from drift, and the technique lacks temporal interpretation of dynamic biofilm processes. In this work, microfabricated sensors featuring gold micro-interdigitated electrodes (μIDEs) were modified with an electrically conductive polymer layer resulting in EIS measurement variability that was significantly reduced compared to unmodified sensors, and enabled highly stable, time-resolved EIS measurements. EIS characterization of *Pseudomonas aeruginosa* biofilm in parallel with high-resolution confocal laser scanning microscopy confocal laser scanning microscopy (CLSM) was performed using a novel 3D-printed flow cell system, resulting in distinct changes to EIS data corresponding with consistent biofilm growth. We have shown that EIS microsensors can detect four stages of biofilm: (*i*) initial biofilm attachment to the sensor substrate, (*ii*) early-stage irreversible biofilm proliferation characterized by sparse biofilm coverage, (*iii*) mature biofilm detection characterized by uniform biofilm coverage, and (*iv*) changes due to detachment and regrowth of biofilm.

Introduction

Most microorganisms exist as organized communities attached to each-other or surfaces embedded in a matrix of extracellular polymeric substance (EPS); creating structures known as biofilms (Azeredo et al., 2017; Costerton et al., 1999). Biofilms can profoundly affect human health, industrial processes, and natural and engineered systems. Collectively, biofilm associated costs have been estimated at around $4 trillion per year globally (Cámara et al., 2022). Biofilms are more resilient against mechanical and chemical treatments compared to planktonic cells, rendering common treatment options ineffective. Strategic solutions for *in situ* sensing of biofilms in environmental, medical, and industrial settings are needed to implement treatments more effectively so that biofilms can be reliably monitored.

Measurement and analysis techniques using quartz crystal microbalance (QCM), open circuit potentiometry (OCP), voltammetry, or amperometry sensors allow for nondestructive monitoring and *in situ* analysis of biofilms at various stages of growth (Becerro et al., 2016; Poma et al., 2020; Ripa et al., 2020). However, these applications are susceptible to ambient vibrations and noise, or are limited to analyzing electroactive analytes, respectively (Ding et al., 2020; Grieshaber et al., 2008). Recently, electrochemical impedance spectroscopy (EIS) has shown potential in detecting biofilm growth *in situ* and has significant advantages over the previously mentioned techniques. EIS has the sensitivity to gather information occurring at the solid-liquid interface and in the bulk solution in real-time without the need of complex reagents and bulky instrumentation. EIS devices can be miniaturized using microfabrication techniques, which increase signal-to-noise, and improve sensitivity compared to conventional electrode geometries. In general, EIS applies a sinusoidal electrical perturbation (*i.e.*, voltage or current) to an

electrochemical system across a range of frequencies and measures the electrical response (*i.e.*, voltage or current), termed complex impedance (Vivier and Orazem, 2022). EIS spectra can be divided into several domains where certain regions embody electrochemical parameters of a system under test. For instance, EIS spectra may show impedance artifacts due to double-layer capacitances, diffusional impedances, solution resistances, and others (Magar et al., 2021). During an EIS measurement containing microorganisms, changes in EIS spectra over time may indicate the attachment, presence, and growth of microorganisms on the electrode surface.

Among EIS techniques, the use of micro interdigitated electrodes (μIDEs) for biosensing applications have stood out for their simplistic design and fabrication, high sensitivity, high signal-to-noise ratio, and their use without the need of a reference electrode during measurements (Dorledo de Faria et al., 2019; Furst and Francis, 2019; Park et al., 2018). For microfabricated EIS sensors, gold is commonly used as an electrode material due to having good chemical stability, low reactivity, good biocompatibility, and high electrical conductivity. While gold μIDEs have been used for the detection of planktonic bacteria (Kim et al., 2012; Simic et al., 2020; Yang et al., 2004), biofilm (van Duuren et al., 2017; Ward et al., 2018), and microbes in icy-conditions (McGlennen et al., 2020), several research limitations can be noted. Most of these studies were performed under static conditions with no fluid shear and may have reached nutrient limitations. Further, confirming the presence of biofilm on μIDEs has largely relied on biofilm-destructive techniques at a finite time point and lack a temporal interpretation of EIS during cell attachment and biofilm development (Goikoetxea et al., 2018; Paredes et al., 2012, 2013, 2014a, 2014b). Electrochemical measurements, including the use of gold μIDEs, suffer from nonlinear, long-term baseline instability, (*i.e.*, signal drift), which decreases measurement reproducibility and leads to

diminished quantitative confidence (Roberts and Sombers, 2018). Lastly, a clear differentiation and interpretation between biotic and abiotic effects on EIS measurements through continuous measurements has been ambiguous or lacking (Blanco-Cabra et al., 2021).

Owing to the complex behavior of biofilms, a single analytical technique is often not sufficient to fully characterize the dynamics of biofilm growth. Herein, microfabricated EIS sensors were combined with live-cell confocal laser scanning microscopy (CLSM) imaging to achieve the analytical depth necessary for interpreting EIS data from biofilms over different stages of growth. The objectives of this work were to: (*i*) minimize EIS signal drift and improve the measurement stability of microfabricated EIS sensors, (*ii*) develop a novel 3D printed flow cell system for capturing EIS and CLSM images during biofilm growth, (*iii*) identify the optimal single-frequency impedance measurement that best characterizes biofilm growth, and (i*v*) validate the suitability of EIS sensors for the real-time detection of biofilm growth.

Material and methods

Sensor fabrication

Sensors were fabricated using standard microfabrication techniques of physical vapor deposition, lithography, and wet etching processes with minor modifications (Neubauer et al., 2019). A 10 nm titanium adhesion promoter was used in lieu of chromium because of its increased resistance to dissolution, and limited oxidation potential (Hoogvliet and van Bennekom, 2001). The titanium film was deposited using electron beam physical vapor deposition in an Angstrom Thermal Evaporator (AMOD, Oxford Instruments, USA). Proceeding gold etching, the titanium adhesion promoter was etched by immersion in 40:1:1 H_20:HF:H_20_2 solution for 12 s, followed by deionized water (DIW) rinse. The µIDEs were designed to be 15 µm in width with a spacing of 10

μm, for a total of 50 electrode pairs. To allow only the μIDEs region of the sensors to participate in EIS, the electrical connection leading up to the μIDEs were encapsulated with SU-8 3010 (Kayaku Advanced Materials, Boston, USA) and were patterned with lithography (Figure 3.1b). The gold-patterned wafers were cleaned with O_2 and Ar^+ plasma for 5 min at 600 W in Ion Wave 10 Batch Plasma System (PVA Tepla, USA), and were immediately spun coated with SU-8 3010 photoresist at 500 RPM for 10 s, 4000 RPM for 30 s, soft baked at 65ºC for 60 s and then 95ºC for 600 s. The wafers were exposed on the contact aligner (ABM inc., USA) for 360 mJ cm^{-2} to a mylar photolithography mask (Cad Art Services; Bandon, OR). Post-exposure bake was performed at 65ºC for 60 s, 95ºC for 180 s, and 65ºC for 30 s, respectively. The wafers were developed in SU-8 developer (Kayaku Advanced Materials, Boston, USA) for 360 s while shaking on an orbital shaker at 60 RPM, followed by a DIW rinse. Finally, the wafers were hard baked at 125ºC for 1200 s on a hotplate.

Additionally, sensors were equipped with a crosshair feature (Figure 3.1a-2) to streamline locating the center of the μIDE during CLSM analysis (see CLSM imaging and data analysis below). The wafers were diced into sensors measuring approximately 8.7 mm wide × 26 mm long using a Disco DAD3221 Dicing Saw (Disco Corp., Japan). The summary of the fabrication process can be found in Supplemental Figure A.1. The microfabricated sensors in this work featured three transducer elements within the same footprint (Figure 3.1), however the primary focus of this study was to use μIDEs.

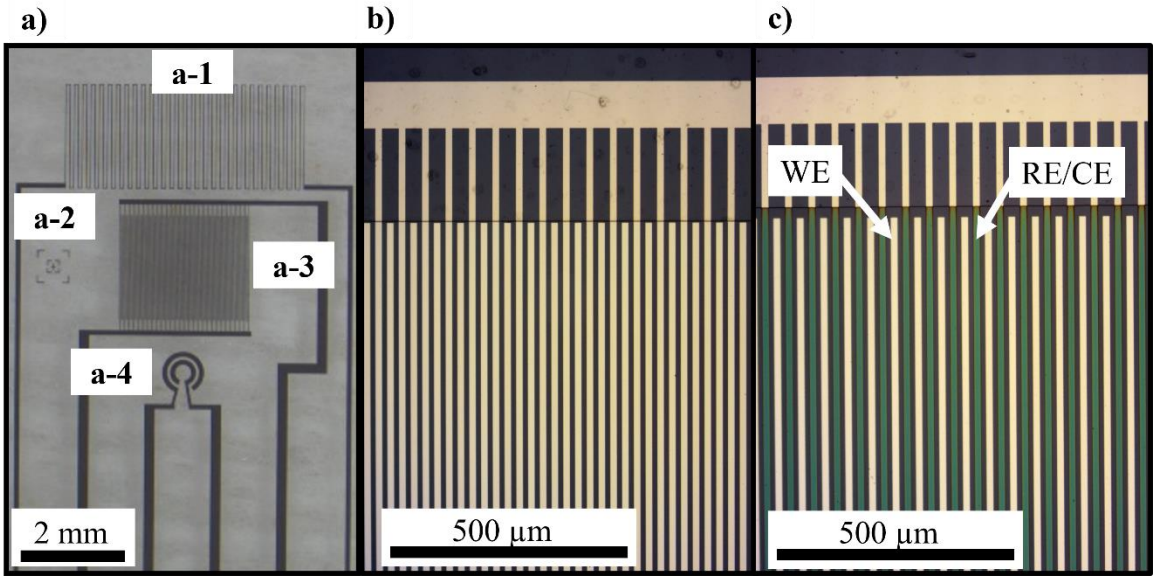

Figure 3.1: Optical microscope images of microfabricated sensors and their features. (a) Layout of the microfabricated sensor. (a- 1) RTD sensor, (a-2) "crosshair" feature used for finding the center of IDE structures (a-3) µIDE structures, (a-4) ring impedance sensor. (b) µIDE sensor before electropolymerization. (c) µIDE sensor showing both bare gold WE and PPy:PSS coated CE/ RE regime. (For interpretation of the references to colour in this figure legend, the reader is referred to the Web version of this article.)

Sensor electropolymerization

Sensors were cleaned by placing a 100 µL drop of 7:2:1 H_2O:NH_4OH:H_2O_2 on the µIDEs for 1 hr, followed by DIW rinse (Kim et al., 2008). Electropolymerization of one side of the µIDEs was adapted from (El Hasni et al., 2017). Briefly, 0.2 M poly (4-styrenesulfonic acid) solution (PSS; Mw ~75,000, 18 wt% in water, Sigma-Aldrich, USA) and 0.2 M pyrrole (PPy; 98%, reagent grade, Sigma-Aldrich, USA) were freshly prepared in DIW. A 100 µL drop of 0.2 M PSS:0.2 M PPy was placed onto the surface of the µIDEs. Two different electrode modification procedures (*i.e.*, one thin, and one thick) were evaluated to optimize the coating parameter that best minimizes measurement variability and drift. Electrodeposition was carried out under galvanostatic conditions with a current density of 0.1 mA cm^2 applied to one side of the µIDEs using a Keithley 2450 source measure unit (SMU). The surface area of one side of the µIDEs was calculated as

0.015 cm^2, which led to deposition times of either 113.33 s or 300.00 s. Resulting deposition charges were 170 µC and 450 µC, respectively (Figure 3.1c).

Design and fabrication of CLSM flow cell system

A flow cell system was designed for monitoring biofilm growth on top of the surfaces of the µIDEs so that simultaneous high-resolution live CLSM images and EIS data could be collected. The design of the flow cell system consisted of four components: (*i*) a base to mount the flow cell system to the CLSM microscope, (*ii*) the flow cell body, (*iii*) three microfabricated EIS sensors, and (*iv*) three electrical connectors (Figure 3.2). 3D CAD of the flow cell system and its associated components were made in Autodesk Inventor 2021 and Eagle (Autodesk, USA). The base was milled out of a 6061-aluminum sheet to fit the clamp width of the CLSM stage. The flow cell body and the electrical connection holders were 3D printed using an Epax X1 4k printer with biocompatible poly lactic acid (PLA) liquid resin (eSUN PLA pro, China). Structurally, the flow cell body was 100/40/10 mm (W/H/D) and housed three independent flow chambers (~35 µL each). Inlet and exit ports were vertically mounted and set at differing heights to minimize bubble formation. A 25 × 75 × 1 mm glass microscope slide (Fisher Scientific, USA) served as a viewing window and was adhered to the flow cell body using silicone (DAP, USA). The planar profile of the flow cell body enabled uninterrupted movement along the X-Y direction on the microscopy stage.

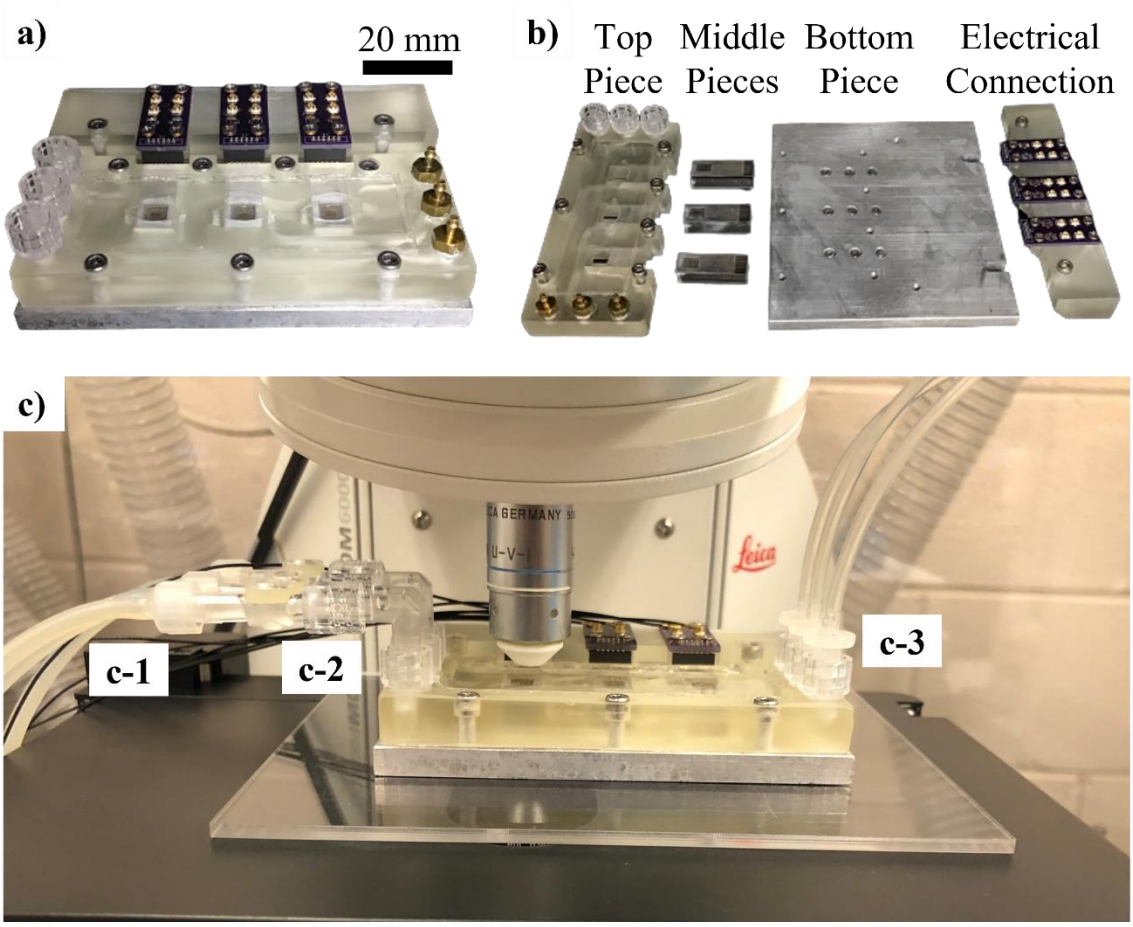

Figure 3.2: Design of the flow cell system with integrated microfabricated sensors used for biofilm growth experiments. (a) Picture of flow cell system prior to experiment. (b) Disassembled view of flow cell system revealing its four major components: (top piece) 3D printed flow cell body with luer-lock and barb-connectors, (middle pieces) silicone gaskets, sensors, and support blocks, (bottom piece) aluminum base for mounting to CLSM, and (electrical connection) PCB boards and holders. (c) The flow cell mounted beneath a wet immersion objective on CLSM, (c-1) influent barb connectors and silicone tubing, (c-2) injection ports, (c-3) effluent barb connectors and silicone tubing.

The flow cell body was fitted with three microfabricated EIS sensors and sealed with laser-cut silicone gaskets (0.01” High-Purity High-Temperature Silicone Rubber, McMaster Carr, USA) pressed between laser cut acrylic blocks and the flow cell body. Plastic threaded barb connectors were used to connect 0.8 mm I.D. silicone tubing (P/S #13, Masterflex, USA) both for the inlet and outlet (Figure 3.2c-1 and 3.2c-3). Cell injection ports (Fisher Scientific, USA) were equipped

with luer-lock connectors and placed in line with the influent tubing (Figure 3.2c-2). Electrical connection was achieved using custom-made printed circuit boards (PCBs) and pogo-pins (Mill-Max, USA), which allowed reliable and non-permanent electrical connection to each sensor (Figure 3.3a). The PCBs were equipped with ultra-miniature connectors (UMC) and were connected to a Hioki IM3533 LCR meter with UMC to subminiature version A (SMA) cables (Cinch Connectors; USA). The entire assembly fastens to the custom-manufactured aluminum base using six M3 socket stainless steel cap screws.

Computational fluid dynamics (CFD) analysis was performed to visualize the flow profiles and wall shear stresses within the flow chambers containing a microfabricated sensor using COMSOL Multiphysics Version 5.3. A physics controlled fine mesh was used for the simulation. Incompressible and steady-state flow conditions were simulated using the experimental flowrate of 1 µL min^{-1}.

EIS measurements and data analysis

EIS measurements were carried out with a Hioki IM3533 LCR meter connected to a Keysight 970A data acquisition system (DAQ) with a DAQ905A RF 2 GHz Dual 1:4 RF Multiplexer, 50 Ohm switching module. The instruments were controlled by a custom-built virtual interface (VI; LabView 2017), providing multiplexed four channel EIS measurements. EIS was collected every 30 min across a frequency range of 200 kHz to 100 Hz and 25 logarithmically spaced data points. The signal source was a sine wave with an amplitude of 10 mV RMS and no DC bias. During EIS data collection sensors coated with PPy:PSS were connected to the LCR meter such that the coated side of the µIDEs served as both the counter electrode (CE) and

reference electrode (RE; Figure 3.1c).Time-dependent changes to impedance were reported given by equation (3.1):

$$\text{Impedance Change (\%)} = \frac{|Z_{(f,t)}| - |Z_{(f,t0)}|}{|Z_{(f,t0)}|} * 100\% \quad (3.1)$$

Where $|Z_{(f,t0)}|$ is the impedance measurement at the frequency of interest (f), measured at the initial timepoint (t_0), and $|Z_{(f,t)}|$ is every subsequent impedance measurement. All EIS data were analyzed in Matlab 2021a and statistical differences were determined by Student's T-test.

Characterization of PPy:PSS coated sensors

To evaluate sensor variability and stability, four µIDEs of each of three different coatings (*i.e.*, 0, 170, and 450 µC terminal deposition charges of PPy:PSS) were submerged in sterile 1:10X tryptic soy both (TSB; Fisher Scientific, USA), inside of 1.5 mL microcentrifuge tubes for 18 hrs while logging EIS every 30 min (see above EIS measurements and data analysis). Impedance changes were measured at 100 Hz to monitor time-dependent changes to low-frequency impedance dominated by the double-layer capacitance. EIS sensor variability and stability at 100 Hz were evaluated statistically using Levene's Test for equality of variances between the three coating parameters at t_0 and between t_{18} and t_0.

Cell culturing conditions

A green fluorescent protein (GFP) labelled *Pseudomonas aeruginosa* PA01 was used for all biofilm related experiments (Nivens et al., 2001). Cell cultures were grown in the presence of 50 µg mL^{-1} carbenicillin (Fisher Scientific, USA) plates. Freezer stocks were transferred to tryptic soy agar (TSA; Fischer Scientific, USA) and were incubated at 37ºC for 24 h prior to experimentation. Cell culture enrichments were made from single colonies and were grown in 1X

TSB at 37ºC while shaking at 150 rpm for 18 h. Subsequently, enrichments were harvested at 10,000×g for 5 min. The resulting cell pellets were resuspended in 1:10 X TSB and incubated at 22ºC while shaking at 150 rpm for 6 hrs to allow cells to adjust to growth conditions selected for the flow cell. Dilute media was used because biofilm growth and EPS production are more substantial under depleted nutrient environments (Zhang et al., 2014). Enrichments were harvested at an optical density of OD_{600}=0.2, resulting in a cell concentration of ~$1x10^8$ colony forming units (CFUs) mL^{-1}. Enrichments were transferred to 10 mL sterile luer lock syringes (Becton Dickinson, USA), equipped with 20 ½ ga. needles (Fisher Scientific, USA) prior to injection into the flow chambers.

Flow cell system operation

The three flow chambers were sterilized by infusing 70% ethanol for 20 min followed by a DIW rinse. Biofilm growth was initiated by first filling each flow chamber with 1:10X TSB from individual 10 mL syringes. A continuous flowrate of 1 µL min^{-1} was provided to each flow chamber for 2 h. Next, the flow chambers were inoculated with 1 mL of cell culture enrichments (~$1x10^8$ CFUs) by aseptically inserting the syringe needle through the injection ports (Figure 3.2c) (seeding phase). Flow was paused during seeding for 2 h to allow cell attachment onto µIDEs. Subsequently, sterile 1:10X TSB was supplied to the flow chambers at a continuous flowrate of 1 µL min^{-1} for 48 h to remove excess planktonic cells in the bulk solution and to promote biofilm formation (growth phase). All experiments were performed in triplicate at 22ºC. Abiotic controls were performed following the same procedure, minus the injection of cell culture enrichments.

Before inoculation of the flow chambers with cell culture enrichments, an initial EIS measurement of the cell free culture media (1:10X TSB) was collected, which served as the

background impedance ($|Z_{(f,t0)}|$). After infusion of cell culture enrichment into the flow chambers, EIS data were recorded every 30 min ($|Z_{(f,t)}|$). A summary of the operation of the flow cell for biofilm growth is shown in Supplemental Figure A.2.

CLSM imaging and data analysis

Biofilm images were acquired using CLSM (SP5 upright confocal, Leica, USA) and analyzed in Imaris 9.8 (Bitplane, Switzerland). To minimize quantitative subjectivity and bias, biofilms were imaged at the same X-Y coordinates for each timepoint. Representative 3D CLSM images were captured using 40X (Leica, 3.3 mm WD, 0.80 NA) magnification. Total biovolume from each CLSM Z-stack was calculated using Imaris 9.8 "surfaces" analysis feature with absolute fluorescence intensity above 20.0, voxel absolute fluorescence intensity above 4.0, and eliminating particle sizes smaller than 2 µm in diameter as filter criteria. Data were normalized to the field of view by using equation (3.2) similarly to (Lim et al., 2016), creating a biofilm index.

$$\text{Biofilm Index} = \frac{\sum Biovolume\ (\mu m^3)}{\text{Field of View}\ (\mu m^2)} \tag{3.2}$$

Differences in biofilm indices were analyzed using a Student's T-test to compare differences in means.

Results

Characterization of electropolymerized µIDEs

A bode plot of impedance and phase angle for all three coatings parameters (*i.e.*, 0, 170, and 450 µC PPy:PSS) of electrodeposited µIDEs displayed typical resistive and capacitive behaviors for electrode/electrolyte systems. The spectra were characterized by three distinct regions: a low-frequency capacitive region (*i.e.*, <2 kHz), a middle frequency capacitive and

resistive region (*i.e.*, 2 kHz<f<20 kHz), and a high-frequency resistive region (*i.e.*, >20 kHz) (Supplemental Figure A.3). Below 2 kHz, phase angle reached its minimum, and impedance reached its maximum. In the middle-frequency region impedance and phase angle were reversed with higher frequencies. Above 20 kHz, the phase angle was highest, and the magnitude of impedance reached its minimum.

Differences in EIS spectra were evident between the three coatings. Sensors coated with deposition charges of 170 µC and 450 µC PPy:PSS resulted in a clear reduction in impedance from 100 Hz to ~150 kHz. Conversely, 170 µC and 450 µC PPy:PSS coated sensors' phase angles were collectively higher than the 0 µC PPy:PSS coated sensors across all frequencies (Supplemental Figure A.3). Of relevance, the phase angle for each of the three coating parameters approached -90º below 2 kHz, where capacitive effects (*i.e.*, electric double-layer capacitance and electrode polarization effect) were the dominating signal. For this reason, 100 Hz was chosen to further characterize sensor variability and stability.

Sensor variability and stability in abiotic media

EIS measurements of µIDEs with and without electrically conductive PPy:PSS coatings were recorded over 18 h in sterile 1:10X TSB to determine measurement stability over time at 100 Hz (Figure 3.3; Supplemental Figure A.4). Impedance signals for uncoated sensors (*i.e.*, 0 µC PPy:PSS) either increased or decreased relative to t_0 with no predictable trend. Sensors with PPy:PSS coatings behaved unidirectionally, with a reduction in total sensor drift variability related to coating thickness.

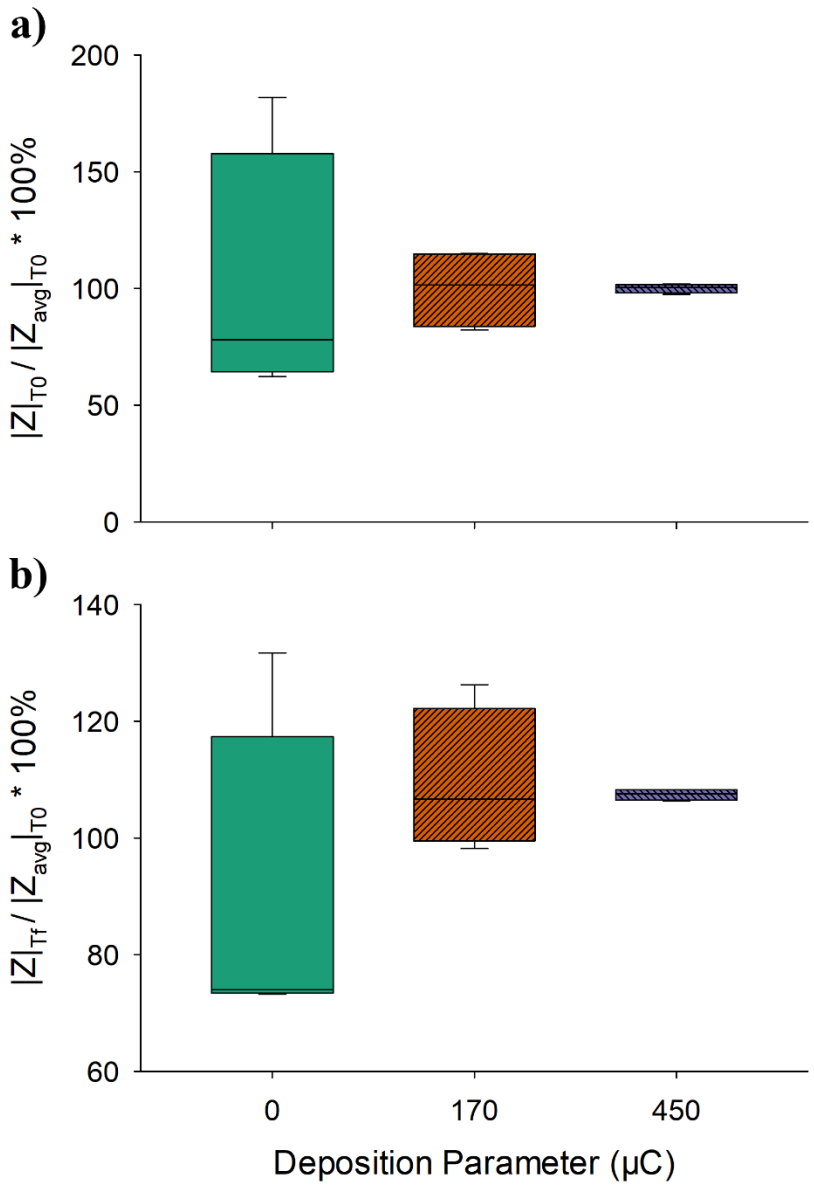

Figure 3.3: Evaluation of sensor variability in abiotic 1:10X TSB from sensors coated with PPy:PSS with deposition charges ranging from 0 to 450 µC. (a) Normalized impedance at t0 for 100 Hz from sensor batches coated with deposition charges of 0 µC, 170 µC, and 450 µC PPy:PSS. (b) Normalized impedance at t18 with respect to t0 for 100 Hz from sensor batches coated deposition charges of 0 µC, 170 µC, and 450 µC PPy:PSS. Values for bare gold are indicated by "0 µC" deposition charge. Please note different scaling on y-axes. (For interpretation of the references to colour in this figure legend, the reader is referred to the Web version of this article.)

Figure 3.3a shows normalized impedance at 100 Hz for each of the three coatings immediately (*i.e.*, t_0) after sensors were submerged in 1:10X TSB. Differences in the variability of

the three conditions of the sensors at t_0 were evident. At t_0, variability of impedance for both 0 µC PPy:PSS and the 170 µC PPy:PSS coated sensors varied largely from 62.1 to 181.8%, and 82.1 to 114.9%, respectively. When coated with 450 µC PPy:PSS, impedance variability at 100 Hz extended from only 97.3 to 101.9%. The variation of normalized impedance of 170 µC PPy:PSS coated sensors was not significantly different from the 0 µC PPy:PSS coated sensors (Levene's Test, F=3.2259, DF=7, P value=0.123). Conversely, the 450 µC PPy:PSS coated sensors were significantly different from the 0 µC PPy:PSS (Levene's Test, F=7.4285, DF=7, P value=0.034) and the 170 µC PPy:PSS coated sensors (Levene's Test, F=89.7715, DF=7, P value<0.001).

Impedance variability at 100 Hz for the three differently coated sensors submerged in 1:10X TSB for 18 h (*i.e.*, t_{18} with respect to t_0) mirrored the initial response (Figure 3.3b). At t_{18}, impedance drift for the coated sensors were bidirectional. Further, impedance drift for both the 0 µC PPy:PSS and 170 µC PPy:PSS coated sensors varied largely over a range of 58.4% to 28.0%, respectively. Conversely, when coated with 450 µC PPy:PSS, the variability of impedance drift was narrow, spanning 2.0% across a slight upward trajectory. The variability of sensors coated with 450 µC PPy:PSS were significantly different from 0 µC PPy:PSS coated sensors (Levene's Test, F=8.3456, DF=7, P value=0.028). Therefore, each sensor was functionalized with 450 µC PPy:PSS for the remainder of our study.

Flow chamber fluid simulation

Fluid flow velocity-profiles and wall shear stresses within the flow chambers were simulated at a steady-state flow rate of 1 µL min^{-1} (Figure 3.4). Cross-sections through the longitudinal plane of the transverse flow profile showed a homogeneous distribution of flow within the active sensor region (Figure 3.4a and 3.4b). The flow velocities along the sensor surface did

not exceed 5 µm s^{-1}, and no eddies were apparent at any position within the boundaries of the flow chambers. Simulated wall shear at the interface of the sensor surface was found to be evenly distributed in the active sensor area averaging ~20 µPa (Figure 3.4c). Higher wall shear at the inlet and outlet of the flow chambers were negligible as shear dissipated prior to reaching the sensor. Collectively, low-flow velocity and wall shear stress provided ideal conditions to validate the EIS response to biofilm formation (Araujo et al., 2016).

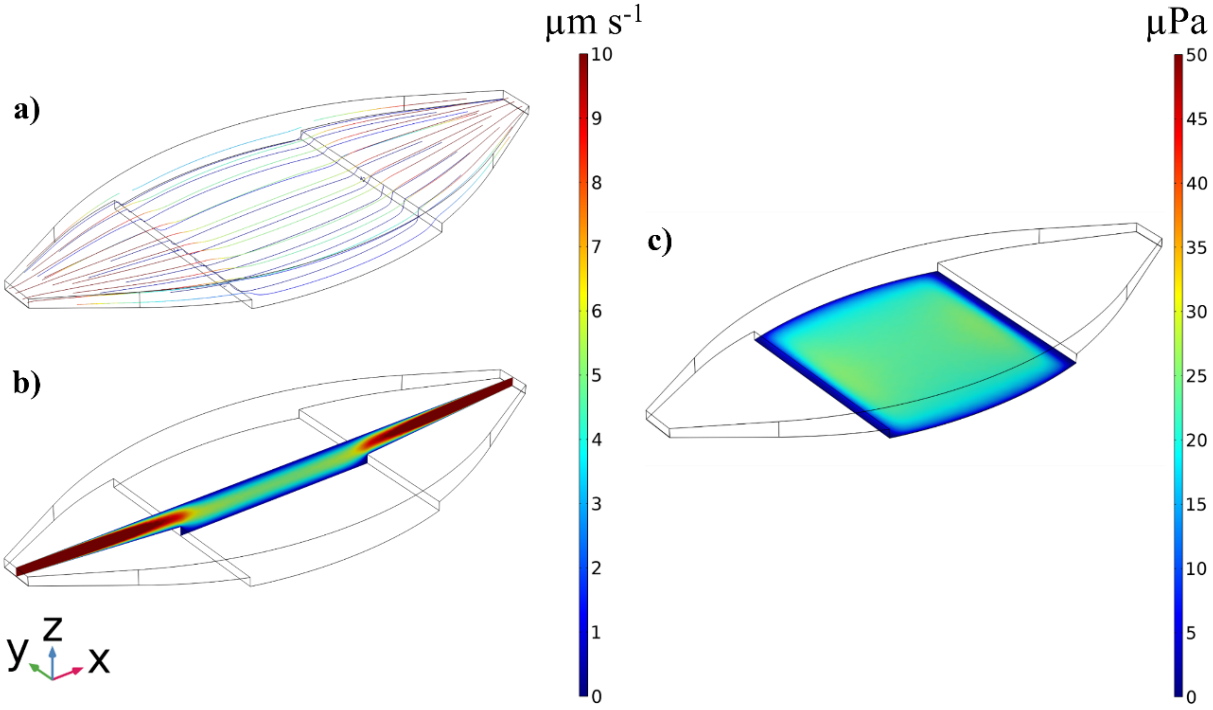

Figure 3.4: Finite element analysis using COMSOL multiphysics of the flow chamber design. (a) flow trajectories indicated by directional arrows within the flow chamber, (b) Z-X cross section of flow profile, (c) wall shear stress of X–Y plane parallel to integrated microfabricated sensor showing homogenous stress distribution across surface.

EIS characterization of biofilm growth

Specific frequency regions of interest were defined at 100 Hz<f<2 kHz, 2 kHz<f<20 kHz, and 20 kHz<f<200 kHz to characterize both abiotic and biofilm growth effects on impedance under

flowing conditions (Supplemental Figure A.5). For abiotic conditions, impedance changes at the low-frequency regime (<2 kHz) remained stable (<4% variation) throughout the experiment and undulated with no discernible trend. In the frequency range of 2 kHz<f<10 kHz, impedance fluctuations were most pronounced (as high as 8% variation) and appeared susceptible to temperature fluctuations in the room (≤2.5ºC). In the highest frequency range of 20 kHz<f<200 kHz, impedance changes remained stable (<3% variation) throughout the experiment. In the presence of biofilm, impedance changes were most pronounced in the low-frequency range (≤25%). Biofilm related changes in the higher frequency ranges were small (≤10%) and less identifiable.

To select a representative frequency that best captures biofilm growth, impedance changes at 100 Hz, 1.26 kHz, 11.6 kHz, and 106.2 kHz were investigated (Figure 3.5). These frequencies represent frequencies that were closest to each power of 10 magnitude. It was evident that 100 Hz and 1.26 kHz displayed the greatest changes in response to biofilm growth and stability to abiotic conditions compared to the other frequencies. Of further relevance, abiotic impedance changes were significantly different at all time points from those caused by biofilm (T-test, P value≤0.010). Since impedance at 100 Hz had a higher experimental variability compared to the impedance at 1.26 kHz, 1.26 kHz was chosen as a single representative frequency to measure biofilm.

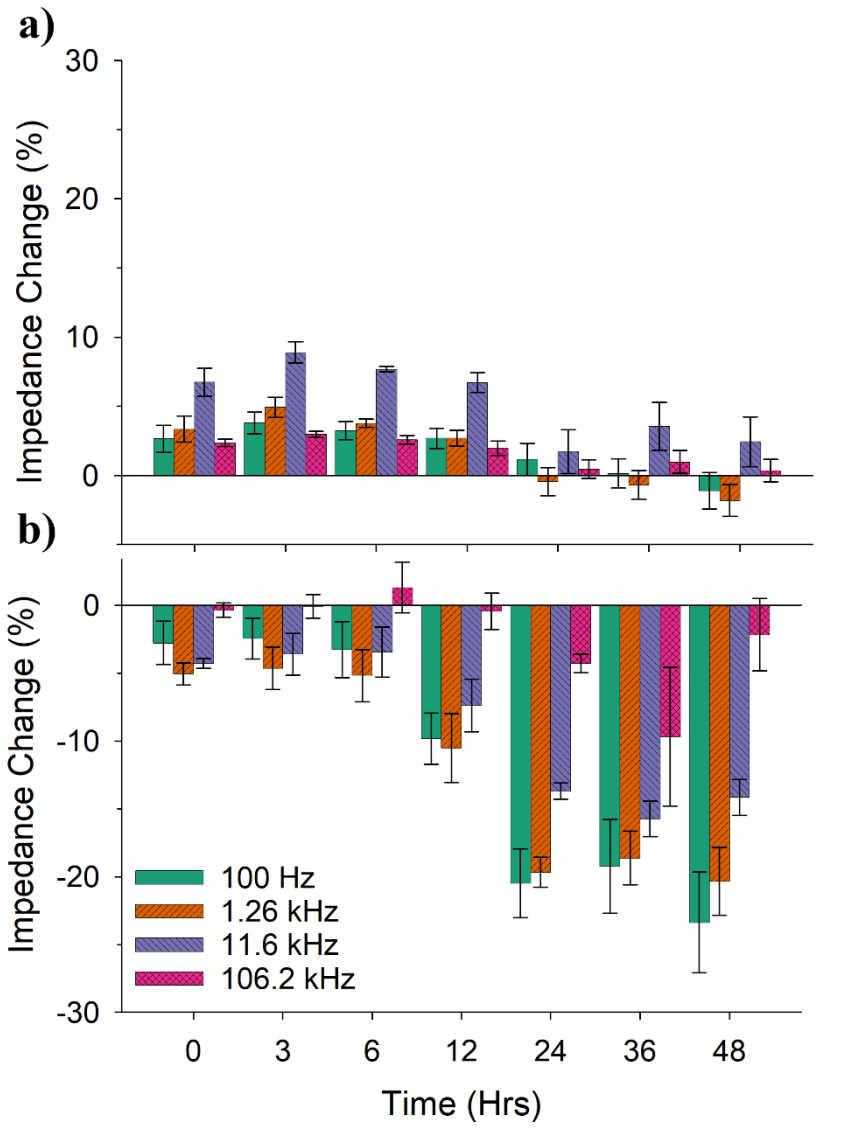

Figure 3.5: Bar chart comparing average impedance changes at select frequencies of 100 Hz, 1.26 kHz, 11.6 kHz, and 106.2 kHz at selected timepoints of 0, 3, 6, 12, 24, 36, and 48 h of media flow. Error bars represent standard error from three repeat experiments.

Real-Time Single Frequency Impedance Analysis and CLSM Imaging of Biofilm

EIS and CLSM were integrated into the same analytical platform to address the overarching objective of this work, whether EIS sensors can reliably detect biofilm. Changes in impedance at the selected frequency of 1.26 kHz for 48 h of biofilm growth were evaluated (Figure 3.6).

Impedance rapidly changed on the order of 5% upon injection of cells into the flow chambers. Following 2 h of seeding, flow was initiated (*i.e.*, t=0 h), and impedance displayed a sigmoidal decrease reaching a plateau by 24 h of growth.

Among the select timepoints, the earliest differentiable timepoint for impedance relative to the abiotic baseline was at 12 h of biofilm growth (T-test, P value ≤0.014), with every subsequent timepoint having significant differences compared to the baseline. Further, impedance at 24 h was significantly different compared to 6 and 12 h of biofilm growth (T-test, P value≤0.028). While impedance tended to fluctuate, no statistical differences were observed between 24 and 48 h of biofilm growth (T-test, P value≥0.055).

The different degrees of biofilm formation on the sensor surfaces were visually confirmed using CLSM (Figure 3.6). Biofilm increased consistently throughout the 48 h of growth and corresponded with impedance changes (Figure 3.6). Significant differences were observed between abiotic baseline conditions compared to 6, 12, 36, and 48 h of biofilm growth (T-test, P value≤0.03). Biofilm indices reached 1.6 μm^3 μm^{-2} and 1.8 μm^3 μm^{-2} at 6 and 12 h, respectively, although they were not significantly different (T-test, P value≥0.67). By 24 h of growth, the biofilm index reached on average 10.6 μm^3 μm^{-2}. High variability across replicates resulted in no significant difference from all other timepoints (T-test, P value≥0.15). After 36 h of growth, sensor surfaces were completely covered by biofilm (Figure 3.6). At 36 h, the biofilm index reached 19.8 $\mu m^3 \mu m^{-2}$ and increased to 35.2 μm^3 μm^{-2} at 48 h of biofilm growth but displayed no statistical difference (T-test, P value=0.166). Both 36 and 48 h of biofilm growth were statistically different from all previous timepoints (T-test, P value≤0.030).

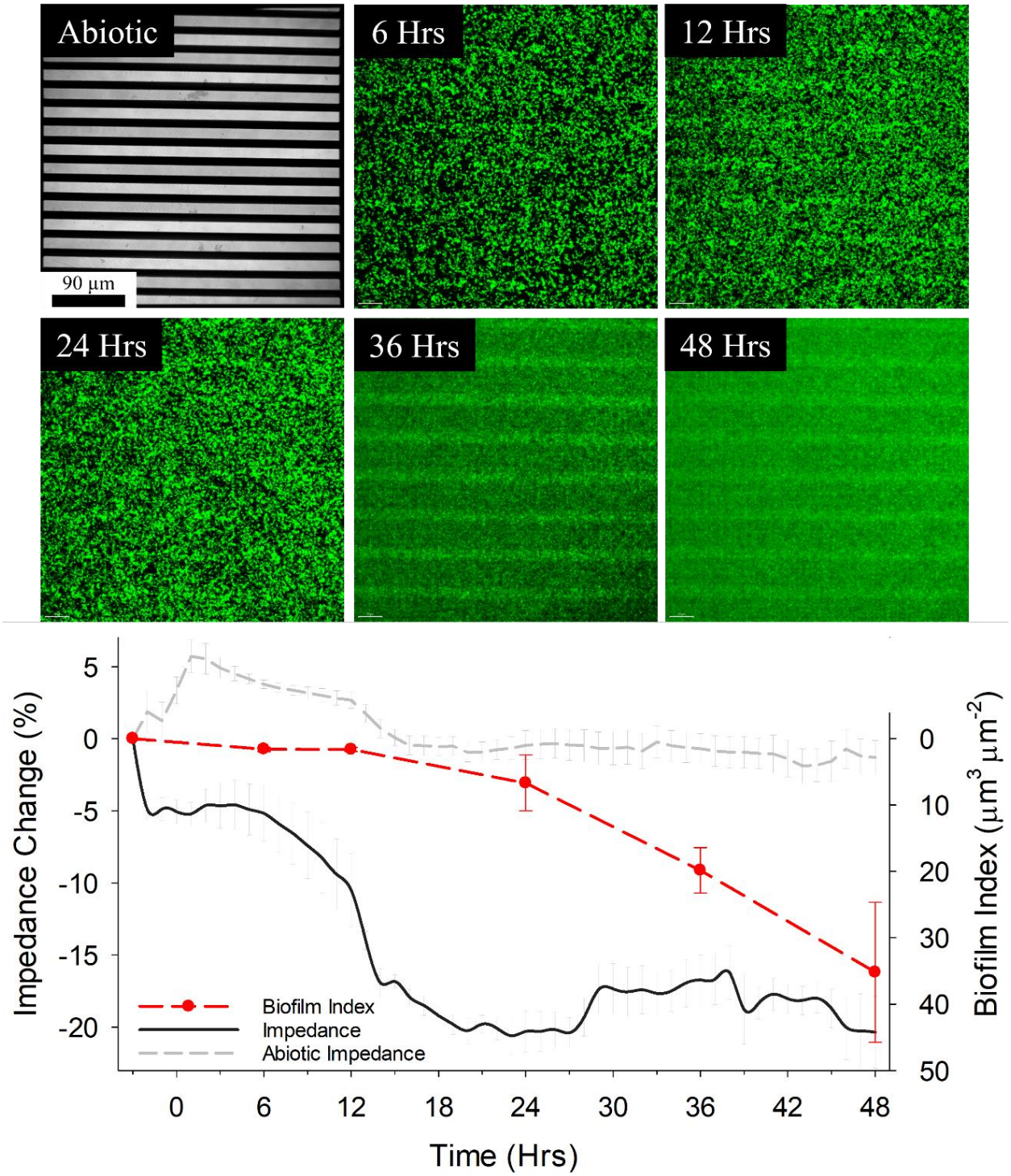

Figure 3.6: (Top) Representative CLSM images captured at abiotic conditions, and 6, 12, 24, 36, 48 h of biofilm growth. (Bottom) Average impedance change from 1.26 kHz frequency collected over 48 h-growth of GFP expressing *P. aeruginosa* biofilm. Left axis is relative change in impedance and right axis is calculated biofilm factor. Error bars represent standard error from three repeat experiments.

Discussion

Crucial parameters for developing biosensors are the reliability and reproducibility of the measurements and a clear understanding of abiotic versus biological signals. Despite the widespread use of gold µIDEs in biosensor applications, they demonstrate low reproducibility and signal drift due to instabilities from adsorption processes at the sensor surface (Lazar et al., 2016). Moreover, the small surface area of µIDEs leads to small capacitances and, therefore high interfacial impedances. Consequently, this reduces sensitivity in the low-frequency range, potentially masking biological interactions with the electrodes. Building on the findings of Kremers and others (Kremers et al., 2021), sensors modified with 450 µC PPy:PSS deposition charges significantly improved electrochemical stability over 48 h of continuous measurements (Figure 3.3; Figure 3.6). Moreover, electropolymerization with PPy:PSS led to lower interfacial impedance and reduced the variation in initial impedance. Previous approaches to improve measurement reproducibility and sensitivity included electrode pretreatment and increasing electrode surface area (Ho et al., 2019; Kılıc, 2020; Zhang et al., 2022). Yet, long-term signal-drift has remained a major hurdle. With respect to time, only PPy:PSS coating led to unidirectional impedance changes and the smallest variability in signal drift. In response to continuous EIS measurements, the PPy:PSS films on the gold electrodes acted as a functionalization material, enlarging the electroactive surface area, and providing lower interfacial impedances, thus enhancing electrochemical signals occurring at the electrode/electrolyte interface (Zheng et al., 2013).

It is important to note that in relation to impedance, microorganisms have varying effects within certain frequency domains. µIDEs, when exposed to microbes, display three distinct

domains within EIS spectra (*i.e.*, a double-layer region, a resistive region, and a region that combines resistive and parasitic effects) (McGlennen et al., 2020). Impedance in the frequency ranges of 10 Hz<f<10 kHz is commonly selected to detect biofilm, bracketing the optimized response seen at 1.26 kHz selected herein. (Liu et al., 2018; van Duuren et al., 2017). Across this frequency range, impedance is likely dominated by effects occurring at the electrode-electrolyte interface, such as the capacitive double-layers (Bratov et al., 2018). Several mechanisms have been proposed that could explain these changes (*e.g.*, the production of redox species, biofilm material deposited on the surface, presence of cells near the surface, biofilm detachment) at the electrode/electrolyte interface in response to biofilm growth (Ward et al., 2014). We argue that electrochemical responses to cell attachment and gradual biofilm development is more complex, portraying all these mechanisms at any given time. For instance, during the early stages of cell attachment (*e.g.*, 0-3 h of biofilm growth), impedance changes are likely attributed to changes in localized ionic species near or on the electrode surfaces (Yang and Bashir, 2008). During later stages, impedance changes may be attributed to biofilm embedded in EPS (Carniello et al., 2018). Of equal importance is the understanding of sensor responses in the absence of biology, as biosensing applications may undergo long periods where sensors are not exposed to microorganisms. In this project, impedance measurements highlighted that abiotic responses were not only statistically different from sensors exposed to biofilm but also that impedance changes in the middle frequency range are more indicative of changes to the bulk solution.

The flow cell system successfully combined microfabricated EIS sensors aided by live-cell imaging with CLSM to characterize biofilm development. Laminar fluid flow and low shear stresses displayed ideal conditions for homogenous biofilm growth (Straub et al., 2020). With

respect to the sigmoidal impedance changes detected throughout biofilm development, sensor signals could be categorized into four distinct responses (Figure 3.6). First, the initial detection of planktonic cell culture enrichments is characterized by an instantaneous decrease in impedance. Next, an apparent "lag" phase of impedance changes spanning several hours. Subsequently, a rapid decrease in impedance in relation to biofilm proliferation. Lastly, a stationary/steady-state region characterized by impedance signals that reached a plateau (Huiszoon et al., 2019, 2021; Subramanian et al., 2017). Beyond 24 h of growth, periodic fluctuations in impedance were evident and are hypothesized to be a result of detachment and regrowth of biofilm clusters on the sensor surface (Hall-Stoodley et al., 2004).

Evidence suggests that biofilms themselves are less conductive (Malvankar et al., 2011), and thus, the decrease in impedance would depend on the presence of charge carriers. Biofilm formation involves a complex phenomenon that among other processes involves the production of EPS and a variety of metabolites. For instance, *P. aeruginosa* is known to produce redox-mediating metabolites such as phenazines and *Pseudomonas* quinolone signal (PQS) that can affect electrochemical properties of biofilms (Oziat et al., 2015, 2021; Robb et al., 2018). EPS may also alter the electron transfer in biofilms as some biofilms are electrochemically active while others are less conductive (Li et al., 2016; Malvankar et al., 2011; Tan et al., 2019; Wang et al., 2022). Elucidating the exact mechanisms responsible for the measured decrease in impedance was, however, beyond the scope of this work. Electrically conductive polymer coatings such as PPy:PSS enhance absorption of polycyclic organic species (e.g. certain phenazines and PQS) and can increase the sensitivity of EIS biosensors (Oziat et al., 2015).

Sensors consist of electrodes with width and spacings of 15 µm and 10 µm, respectively, which has been shown to be the optimal spacing ratio for biosensing applications (Jun et al., 2018). Previous work has concluded that ~90% of the EIS signal occurs in the region above the electrodes, equivalent to ~twice the spacing between the electrodes (Van Gerwen et al., 1998). Hence, the present sensor geometry would limit differentiable EIS to a biofilm index threshold of ~20 um^3 um^{-2}, an estimate that is supported by the insignificant impedance changes after 36 h (Figure 3.6). Increasing the spacing between electrodes might allow the detection of thicker biofilm. Depending on the objective or scope of the experiment, the design of the electrodes should match the targeted biofilm thickness.

Among the numerous techniques available for fabricating microfluidic devices, 3D printing has shown promise for rapidly creating microfluidic devices (Chen et al., 2016; Pousti et al., 2018). The 3D printed flow cell system presented herein has several advantages and could be used to evaluate the growth of biofilm forming microorganisms using various electrochemical or mechanical sensors. For example, design changes can be quickly implemented using commercial and open-source CAD software, allowing rapid design implementation, such as expanding the number of flow chambers or altering the opening size to accommodate new sensor designs.

Conclusions

This work demonstrated that microfabricated sensors modified with PPy:PSS coatings enabled highly stable time-resolved EIS measurements under abiotic and biofilm growth conditions. Modified EIS sensors were integrated into a novel 3D-printed flow cell that allowed for time-resolved live-cell CLSM imaging of attached biofilm and impedance measurements. Future work may evaluate sensor response to different microbial species and bulk solutions.

Beyond lab-based testing, the integration of microfabricated sensor systems into modern infrastructure susceptible to biofilm growth should be considered. Overall, this may enable a deeper understanding of the electrochemical properties of biofilms or other biological materials in environmental, medical, and industrially relevant environments.

Supporting Information to this Chapter is presented in Appendix A.

APPLICATION OF IMPEDANCE SENSORS

FOR BIOFILM CONROL IN REAL-TIME

Contribution of Authors and Co-Authors

Manuscript in Chapter 4

Author: Matthew McGlennen

Contributions: Investigation, Conceptualization, Methodology, Formal analysis, Data curation, Writing – original draft.

Co-Author: Markus Dieser

Contributions: Conceptualization, Formal analysis, Writing – review & editing.

Co-Author: Christine M. Foreman

Contributions: Conceptualization, Supervision, Funding acquisition, Writing – review & editing.

Co-Author: Stephan Warnat

Contributions: Conceptualization, Supervision, Funding acquisition, Writing – review & editing.

Manuscript Information

Matthew McGlennen, Markus Dieser, Christine M. Foreman, Stephan Warnat

Industrial Microbiology and Biotechnology

Status of Manuscript:
__x__ Prepared for submission to a peer-reviewed journal
____ Officially submitted to a peer-reviewed journal
____ Accepted by a peer-reviewed journal
____ Published in a peer-reviewed journal

Publisher: Oxford University Press

Abstract

Microbial biofilm contamination is a widespread problem that requires precise and prompt detection techniques to effectively control its growth. Microfabricated electrochemical impedance spectroscopy (EIS) biosensors offer promise as a tool for early biofilm detection and monitoring of elimination efforts. This study utilized a custom flow cell system with integrated sensors to make real-time impedance measurements of biofilm growth under flow conditions, which were correlated with confocal laser scanning microscopy (CLSM) imaging. Biofilm growth in tryptic soy broth (TSB) resulted in a 22±7% decrease in impedance over 24 hours. Treatment with either chlorine or biocide at 24 hours increased impedance towards abiotic levels by 13±3% or 14±3%, respectively, over the ensuing 12 hours. Both growth and dispersal were validated by CLSM imaging. Biofilm grown with Furanone C-30, a quorum sensing inhibitor (QSI), maintained stable impedance for 18 hours, then declined 14±3% by 36 hours. Sensors were also tested for 72 hours in an oil-water emulsion of metalworking fluid (MWF) to demonstrate utility in industrial biofilm monitoring. Biofilm growth in MWF decreased impedance similarly to TSB. MWF is opaque, making CLSM imaging impossible. In MWF, treatment with biocide at 24 hours caused an abrupt decrease in impedance, which gradually increased over the ensuing 36 hours to within 8±3% of the abiotic baseline. Biofilm in MWF exposed to QSI maintained level impedance for 72 hours. Overall, these results support the utility of microfabricated EIS biosensors for evaluating the growth and dispersal of biofilm *in situ* and demonstrate potential for use in industrial settings.

Introduction

Biofilms are complex, structured microbial communities encased in a self-produced extracellular polymeric substance (EPS) adhered to surfaces. The formation of microorganisms into biofilms is the most common mode of growth for microorganisms on Earth (Costerton et al., 1999) and provides protection from chemical, mechanical, and physical stressors, improves evasion of host defense mechanisms, and increases virulence factors (Lappin-Scott and Costerton, 1989; Azeredo et al., 2016). Globally, microbial biofilm contamination is a problem in natural, industrial, and medical settings, costing roughly $4 trillion annually (Cámara et al., 2022).

Current standard techniques to assess/identify biofilm growth vary in analysis time, sensitivity, cost, and complexity. Standard wet lab techniques include plate counts, dip slides, polymerase chain reactions (PCR), enzyme-linked immunosorbent assays (ELISA), fluorescent *in-situ* hybridization (FISH), and spectroscopic methods such as infrared, ultraviolet, and visible light spectroscopy (Saha et al., 2012; Saha and Donofrio, 2012; Assenhaimer et al., 2017; Kiefer et al., 2018; Passman and Küenzi, 2020). Microsensors have been designed to detect biofilm indicated by changes in oxygen, pH, and temperature (Saccomano et al., 2021; Funari and Shen 2022) to name a few. Each technique shows both strengths and weaknesses based on their application, highlighting the lack of a one-size fits all approach. Moreover, many of these techniques are destructive endpoint diagnostic tools and cannot be easily deployed to assess in real-time the onset of biofilm formation up to maturation and treatment response.

Over the last decade, microfabricated electrochemical impedance spectroscopy (EIS) biosensors have expanded to the field of microbiology. Compared to standard microbiology techniques, EIS biosensors can obtain information about microbes both in planktonic (Mallén-

Alberdi et al., 2016; Brosel-Oliu et al., 2018; McGlennen et al., 2020; Sidhu et al., 2020) and biofilm stages (Chabowski et al., 2017; Liu et al., 2018; Huiszoon et al., 2021) in real-time. In general, EIS is a technique used to the characterize electrochemical properties of solids, liquids, and gasses, and is achieved by supplying a sinusoidal electrical perturbation to an electrochemical system and measuring the time-varying response. The measurement is carried out across a frequency sweep (typically ~1MHz to 1 mHz) (Magar et al., 2021). When applied to biosensors, changes to EIS spectra over time can indicate the presence microbes at or near the sensor surface. Furthermore, impedance measurements can be carried out at single-frequencies which reduces data acquisition time, simplifies analysis, and improves efficiency. Most recently, McGlennen et al., showed that microfabricated EIS sensors using optimized single-frequency impedance measurements could differentiate stages of biofilm growth, starting with the initial attachment of cells through the maturation of biofilm (McGlennen et al., 2023). Based on sensor characteristics and affinity, the analytical detection limit of microfabricated EIS sensor measurements can be less than 10 colony forming units (CFUs) mL^{-1} (Abdelrasoul et al., 2020). Moreover, EIS sensors are non-invasive and label-free, making them desirable for industrial applications and could be expanded into the analysis of additional fluid formulations.

Biofilm formation is a complex process, beginning with initial attachment, proliferation, maturation and subsequent detachment. Biofilm management has been approached by targeting both the formation process of biofilms and their eradication. Focus has been placed on various additives that interfere with bacterial signaling pathways (*i.e.*, quorum sensing) or disrupt extracellular DNA, proteins, lipopolysaccharides, and exopolysaccharides during early stages of biofilm formation (Lu et al., 2019; Ozcan et al., 2019). Alternative strategies have also been

explored including development of antiadhesion coatings, material modifications (Rather et al., 2021; Lisoń et al., 2022), or incorporation of mechanical removal procedures (Sadekuzzaman et al., 2015). Nonetheless, the use of antimicrobials remains the standard approach to prevent and remove biofilm (Bott, 2009; Di Pippo et al., 2018). Mature biofilms consist of cells securely attached to the substrate, encased by protective EPS making them resistant to chemical and mechanical forces (Lebeaux et al., 2014; Peterson et al., 2015). However, despite extensive efforts to remove biofilms, microbial contaminants persist, leading to rapid recolonization (Davies, 2003; Hall-Stoodley et al., 2004; Trafny, 2013; Stewart et al., 2019). Compared to mature biofilms, early-stage biofilms are less securely established, less resistant to antimicrobials, and more susceptible to other chemical treatments (Fu et al., 2021; Høiby et al., 2001). Thus, it is postulated that early detection and treatment could be a highly effective strategy for combating biofilm.

The potential of EIS biosensors to detect early-stage biofilm formation make it particularly attractive tool for combatting biofilms. Herein, EIS biosensors were deployed to monitor treatment responses using commercially available anti-biofilm compounds that target a range of different control strategies (*e.g.*, chlorine, biocide, and quorum sensing inhibitor (QSI)). Furthermore, the EIS biosensors were tested against biofilms grown in metalworking fluid (MWF), a complex mixture of oils, emulsifiers, and other additives, to extend their utility beyond simple aqueous environments, as biofilm contamination poses a significant problem in industrial settings (Passman and Küenzi, 2020).

Material and methods

System overview

A 3D printed flow cell system with integrated interdigitated electrode (µIDE) sensors was designed to monitor the growth and treatment of biofilm in a controlled manner, as previously described (McGlennen et al., 2023). The overarching methodology for using the system is depicted graphically (Figure 4.1). Briefly, biofilm growth occurs within flow chambers composed of a microfabricated sensor as the bottom substrate, and a glass microscope slide serving as the top substrate viewing chamber (Figure 4.1b). Single frequency impedance analysis indicates the initial attachment of cells to the sensor substrate, early-stage irreversible biofilm proliferation, mature biofilm establishment, and changes due to detachment and regrowth of biofilm (Figure 4.1c). Abiotic baseline impedance starts at 0% and decreases correspondingly to increasing biofilm biomass. Impedance changes tend to reach a maximum and stabilize upon uniform biofilm substrate coverage. At this stage, biofilm treatment is introduced, reducing biofilm biomass, and impedance response correspondingly increases.

Sensor design

µIDEs were selected for this application as they have proven to be easily fabricated, are highly sensitive, and do not require the use of a reference electrode (Park et al., 2018; Dorledo de Faria et al., 2019; Furst and Francis, 2019). EIS sensors were microfabricated as previously described (McGlennen et al., 2023). Briefly, the sensor design consisted of interdigitated electrodes 15 µm in width with a spacing of 10 µm for a total of 50 electrode pairs. Sensor surfaces were modified with poly (4-styrenesulfonic acid) doped with pyrrole, termed PPy:PSS, to enhance

electrochemical stability and increase sensitivity. One side of each of the µIDEs were coated with 450 µC PPy:PSS before experimentation (McGlennen et al., 2023).

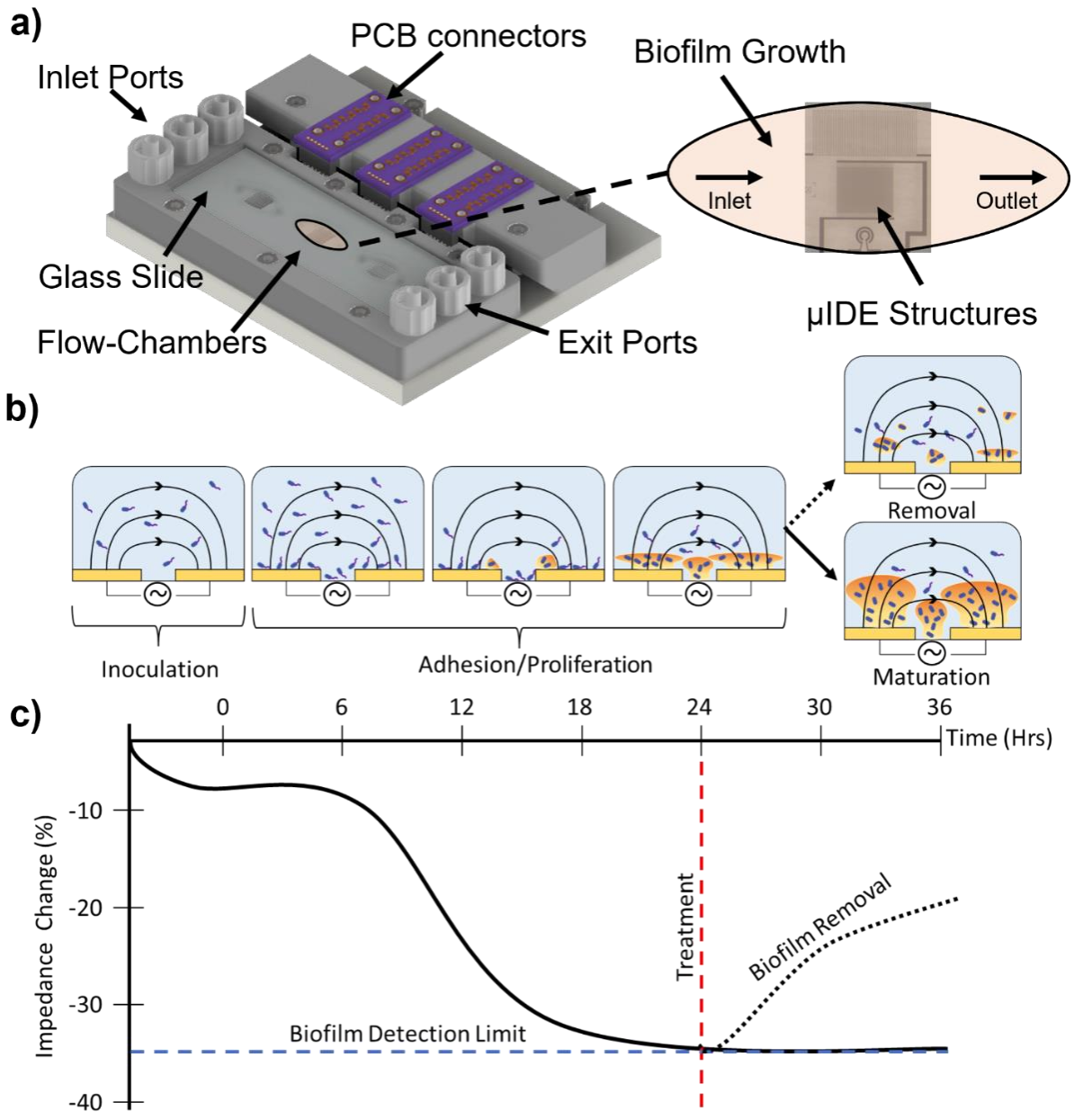

Figure 4.1: Graphical representation of platform design and experimental setup for analyzing biofilm: a) 3D printed flow cell system CAD rendering with detailed top view of flow-chamber with integrated EIS biosensor for biofilm growth and analysis, b) cross section schematic of biofilm development stages on EIS biosensor electrodes within flow chambers, and c) anticipated impedance changes in response to biofilm growth and removal.

Flow cell operation

As previously described, biofilm cultivation was carried out in 3D printed flow cell systems (McGlennen et al., 2023). Briefly, the flow cell was filled with sterile media (*i.e.*, 1:10X TSB, or 5% MWF) and an initial EIS measurement was collected. Subsequently, 1 mL of cell culture enrichments were injected into the flow chambers and left to adhere to the senor surface for 2 hrs. Following the 2 hrs of incubation, a continuous flow of sterile media was initiated to the flow chambers at a rate of 1 µL min^{-1} (Genie Touch Syringe Pump, Kent Scientific, USA). Abiotic (no biofilm) control trials were used to determine the effect of treatment amendments on impedance following the same methods.

Bacterial strain selection and culturing conditions

The model biofilm-forming bacterial strain *Pseudomonas aeruginosa* PA01 expressing green fluorescent protein (GFP) was used. Freezer stocks were transferred to tryptic soy agar (TSA; Fischer Scientific, USA) plates and incubated at 37ºC for 24 hrs. All cell cultures were grown in the presence of 50 µg ml^{-1} of carbenicillin (Fisher Scientific, USA). Enrichments were made from single colonies grown in 1X tryptic soy broth (TSB; Fisher Scientific, USA) at 37ºC while shaking at 150 RPM for 18 hrs.

Following 18 hrs of incubation, enrichments were harvested by centrifugation at 10,000xg for 5 min. The resulting cell pellets were either resuspended in 1:10X TSB or a complex, industrial, oil-water emulsion (*i.e.*, SC-506 CF metalworking fluid (MWF), Hangsterfer's, USA). Cells, which were resuspended in 1:10X TSB, were incubated at 22ºC while shaking at 150 RPM for 6 hrs to allow cells to adjust to ambient conditions selected for biofilm growth in the flow cell. Enrichments were harvested at an optical density at a wavelength of 600 nm of OD_{600}=0.2,

resulting in a cell concentration of ~1x10^8 CFUs mL^{-1}. For assays in MWF, cells were washed twice in autoclaved municipal tap water before resuspending cell pellets in autoclaved municipal tap water mixed with MWF (final conc. 5% v/v). The cell concentration of the final mixture was ~1x10^8 CFUs mL^{-1}. All enrichments were transferred to 10 mL sterile luer lock syringes (Becton Dickinson, USA), equipped with 20 ½ ga. needles (Fisher Scientific), prior to injection into flow chambers.

Biofilm treatment

The effect of three different biofilm treatments were investigated. After 24 hrs of growth in the flow cell, established biofilms were treated with either chlorine (Sodium hypochlorite solution; 20% w/v, Sigma-Aldrich, USA) or a biocide (Proxel GXL; Lonza Inc., USA). Treatment concentrations were 1.41 mM chlorine and 0.1% biocide (v/v) in 1:10X TSB, and 1.0% biocide (v/v) in 5% MWF. The chlorine concentration was chosen as it has been shown to disperse biofilm in a flow-cell based system with only partial destruction of biomass (Davison et al., 2010). Proxel GXL was applied at concentrations of 4X and 40X above the recommended minimum inhibitory concentration for planktonically growing *P. aeruginosa*, respectively (Lonza inc., USA). Chlorine solutions were manually injected as a one-time treatment into each of the three flow chambers (Figure 4.1b) at a rate of 1 mL min^{-1} for 1 min. Sterile media flow was paused during chlorine injection and resumed thereafter at a flowrate of 1 µL min^{-1} for 12 hrs. Biofilm was in contact with chlorine for ~1.5 hrs. Conversely, the biocide Proxel GXL was applied as a continuous treatment, in accordance with the manufacturer's recommendations. Sterile media was exchanged with media containing biocide and applied at a flowrate of 1 µL min^{-1} for 12 hrs.

As a third treatment, biofilm formation was suppressed by targeting quorum sensing, a communication process between bacterial cells that regulates the growth and behavior of the microbial population (Miller and Bassler, 2001). Biofilm formation was investigated both in the presence and absence of the quorum sensing inhibiting (QSI) reagent (Z-)-4-Bromo-5-(bromomethylene)-2(5H)-furanone (Furanone C-30; Sigma Aldrich, USA). Cells, either resuspended in 1:10X TSB or MWF as described above, were supplemented with 75 µM Furanone C-30, as this concentration showed high efficiency at reducing biofilm formation (Ozcan et al., 2019). Enrichments were incubated for 60 min at 22ºC while shaking at 150 RPM to allow time for the QSI inhibitor to block cell communication prior to flow chamber injection. After inoculating the flow chambers, 75 µM Furanone C-30 mixed with 1:10X TSB or 5% MWF were continuously supplied at a flowrate of 1 µL min^{-1} for either 36 for 1:10X TSB or 72 hrs for 5% MWF.

Electrochemical impedance spectroscopy measurement

EIS measurements were carried out with a Hioki IM3533 LCR meter connected to a Keysight 970A data acquisition system (DAQ) with a DAQ905A RF 2 GHz Dual 1:4 RF Multiplexer, 50 Ohm switching module. The instruments were controlled by a custom-built virtual interface (VI; LabView 2017), providing multiplexed four-channel EIS measurements. During EIS data collection, PPy:PSS coated sensors were connected to the LCR meter such that the coated side of the µIDEs served as both the counter electrode (CE) and reference electrode (RE). Impedance spectra were collected every 30 min across a frequency range of 200 kHz to 100 Hz and 25 logarithmically spaced data points with a signal source that was a sine wave with an amplitude of 10 mV RMS and no DC bias for both 1:10X TSB and 5% MWF. A previous study

showed that biofilm detection was most sensitive using 1.26 kHz as the source frequency for impedance measurements in 1:10X TSB (McGlennen et al., 2023). The single frequency that best-captured biofilm growth in 5% MWF was 200 kHz (see supplemental material). In both cases, time-dependent changes to impedance were reported given by Equation 4.1:

$$\text{Impedance Change (\%)} = \frac{|Z_{(f,t)}| - |Z_{(f,t0)}|}{|Z_{(f,t0)}|} * 100\% \quad \text{(Equation 4.1)}$$

where $|Z_{(f,t0)}|$ is the impedance measurement at the selected frequency of interest (f), measured at the initial timepoint (t_0), and $|Z_{(f,t)}|$ is every subsequent impedance measurement.

Biofilm assessment with confocal laser scanning microscopy and image analysis

Biofilm experiments and EIS data collection were performed while the flow-cell was mounted on a confocal laser scanning microscope (CLSM; SP5 upright confocal, Leica, USA). GFP expressing *P. aeruginosa* PAO1 was used for all biofilm related experiments, allowing visualization under the microscope without the need of staining (Nivens et al., 2001). Total biovolume from each CLSM image stack was calculated using Imaris 9.8 surfaces analysis with a custom fluorescence intensity filter, and by eliminating particle sizes smaller than 2 μm. The resulting calculation represents the total biovolume present in each confocal stack. The data presented here was normalized to the field of view by using Equation 4.2, similarly to (Lim et al., 2016), creating a biofilm index.

$$\text{Biofilm Index} = \frac{\sum \text{Total Biovolume } (\mu m^3)}{\text{Field of View } (\mu m^2)} \quad (4.2)$$

Statistical analyses

Data were processed with Matlab 2021a. Significant impedance changes and biofilm index differences were analyzed using an unpaired T-test. Student's T-test determined statistical differences between EIS data.

Results

Real-time impedance measurements of biofilm growth

The flow cell allowed for non-destructive, real-time visualization of biofilm growth and removal without disruption in flow and EIS measurements (Figure 4.1). To establish a baseline understanding of the effect of media and the absence/presence of microbial cells, impedance was measured at 1.26 kHz and 200 kHz in 1:10X TSB and in a complex industrial oil-water emulsion fluid (5% MWF), respectively (Figure 4.2), every 30 min for 36 hrs.

Under continuous flow of abiotic 1:10X TSB, impedance remained stable (Figure 4.2a, ≤4% variation) and displayed no statistical difference between 0 and 36 hrs (T-Test, P value≥0.079). Injection of planktonic cells into the flow chambers resulted in an instantaneous decrease of ~5% in impedance. When flow was initiated after 2 hrs of seeding (*i.e.*, 0 hrs) impedance decreased in a sigmoidal decay pattern until reaching a plateau at ~ -22% by 24 hrs of growth (24 to 36 hrs, T-Test, P value=0.956). Visual confirmation of the different biofilm stages from seeding to monolayer establishment in relation to EIS can be found in McGlennen et al., 2023.

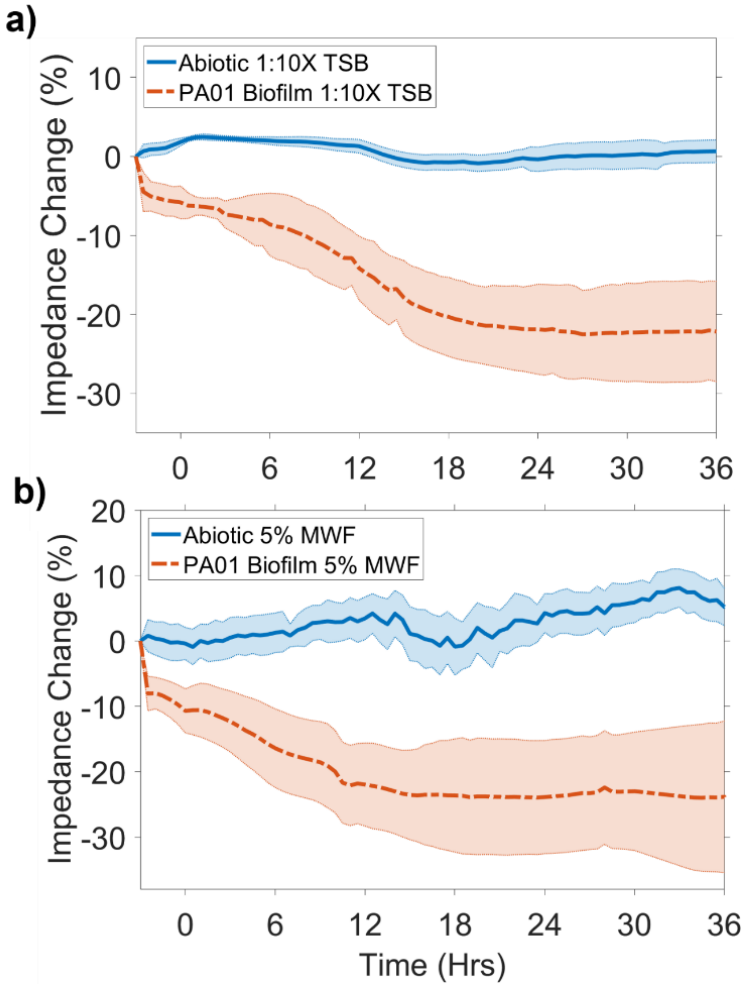

Figure 4.2: Impedance changes for abiotic controls and biofilm growth in (a) 1:10X TSB and (b) 5% MWF. Shaded regions represent standard deviation.

Similarly, impedance measurements in 1:10X TSB displayed no statistical difference between 0 and 36 hrs of continuous flow under abiotic condition in 5% MWF (T-Test, P value≥0.051). In the presence of cells, impedance attenuated in a sigmoidal decay pattern reaching a plateau of ~ -25% by 24 hrs of growth (24 to 36 hrs, T-Test, P value=0.996).

Real-time impedance measurements of biofilm treatment

To investigate biofilm removal using EIS biosensors, established biofilms grown for 24 hrs were treated with either 1.41 mM chlorine or 0.1% biocide. The addition of these agents altered

the electrochemical properties of 1:10X TSB and 5% MWF, hence the impedance baseline. Effects on impedance were noisier in the abiotic media compared to biosensors overgrown with biofilm, which increased impedance variability by 10% and 7% on average in abiotic 1:10X TSB and 5% MWF, respectively (Figure 4.3a, b). The addition of chlorine decreased impedance sharply by ~ 5% in abiotic 1:10X TSB and plateaued 6 hrs after treatment with an overall impedance increase of ~ 5% (Figure 4.3a). Impedance changes caused by the addition of chlorine and biocide to 1:10X TSB were, however, not statistically significant (T-test, P value≥0.414; Figure 4.4). In 5% MWF, the addition of the biocide triggered a large drop in impedance of ~30% before stabilizing 12 hrs later, for both abiotic sensors and sensors exposed to biofilm (Figure 4.3d). Impedance remained stable between 36 and 72 hrs in abiotic 5% MWF (T-Test, P value=0.339; Figure 4.4); thus, the impedance at 36 hrs was selected as the new baseline for treatment effect calculations.

All biosensors covered with biofilm reflected a treatment response upon contact with chlorine and biocide, with impedance changes nearing abiotic baselines (Figure 4.3). Differences were evident with respect to response time. Impedance changes for biosensors treated with a one-time injection of chlorine was instant and followed a saturation curve pattern (Figure 4.3a). During continuous treatment of biofilm in both 1:10X TSB and 5% MWF with a biocide, impedance changes followed a sigmoidal pattern with a pronounced lag-phase (Figure 4.3b, d). Overall, impedance increased by 13±3% and 14±3% for chlorine and biocide treated EIS biosensors in 1:10X TSB, respectively, and by 41±3% for biocide treated EIS biosensors in 5% MWF, corresponding to decreases in biofilm. Importantly, changes in impedance were statistically significantly different between key timepoints of pre-treatment (24 hrs) and post-treatment (36 hrs) for EIS biosensors treated with chlorine (T-Test, P value=0.003) and biocide (T-Test, P

value=0.002) in 1:10X TSB (Figure 4.4). Likewise, in response to biofilm treated with biocide in MWF, the impedance change was statistically different between pre-treatment (36 hrs) and post-treatment (72 hrs) (T-Test, P value<0.001).

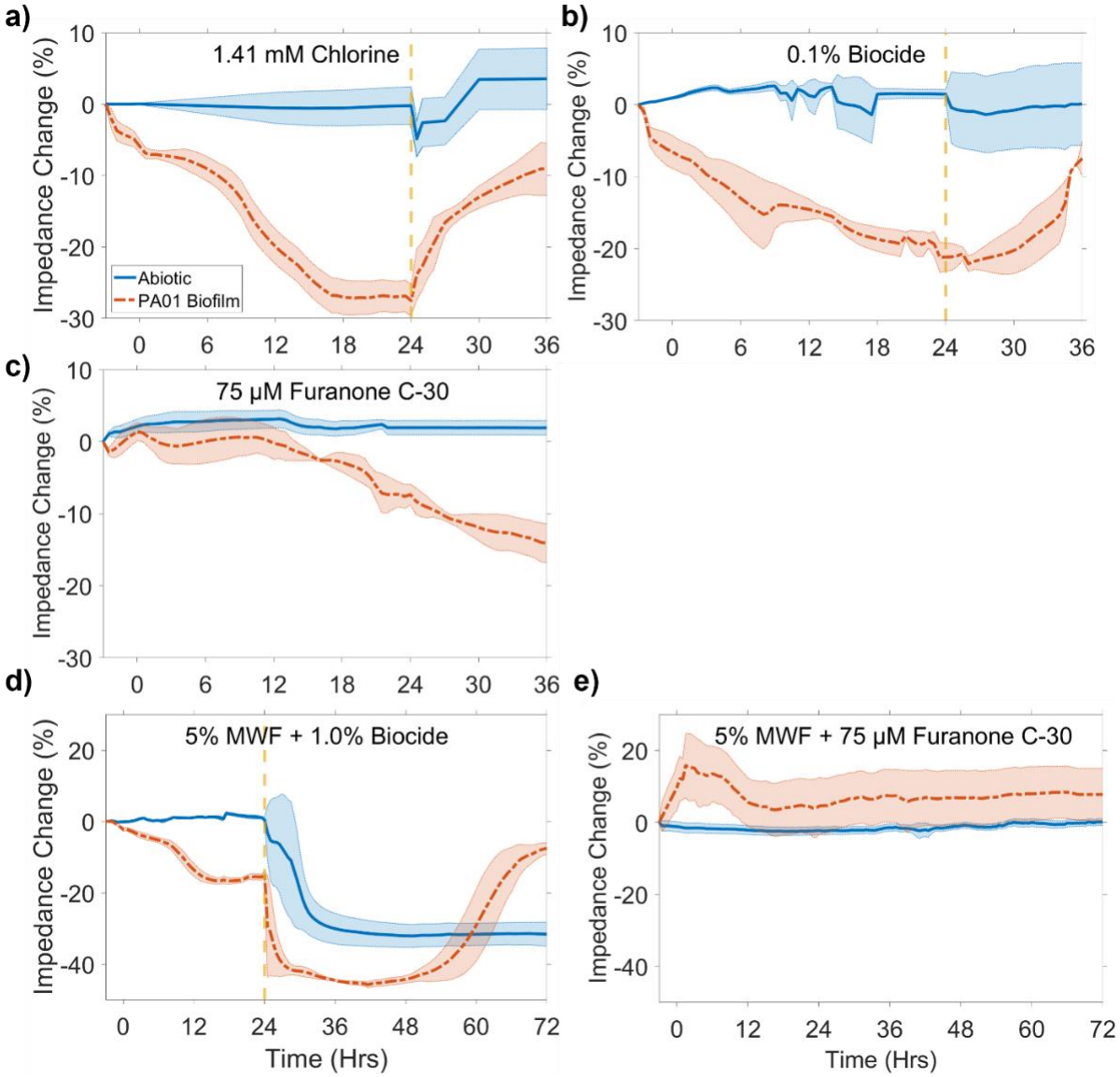

Figure 4.3: Impedance changes at 1.26 kHz over time for abiotic controls and biofilm grown in 1:10X TSB: (a) treated at 24 hrs with 1.41 mM chlorine, (b) treated at 24 hrs with 0.1% biocide (c) exposed to 75 µM Furanone C-30 for 36 hrs, (d) Impedance changes at 200 kHz over time for abiotic controls and biofilm grown in 5% MWF, (d) treated at 72 hrs 1.0% biocide, (e) exposed to 75 µM Furanone C-30 for 72 hrs. Shaded regions represent standard deviation. Yellow dashed lines indicate time of treatment implementation.

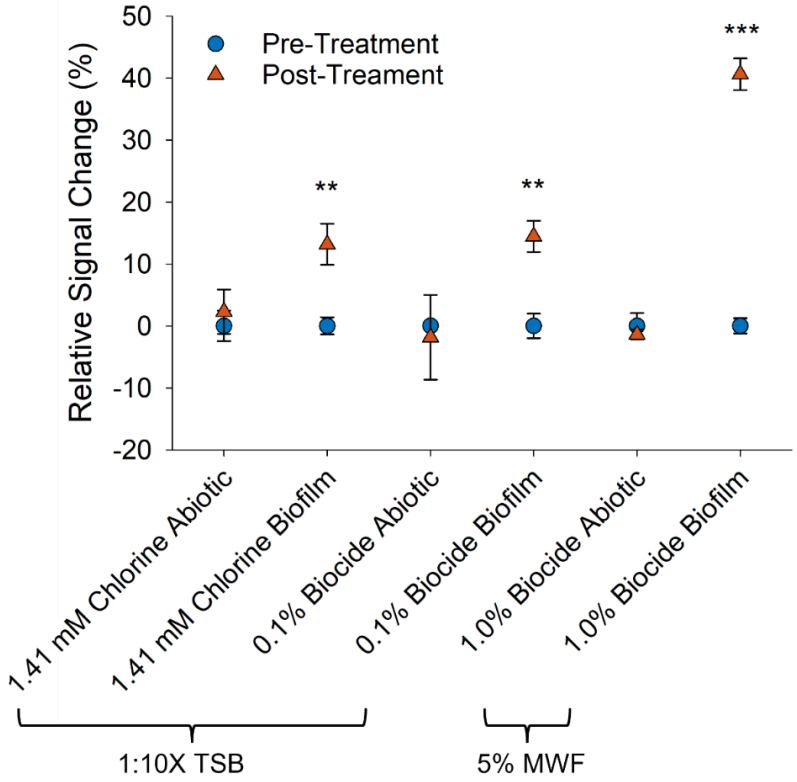

Figure 4.4: Magnitude of impedance change between pre-treated and post-treated biofilm grown in 1:10X TSB and 5% MWF. Error bars indicate standard deviation, differences that met significant levels are shown as *≤0.05, **≤0.01, ***≤0.001.

Real-time impedance measurements of delayed biofilm development

To investigate whether EIS biosensors could monitor the effects of quorum sensing inhibition on biofilm formation, cell enrichments were grown in the presence of 75 µM of the QSI compound Furanone C-30 for 36 and 72 hrs in 1:10X TSB and 5% MWF, respectively. Electrochemically, the addition of Furanone C-30 had negligible effects on impedance (Figure 4.3c, e). Compared to 0 hrs, impedance remained stable in abiotic 1:10X TSB for (T-test, P value=0.811) and abiotic MWF (T-test, P value=0.246) for 36 and 72 hrs, respectively. Biofilm proliferation was suppressed in 1:10X TSB and 5% MWF for 18 and 72 hrs, respectively (Figure 4.3c and Figure 4.3e) as indicated by impedance (T-test, P value≥0.329). After 18 hrs, changes in

impedance became statistically different from 0 hrs in 1:10X TSB (T-test, P value=0.016). A gradual decrease in impedance, reaching ~-17% by 36 hrs, suggested that cells eventually overcame the inhibitory effects of Furanone C-30 and biofilm began to develop.

Validation of biofilm removal and delay by CLSM imaging

CLSM imaging was used to confirm biofilm development and treatment in 1:10X TSB media, but was not possible in 5% MWF as the fluid is opaque. CLSM images at key timepoints of pre-treatment (24 hrs) and post-treatment (36 hrs) were evaluated (Figure 4.5). Consistently, biofilm monolayers attached to biosensor substrata had formed after 24 hrs (Figure 4.5a-1, 4.5b-1, and 4.5c-1) and continued to proliferate without treatment (Figure 4.5a-2). Conversely, exposure to either chlorine or biocide removed biofilm (Figure 4.5b-2 and 4.5c-2). Biofilm removal was quantified using Imaris 9.8 by calculating changes in biofilm index (B.I.; Equation 4.2) between pre-treatment and post-treatment. Chlorine and biocide treatment resulted in an average B.I. reduction of 1.87±0.75 $\mu m^3\ \mu m^{-2}$ and 2.13±0.89 $\mu m^3\ \mu m^{-2}$ between pre-treatment and post-treatment, respectively. Both treatments, resulted in significant reduction of biofilm when compared to biofilm without treatment (T-Test, P value≥0.024). While Furanone C-30 did not appear to affect the number of viable cells at 36 hrs, cells treated with 75 µM Furanone C-30 developed thinner biofilms, exhibiting ~ 40 % reduction in overall thickness compared to untreated biofilms (Figure 4.6).

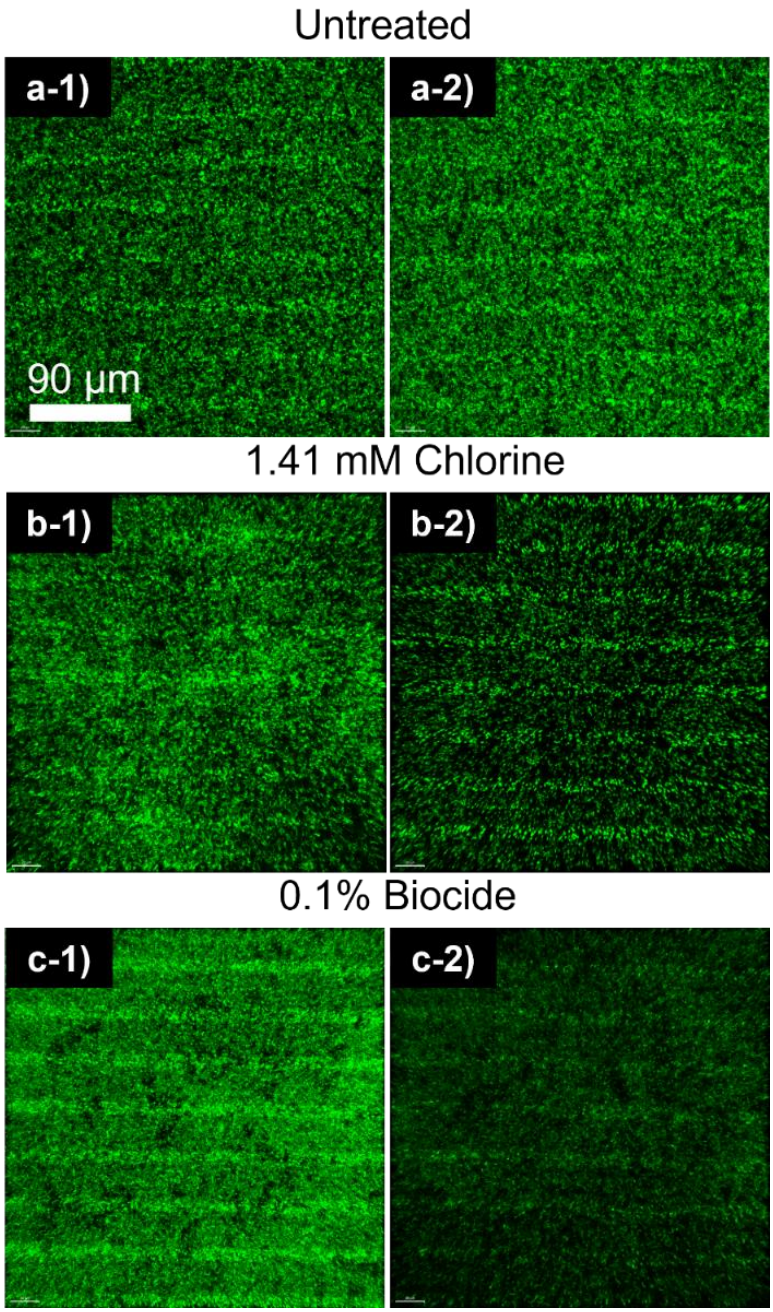

Figure 4.5: CLSM images of (left panel: -1) pre-treatment (24 hrs) and (right panel: -2) post-treatment (36 hrs) biofilm. a) untreated, b) chlorine treatment, and c) biocide treatment. Scalebar represents 90 µm.

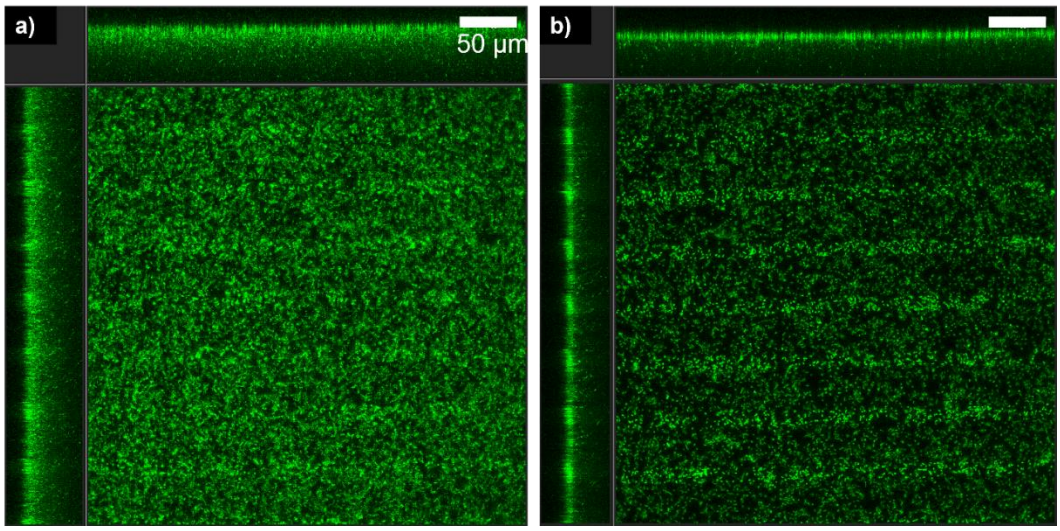

Figure 4.6: CLSM images of a) untreated biofilm at 36 hrs, and b) biofilm exposed for 36 hrs to 75 µM of the quorum sensing compound Furanone C-30. Scalebar represents 50 µm. Top and side panels show side-view profiles of biofilm z-stacks.

Discussion

The developed platform consisted of EIS biosensors integrated into a microfluidic flow environment, allowing for impedance measurements that reflect naturally proliferating biofilm conditions. Live-cell imaging from CLSM supplemented impedance data as a non-destructive visual confirmation of adherent biofilm. The marriage of these characteristics makes the current report unique in that biofilm growth under flow conditions and the expansion of the sensors into alternative fluids and quorum sensing inhibition is explored. Extending findings by McGlennen et al., 2023 on linking biofilm growth to EIS measurements, this study assessed the applicability of impedance to monitor biofilm treatment and the application of QSI in real-time. The behavior of microfabricated sensors used to evaluate biofilm growth is highly dependent on the experimental setup, such as the type of media, flow characteristics (*e.g.*, static vs. continuous flow), organism selection, electrode geometry (*e.g.*, 2 vs. 3-dimensional), and selected frequency range (Furst and

Francis, 2019; Subramanian et al., 2019; Funari and Shen, 2022). All of these factors complicate direct comparisons between reports.

In the present study, a flow-based system using μIDEs coated with an electrically conductive polymer (*i.e.*, PPy:PSS), measured at an optimized single-frequency (*i.e.*, 1.26 kHz and 200 kHz) was deployed. Impedance decreased in the presence of proliferating biofilm following sigmoidal decay curves (Figures 4.2 and 4.3). Others have found a similar relationship between biofilm growth and impedance (Paredes et al., 2012; Paredes et al., 2013; Paredes et al., 2014; Paredes et al., 2014; Subramanian et al., 2017; Huiszoon et al., 2019). These studies reported impedance changes ranging from ~10 to ~40%, and plateaus were reached between 10 and 48 hours, bracketing our findings of 20 to 25% before levelling off at ~24 hrs. Likewise, impedance in the low-frequency ranges (*i.e.*, 10 Hz-10 kHz) was most representative of signals from the electrode/electrolyte interface and provided the highest sensitivity towards biofilm growth (McGlennen et al., 2023; Paredes et al., 2014). While the frequency range in 1:10X TSB growth medium was optimized at 1.26 kHz, this frequency was not suitable for MWFs. Complex industrial oil-water emulsions can form rigid dielectric barriers that hinder the mobility of charge carriers at the interface of the electrode (Perini et al., 2012), suggesting that higher frequencies may be more effective in measuring biofilm. We found that the most appropriate frequency range for measuring biofilm in 5% MWF was ≥100 kHz, as detailed in the supplemental information. However, it should be noted that the degree of hindrance to charge carriers can vary depending on the amount of water in the emulsion, and optimal sensor signal responses may need to be tailored to individual systems. MWF was chosen as a representative media to test EIS biosensors since MWF is prone to *P. aeruginosa* biofilm contamination (Di Maiuta et al., 2017; Passman and Küenzi, 2020).

Importantly, EIS detected biofilm growth in MWF with the same degree of sensitivity as in 1:10X TSB (Figures 4.2 and 4.3).

While the exact mechanisms behind the impedance decrease in response to biofilm are not fully understood, we hypothesize that biofilm metabolic processes modify ionic concentrations at the capacitive double-layer of the sensor electrodes. This leads to a decreased Debye length, and thus, an elevated capacitive double-layer that results in a decline in impedance (Huiszoon et al., 2019; 2021; McGlennen et al., 2023). Additionally, upon the production of EPS, electrochemically active metabolites such as phenazine, pyocyanin (PYO), or *Pseudomonas* quinolone signal (PQS) may become entrapped within the EPS matrix, leading to the accumulation of electrochemically active sites (Becerro et al., 2016; Bosire et al., 2016). Cells may also act as small capacitors, decreasing impedance (*i.e.*, capacitance increase; Turick et al., 2019). Conversely, biofilm treatment causes damage to cells and/or disruption of the EPS matrix, and decreases metabolic processes, resulting in the release and subsequent decrease in the concentration of electroactive redox compounds. These compounds are then carried away by the flow and thus, the impedance increases. With regards to these mechanisms, chlorine causes the detachment of biofilm clusters and the breakdown of metabolites by oxidation of organic materials (Davison et al., 2010), whereas 1,2-benzisothiazolinon-3-one (*i.e.*, biocide) is believed to inhibit bacterial growth and metabolic activity (Green et al., 2018; Silva et al., 2020). Both chlorine and biocide treatment resulted in impedance increases (Figures 4.3b and 4.3c). While indicative of biofilm reduction, impedance did not fully rise to abiotic levels. Further, the reduced slope of the impedance curves not only implied incomplete removal of biofilm but also that biofilm became less susceptible to the treatment. Incomplete biofilm removal was confirmed by CLSM (Figure 4.5). The measured ~14%

impedance increase corresponded to an ~68% decrease in biomass. However, it is important to note that this study aimed to detect changes in impedance in response to biofilm treatment rather than optimizing biofilm treatment doses.

Furanone C-30 is a QSI compound and has been demonstrated to delay biofilm formation and maturation (Wu et al., 2004; He et al., 2012; Zhao et al., 2018). Quorum sensing is a type of bacterial communication to sense and respond to cell population density, mediated by chemical signalling molecules (Mukherjee and Bassler, 2019). Briefly, the abundance of signalling molecules is low or absent at low cell densities. The production, release, and extracellular concentration of signalling molecules increase as a function of growing cell density, ultimately triggering a synchronized cell population-wide response such as biofilm formation and architecture (Davey et al., 2003). As such, QS systems are autoregulated and depend on a threshold concentration of signalling molecules (Miller and Bassler, 2001). By destabilizing QS regulatory proteins, Furanone C-30 decreases the synthesis of signalling molecules (*i.e.*, acyl-homoserine lactones (AHLs) and PQS) (Skindersoe et al., 2008; Markus et al., 2021), which further downregulates the production of other redox mediators such as phenazine and PYO (Davies et al., 1998; Hentzer et al., 2003; Proctor et al., 2020). When biofilm was grown in the presence of Furanone C-30, impedance remained unchanged for 72 hrs in 5% MWF (Figure 4.3e). In 1:10X TSB, impedance remained stable for 18 hrs (Figure 4.3c) and the subsequent decrease in impedance indicated that QSI was overcome. Ozcan et al., tested *P. aeruginosa* PAO1 biofilm growing in both TSB and MWF in the presence of Furanone C-30, and reported lower concentrations of signaling molecules (PQS and AHLs) critical to biofilm development (Ozcan et al., 2019), affirming the potential role of these mediators in affecting impedance.

The use of µIDEs in combination with PPy:PSS electrode coatings results in highly sensitive biofilm detection, and enhanced measurement integrity/repeatability (this study; McGlennen et al., 2023). Recent reviews have identified four criteria relevant for developing robust biofilm detection tools: analytical techniques need to be (*i*) non-invasive (*i.e.,* cannot perturb or damage biofilm), (*ii*) provide real-time analysis with high temporal and spatial resolution, (*iii*) be applicable to diverse analytes and settings, and (*iv*) be cheap, require low maintenance, and operate continuously for a long time (Saccomano et al. 2021; Funari and Shen 2022). The EIS biosensors developed herein hold promise to fulfill these criteria as they have the advantages of being able to be manufactured at low-cost and can be configured for automated data collection and interpretation, all of which results in a higher efficiency and real-time evaluation of biofilm. To take advantage of the capabilities of EIS, further research is needed to better understand the mechanisms that drive changes in impedance. For instance, this study investigated the model organism, *P. aeruginosa* PA01, but other organisms likely have different electrochemical compositions. It will be necessary to assess the performance of these sensors in diverse biofilm compositions (*e.g.,* mixed species and/or inter-kingdom), different types of supporting fluids (*e.g.,* opaque, complex formulations), and under varying environmental conditions (*e.g.,* fluctuations in temperature, conductivity, or pH). If further validated, impedance sensors would be a significant advancement where biofilm contamination is prevalent and the reliance on current monitoring techniques are inadequate.

Conclusion

In this study, microfabricated EIS biosensors were effective at assessing the growth and removal of *P. aeruginosa* biofilm in 1:10X TSB and 5% MWF. Additionally, EIS biosensors could

observe the delayed effects of biofilm growth from targeting bacterial QS inhibition. The use of EIS biosensors holds great potential for the early detection and continuous monitoring of biofilms. Expanding our understanding of the sensors' uses and limitation beyond laboratory-based testing is vital to ensure future technological expansion into industrial, medical, and natural environments.

Supporting Information to this Chapter is presented in Appendix B.

MICROSENSORS IN ICY ENVIRONMENTS TO DETECT MICROBIAL ACTIVITIES

Contribution of Authors and Co-Authors

Manuscript in Chapter 5

Author: Matthew McGlennen

Contributions: Methodology, Investigation, Formal analysis, Writing - original draft, Visualization

Author: Michael Neubauer

Contributions: Conceptualization, Resources, Writing - review & editing

Author: Matt Driesler

Contributions: Conceptualization, Resources, Writing - review & editing

Co-Author: Markus Dieser

Contributions: Conceptualization, Resources, Writing - review & editing

Co-Author: Christine M. Foreman

Contributions: Supervision, Resources, Writing - review & editing

Co-Author: Stephan Warnat

Contributions: Supervision, Resources, Writing - review & editing

Manuscript Information

Matthew McGlennen, Michael Neubauer, Matt Driesler, Markus Dieser, Christine M. Foreman,

Stephan Warnat

Journal of Microelectromechanical Systems

Status of Manuscript:
____ Prepared for submission to a peer-reviewed journal
____ Officially submitted to a peer-reviewed journal
____ Accepted by a peer-reviewed journal
_x_ Published in a peer-reviewed journal

Publisher: IEEE
Volume: 29, Issue: 5
Published: August 7, 2020
DOI: 10.1109/JMEMS.2020.3012420

Abstract

Electrochemical techniques such as impedance spectroscopy offer a non-invasive approach to monitor microorganisms in natural and engineered environments. Here, we present data on the use of microfabricated impedance spectroscopy sensors for the detection of microbes in icy environments. Under controlled laboratory settings, the effects of different cell concentrations of the Antarctic isolate *Flavobacterium* sp. ANT 11 on impedance spectroscopy was investigated at ambient temperature (22°C) and -10°C. Results show that varying cell concentrations of the bacterial isolate generate unique spectral responses that vary with temperature. Subsequent tests on the performance of microfabricated impedance sensors on natural microbial communities in icy environments in the Beartooth Mountains, WY, USA, confirmed laboratory findings. Different environmental samples at varying microbial concentrations in liquid, semi-frozen (slushy), or frozen states generated discrete impedance spectra. While caution is advised to generalize these results due to the potential contribution of unknown environmental variables, our data provide fertile territory for research in cryo-microbiology, as information on the applicability of impedance spectroscopy under frozen conditions is limited.

Introduction

Electrochemical impedance spectroscopy (EIS) is an innovative technique to measure changes in electrochemical properties in aqueous, solid, and gas systems (Lvovich, 2012). The technique is based on applying a sinusoidal perturbation across a frequency range to a system and measuring the opposition to current, which can determine bulk and interfacial properties of electrochemical systems (Dhillon and Kant, 2017). While EIS is typically used in industrial

applications (Barsoukov, 2005), the importance of EIS microsensors for biosensors applications has increased significantly in recent years (Brosel-Oliu et al., 2019). Microorganisms exchange electrons with their surrounding environment (Shi et al., 2016), which, in turn, are associated with an increase in the electrical conductivity of the surrounding media. EIS can detect the electrical variations caused by cellular electron exchanges that occur at the EIS electrode interface (Randviir and Banks, 2013); thus, providing a label-free approach for measuring the 'electrochemical' fingerprint of microbial activity. For instance, Neubauer et al. combined a simple interdigitated electrode structure on glass with a 3D printed microfluidic channel to measure changes in cell concentrations of *Escherichia coli* K12 (Neubauer et al., 2019). Liu et al. were able to closely monitor changes in impedance related to the growth of Salmonella and *E. coli* biofilms using interdigitated electrode (IDE) microsensors (Liu et al., 2018). However, while a large body of research espouses the importance of EIS microsensors as microbial biosensors (Furst and Francis, 2019), practical industrial, medical, or environmental applications for detecting bacteria are still limited.

Glaciers and ice sheets cover ~11% of the Earth's terrestrial surface and provide a distinct biome for diverse biological communities that affect local and global geochemical cycles (Anesio et al., 2017). Microorganisms in icy environments can be used as bioindicators to monitor dynamic variations caused by climate change and fluctuations in the surrounding environment (Cook et al., 2020). Existing techniques such as Raman spectroscopy (Fukazawa et al., 1997) and nuclear magnetic resonance (NMR) spectroscopy (Brox et al., 2015) have significant limitations to be deployed in advanced telemetry systems because i) costs are prohibitively expensive to deploy multiple systems simultaneously; ii) power consumption is too high to monitor icy environments

for an extended time (~ 1 winter season) without maintenance, and iii) the spatial resolution of the portable spectroscopy tools do not match the microenvironments of ice (Dani et al., 2012). Conversely, EIS microsensors have the potential to overcome challenges associated with traditional biomarker assays, as this modern technology has significantly reduced dimensions, low primary and maintenance costs, and is easy to use. Environmental applications require several sensors to be deployed at low-cost, and low-power to monitor changes. A high spatial density of sensors would increase the probability to detect bioindicators and life in unknown territories. In addition, microsensors have the sensitivity to detect microbial presence in snow and ice.

In this study, we present to the best of our knowledge the first use of microfabricated impedance spectroscopy sensors as a method to study microbial activity in icy environments. Impedance microsensors were tested under both laboratory and field conditions.

Materials & Methods

Sensor and Probe Fabrication

Impedance spectroscopy sensors were fabricated using standard physical vapor deposition, lithography, and wet etching surface micromachining techniques. Briefly, a thin film of 10 nm chromium (thermal evaporation) followed by 100 nm gold (electron-beam evaporation) were deposited on a borosilicate glass wafer (100 mm in diameter) in an Angstrom AMOD PVD evaporator. The wafer was patterned with micro-interdigitated electrode (μIDE) structures by lithography (i.e., spinning positive photoresist, exposure, development) and wet etching. Prior to photolithography, the wafer was cleaned with three solvents (acetone, methanol, and isopropanol), followed by a 10 min dehydration bake at 120°C on a hotplate (Electronic Microsystems Ltd. Model 1000-1). A 1.5 μm layer of positive photoresist (Microchem AZ1512HS) was spun onto

the gold coated wafer with spin speeds of 500 rpm for 10 s, and 4000 rpm for 35 s. The photoresist coated wafer was then soft baked on a hotplate for 1 min at 110°C. Subsequently, the wafer was exposed with a light intensity of 15 mW cm^{-2} for 3.2 s on a contact aligner (ABM contact aligner). The wafer was submerged in developer solution (MicroChem AZ300 MIF) for 1 min 30 s and then hard-baked for 2 min at 115°C on a hotplate. Etching was performed at 22°C by wafer submersion for 40 s in gold etchant (Transene Gold Etch TFA), followed by a deionized water (DIW) rinse and subsequent chromium etching (Transene Chromium etchant 1020) for 20 s. Nominal deposited metal layer thickness was 108 nm after etching, calculated from the average step height from a profilometer scan (Ambios XP2 Profilometer). The wafer was diced into individual sensors, 15 mm x 15 mm in size. The µIDE structures were designed to have electrodes that were 30 µm in width and have spacing between electrodes of 60 µm (Figure 5.1). However, undercutting during the etching process caused the average electrode width to be 26 µm, measured using an optical microscope (Olympus BX41; 20X objective; AmScope MU503 camera). The IDE arrays were chosen based on their ease of manufacturing and miniaturization, low signal-to-noise ratio, fast establishment of steady-state conditions, and for eliminating the need of a reference electrode (Varshney and Li, 2009). Additionally, sensitivity is maximized by increasing the surface area in contact with the media under test, which is favorable to biological applications (Ibrahim et al., 2013).

Based on application requirements, two setups with an integrated impedance sensor were designed: i) a laboratory setup for freezing on a Peltier element (Figure 5.2A), and ii) a 30 cm long field probe (Figure 5.2B).

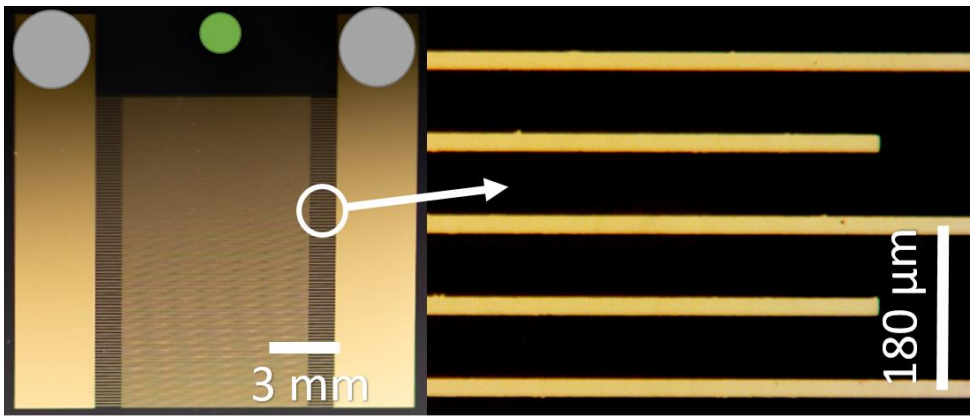

Fig. 5.1: Left: Microfabricated impedance spectroscopy sensor. Right: Micro-interdigitated electrode (µIDE) structures on impedance spectroscopy microsensors. Position of solder connections (grey circle). Position of set screw (green circle).

The manufacturing of the field probe was as follows: a sensor holder (Figure 5.2C) was 3D printed with PLA plastic filament using a LulzBot Taz 6 3D printer. The sensor was soldered to copper cables (Figure 5.1). Solder connections were coated with three layers of silicone (MG Chemicals 422B Silicone Modified Conformal Coating) to protect electronic circuitry from moisture. The sensor was held in place with a set screw (Figure 5.2C), and spaces were sealed with a silicone elastomer (DAP Aquarium Clear Silicone Rubber Sealant). The ends of the cables were routed through a 30 cm long polycarbonate tube and connected to a BNC adapter. The polycarbonate tube was machined from 25.4 mm (1 inch) polycarbonate bar stocks into hollow tubes with an inner diameter of 12.7 mm (½ inch) and an outer diameter of 19 mm (3/4 inch) on a manual lathe. A topical coating of silicone (MG Chemicals 422B Silicon Modified Conformal Coating) was applied to the entire probe assembly (with the exception of the sensor) to enhance waterproofing.

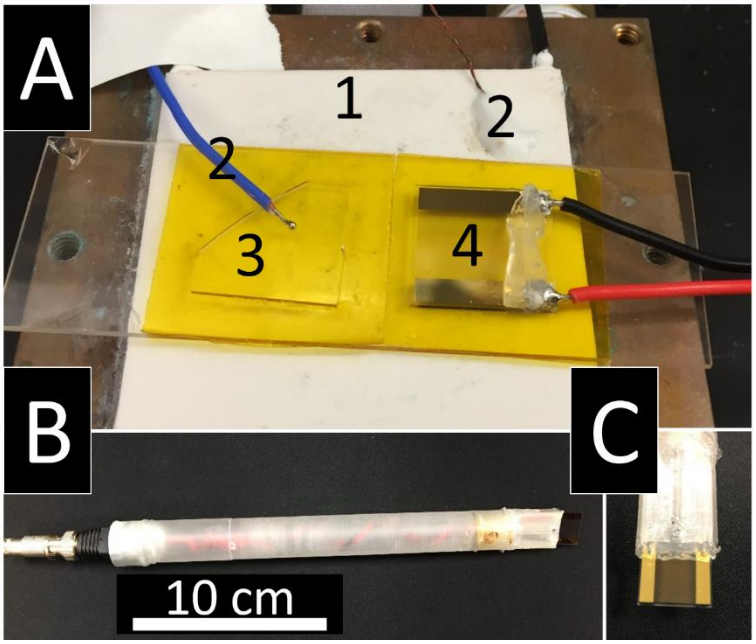

Figure 5.2: Impedance sensors for laboratory and field applications. (A) Laboratory setup for impedance of unfrozen and frozen microbial cell suspensions. (A-1) Peltier element, (A-2) thermocouples for temperature control, (A-3) BSG wafer coupon for measuring temperature directly within unfrozen and frozen cell suspension, (A-4) impedance sensor for measuring cell suspensions, (B) field-deployable probe with impedance microsensor, (C) 3D printed sensor holder with silicone elastomer.

To confirm waterproofing, the assembly was submerged in municipal drinking water for 24 hours at 22°C. Subsequently, the sensor was disassembled and checked for moisture buildup inside the assembly. Electrical contacts and thus, the performance of the impedance sensors, were validated in DIW and standard KCl conductivity solutions, as described below.

Culturing Conditions for Laboratory Experiments

An enrichment of a microbial isolate from Antarctica (*Flavobacterium sp.* ANT 11, GenBank: GU592435; (Dieser et al., 2010)) was grown in R2A media (Reasoner and Geldreich, 1985) at 10°C while shaking at 125 rpm for five days. Cell cultures were harvested by centrifugation at 10,000×g for 5 min. Cell pellets were washed twice and resuspended in autoclaved DIW at a cell concentration of 10^9 colony forming units (CFU) ml^{-1}. CFU were

enumerated by spread plating *Flavobacterium sp.* ANT 11 cultures onto R2A agar plates. For impedance measurements, tenfold dilution series of the cell culture (*i.e.*, 9 parts DIW and 1 part cell solution) were prepared in 1.5 ml microcentrifuge tubes and kept at 4°C (<2 hours) until impedance measurements were taken.

Laboratory Tests

The laboratory tests were carried out using an impedance sensor mounted to a microscope slide with Kapton tape (Figure 5.2A). Different cell concentrations of the microbial isolate were pipetted (200 µl) onto the sensor surface and a blank BSG wafer sample. The blank BSG wafer coupon was equipped with a thermocouple (Fisher Scientific Traceable Total-Range Thermometer) to verify temperature during impedance collection (Figure 5.2A-2). Samples were measured in ascending order of cell concentrations. Each microbial dilution was prepared and measured in triplicate. Impedance spectra for each cell concentration were first recorded at room temperature (22°C). Subsequently, samples were frozen on a thermoelectric/Peltier module (Custom Thermoelectric #12711-5P31-12CW), which was mounted to a copper block and chiller (Thermo Scientific NESLAB RTE 740) with circulating propylene glycol (Cryo-Tek 100 anti-freeze). Impedance spectra were recorded once the temperature reading of the submerged thermocouple stabilized at -10°C (± 1°C, approx. 15 min). Impedance spectroscopy was measured using a Hioki IM3536 LCR meter with 100 mV_{RMS} sine wave and frequency range of 10 Hz to 8 MHz with 176 data points.

Field LCR Meter

Since the Hioki IM3536 LCR meter could not be transported to the field, impedance measurements were performed using a field portable Keysight LCR handheld meter (U1733C).

This LCR meter has a predefined output voltage of 1 VP and frequency settings of 0.1, 1, 10, 100 kHz. In comparison, the output voltage for the Hioki IM3536 LCR meter for laboratory tests was 100 mVRMS. It should be noted that higher output voltage increases the risk of non-linear signals. To determine whether the measurements from the two LCR meters are similar, two tests were performed. (i) Both LCR meters were connected to an EIS dummy cell (Gamry Instruments Universal Dummy Cell 2). The dummy cell had a 2 kΩ resistor in series with a parallel 100 nF capacitor and 2 kΩ resistor. (ii) Impedance was measured in DIW (~0.05 µS cm^{-1}), and a 1413 µS cm^{-1} certified KCl conductivity standard (Biopharm) including ten-fold dilutions (141 µS cm^{-1} and 14 µS cm^{-1}) of the standard. Output voltage was 1 V_p for both LCR meters. Measurements were repeated five times.

Field Tests

As proof of concept that the sensors would be practical in natural microbial environments, the sensors were deployed in the Beartooth Mountains (Wyoming, USA; 44.95024, -109.48384). Snow patches and alpine ponds and lakes covered with slushy ice last well into the summer months, which provide favorable conditions for microbial growth. A minimum of four in situ measurements were performed on June 22, 2020, on slushy lake ice and snow where red algae and other organisms are present. Field impedance was measured with a Keysight U1733 handheld LCR meter.

In vitro measurements (five replicates) were also performed on melted samples (one each) of snow covered with red snow algae and white (*i.e.,* visibly clean) snow. Tenfold dilutions of red snow algae samples were prepared with 0.2 µm filtered snowmelt (Figure 5.3).

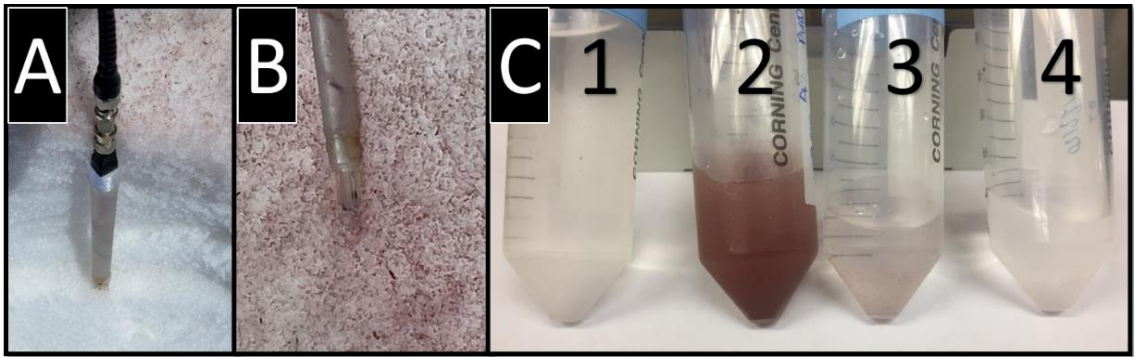

Figure 5.3: Impedance sensors deployed in natural low temperature environments. (A) White snow (B) red snow algae (C) melted samples of snow measured with field probe (C-1) 0.2 µm filtered snow, (C-2) red snow algae, (C-3) 1:10 diluted red snow algae, (C-4) 1:100 diluted red snow algae.

Results and Discussion

Laboratory Impedance Measurements

Nyquist spectra from the laboratory experiments are presented in Figure 5.4 (left, top, and bottom). Differences in impedance spectra were not only evident between different cell concentrations, but also between aqueous and frozen cell suspensions. Measurements for both aqueous and frozen cell suspensions contained characteristic semicircles and tails, typical features of electrode/electrolyte interactions in EIS experiments. This suggests that electrochemically active compounds and metabolites released by bacteria into the solution (Yang, 2008) contribute to double layers, resistive, and diffusion phenomenon at the microsensor interface. Importantly, a higher magnitude of impedance was observed for the frozen samples (Figure 5.4 bottom). Upon freezing, the diameter of the semicircles for each dilution was increased. This is thought to be a combined effect of temperature and matrix change (i.e., liquid vs. frozen), resulting in an increase in the solution resistance between the electrodes and the media. The frequency dependent magnitude of impedance was also evident in the Bode plots (Figure 5.4, right) for each cell concentration. Three characteristic domains throughout the frequency range were identified: i) a

double layer region that spans from approximately 10^1 Hz to 10^3 Hz, ii) a resistive region that spans from approximately 10^3 to 10^5 Hz, and iii) a high frequency region that combines effects of capacitance and resistance above 10^5 Hz.

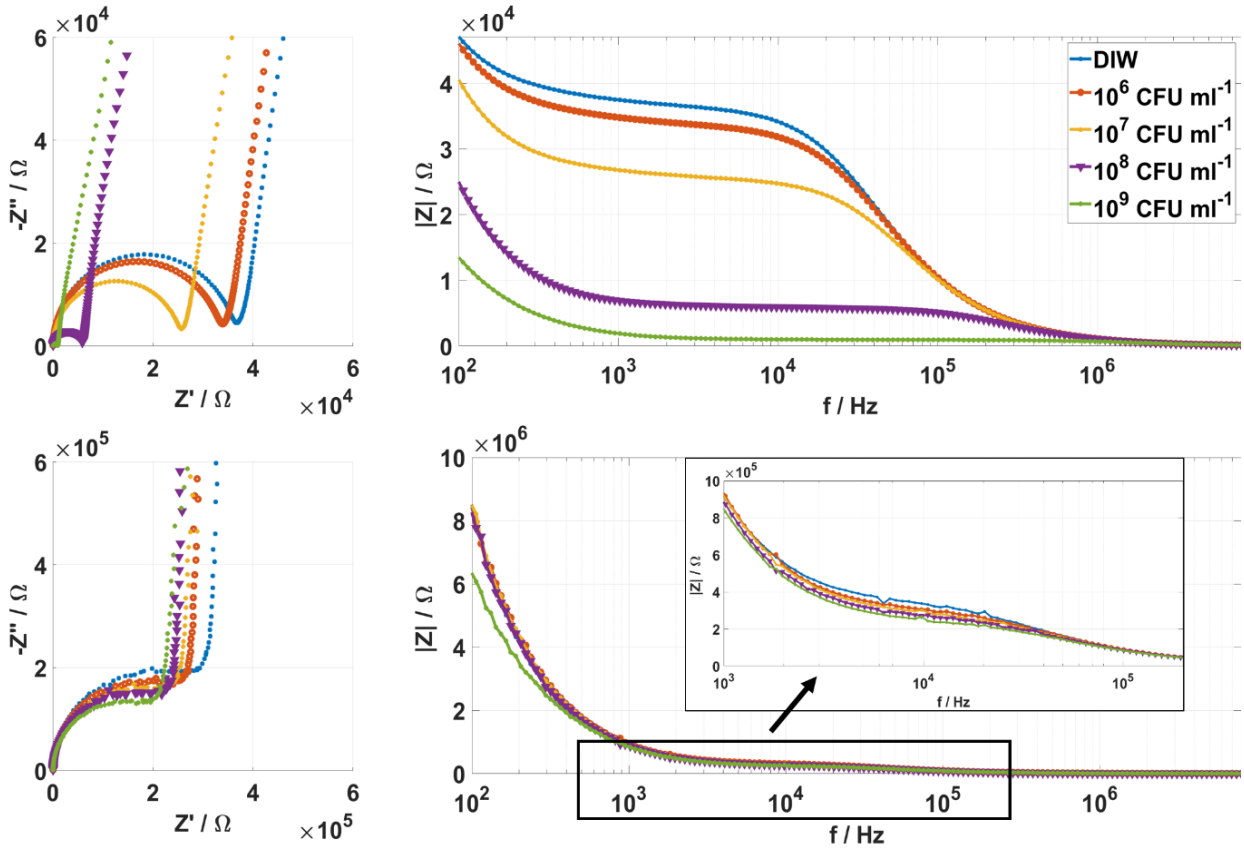

Figure 5.4: *Left:* Nyquist plot of *Flavobacterium* sp. ANT 11 at 22°C (Top) and -10°C (Bottom). *Right:* Bode plot of *Flavobacterium* sp. ANT 11 at 22°C (Top) and -10°C (Bottom). Detailed view of frequency range 10^3 to 2 x 10^5 for *Flavobacterium* sp. ANT 11 at -10°C (Bottom insert). Note the difference in scaling on the y-axes.

To further investigate the electrochemical mechanisms underlying the impedance spectroscopy measurements, impedance spectra of the frozen cell cultures were fit to an electrical equivalent circuit using the model fitting software EIS Spectrum Analyzer. As an example, the Nyquist plot from the frozen cell culture at 10^6 CFU ml^{-1} and the fitted data are shown in Figure 5.5. The slope of the fitted curve in the low frequency range was greater than 45°. Therefore, in

the equivalent circuit model, the Warburg element that is traditionally used in a Randles circuit was replaced with a double layer constant phase element (CPE_{DL}). In the circuit representation (Figure 5.5), R_c describes the connection resistance, C_G geometric capacitance, R_s bulk solution resistance, and CPE_{DL} the interfacial phenomenon during an impedance measurement containing microorganisms. The equivalent circuit model showed a fit over the range of frequencies that closely mimicked the response of the laboratory measurements. It was observed that the fitted values of R_s and CPE_{DL} change between cell concentrations. Specifically, as the cell concentrations increased, the fitted values of R_s decreased. Variations in R_s are associated with interactions with charged species due to the presence of bacteria cells (Yang, 2008). While differences were apparent, no particular trend was observed for CPE_{DL} values across cell concentrations. The equivalent circuit that was fitted to the experimental data suggests that it could serve as a basis for future experiments in icy-microbial environments where microbial concentrations are unknown.

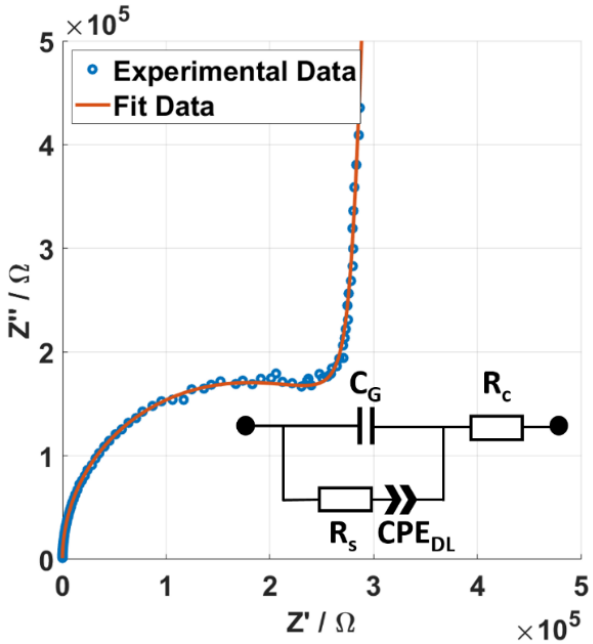

Figure 5.5: Equivalent circuit representation of experimental data for the frozen cell suspension of *Flavobacterium* sp. ANT 11 with 10^6 CFU ml^{-1} and the fit data.

To determine the sensitivity of the measurements, the magnitude of impedance at 20 kHz was plotted versus different cell concentrations of Flavobacterium sp. ANT 11 (Figure 5.6). Impedance at 20 kHz was chosen since the interfacial effects at the electrodes are negligible at this frequency and bulk solution resistance becomes the dominant factor. It was observed that changes in microbial concentrations likely lead to changes in resistive properties. A linear relationship between the logarithmic concentration and the measured magnitude of impedance at 20 kHz yielded the equation: $y=12440*(\text{Log}(\text{CFU ml}^{-1}))+337500$ and gives a correlation of $R^2=0.994$. This equation suggests that changes in the impedance at 20 kHz have a linear relationship between the logarithm of cellular concentrations. The sensitivity was calculated to be 12440 Ω/Log(CFU ml^{-1}). We hypothesize that the electrical conduction through ice occurs mainly through the aqueous grain boundaries where the microorganisms are present (Dani et al., 2012). This could have contributed to higher sensitivity between microbial concentrations. While impedance signals become noisier at lower cell concentrations (10^6 CFU ml^{-1}), the signal to noise ratio can be improved if the electrode sizes and spacing are scaled appropriately (Couniot et al., 2012). Similarly, the measured impedance at 20 kHz for the aqueous cell suspensions yielded the equation: $y=9846*(\text{Log}(\text{CFU ml}^{-1}))+91240$ with a correlation of $R^2=0.965$. The sensitivity was determined to be 9846 Ω/Log(CFU ml^{-1}). Percent differences between impedance measurements were <10% below 100 Hz, <5% between 1 kHz and 100 KHz, <1% above 100 kHz for frozen samples, and <2% across all frequencies for aqueous samples. The higher error observed in the frozen samples was likely due to differences in ice formation on the sensor surface between replicates.

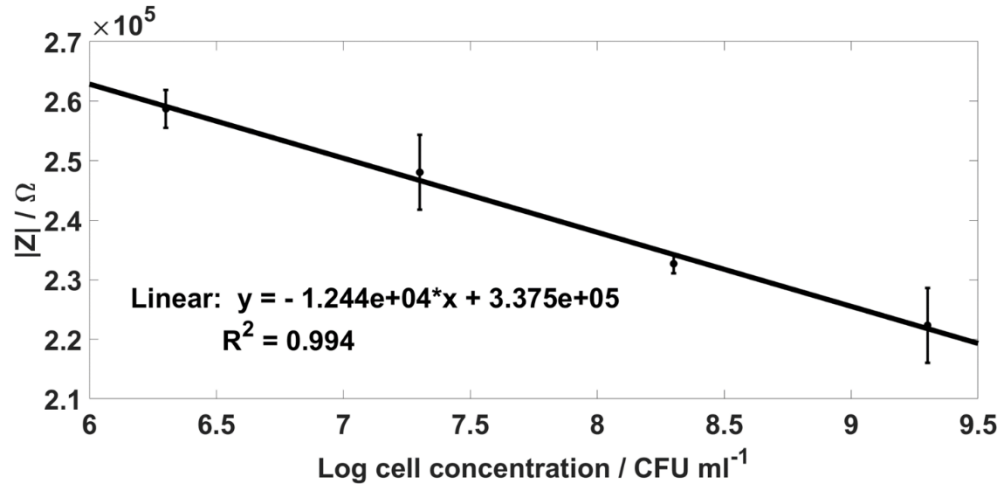

Figure 5.6: Logarithmic plot of different cell concentrations of the bacterial isolate *Flavobacterium* sp. ANT 11 frozen at -10°C versus magnitude of impedance at 20 kHz. The plot shows a linear correlation ($R^2 = 0.994$), error=σ.

Comparison of the Laboratory and Handheld LCR Meters

To validate the use of the handheld LCR meter, impedance measurements of the portable Keysight U1773C were compared to those of the Hioki IM3536 LCR meter. Impedance for both LCR meters was measured at the four frequency setting available on the handheld Keysight U1773C LCR meter and 1 V_P output voltage. All impedance measurements between the two LCR meters were significantly different (unpaired T-test, P-value <0.001) (Figure 5.7 Top). When comparing the performance of the LCR meters using solutions with different concentrations of ions, impedance measurements of DIW (unpaired T-test, P-value <0.001) and the 1413 µS cm^{-1} conductivity standard (unpaired T-test, P-value = 0.04) were significantly different at 100 kHz (Figure 5.7 Bottom).

Differences in the measured impedance values was likely associated with the different measurement conditions: the Hioki LCR meter uses four-wire measurement, whereas the handheld LCR meter uses only two. This may have led to parasitic capacitance in the connections. Additionally, the cables used with the handheld LCR meter are less suited for high frequency

applications. However, while there was a statistical difference between the two meters in a controlled test circuit, they can be deemed negligible from a resolution/interpretation standpoint. Differences in impedance between the two LCR meters were <0.1% (i.e., 2Ω) for each frequency (Figure 5.7 Top) and <1% (excluding the highly pure DIW) for the dummy cell and measurements across solutions of different conductivity, respectively.

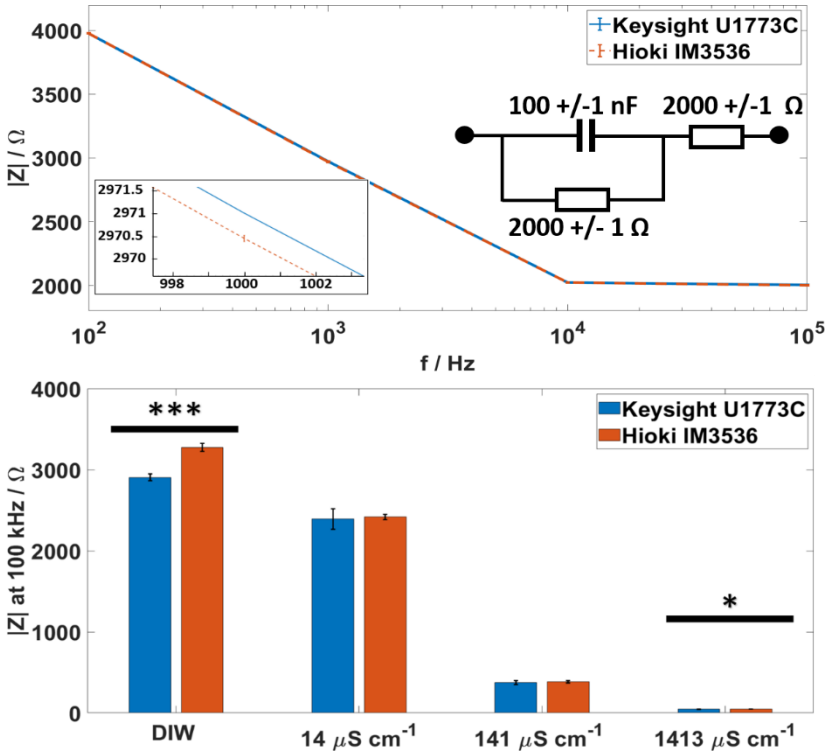

Figure 5.7: (Top): Bode plot of impedance measurements of the dummy cell between the handheld Keysight U1773C and benchtop Hioki LCR meters. The circuit contained a 2 kΩ resistor in series with a 2 kΩ resistor in parallel with a 100 nF capacitor (insert). Close up of impedance measurements at 1 kHz. Error bars = 3σ. (Bottom): Impedance measurements of the Keysight U1773C and Hioki IM3536 LCR meters at 100 kHz for DIW (~0.05 µS cm^{-1}), and KCl conductivity standards. *** P<0.001 * P<0.05.

Field Tests

Impedance measurements on slush and snow from the Beartooth Mountains were performed in vitro and in situ, to investigate the effect of cell concentration and matrix (aqueous

vs. slush and snow) (Figure 5.3). The impedance spectra of the field measurements are shown in Figure 5.8. Bode plots reinforce the three distinct domains throughout the measured frequency range (Figure 5.8), similar to those tested in the laboratory (Figure 5.4). Measurements showed clear differences between cell concentrations and matrix of the solution. All in vitro measurements were significantly different across all measured frequencies (unpaired T-test, P-value≤0.03; Figure 5.8 Top). Despite these statistical differences, the data could not be fit to the equivalent circuit model due to the limited frequency setting of the handheld LCR meter.

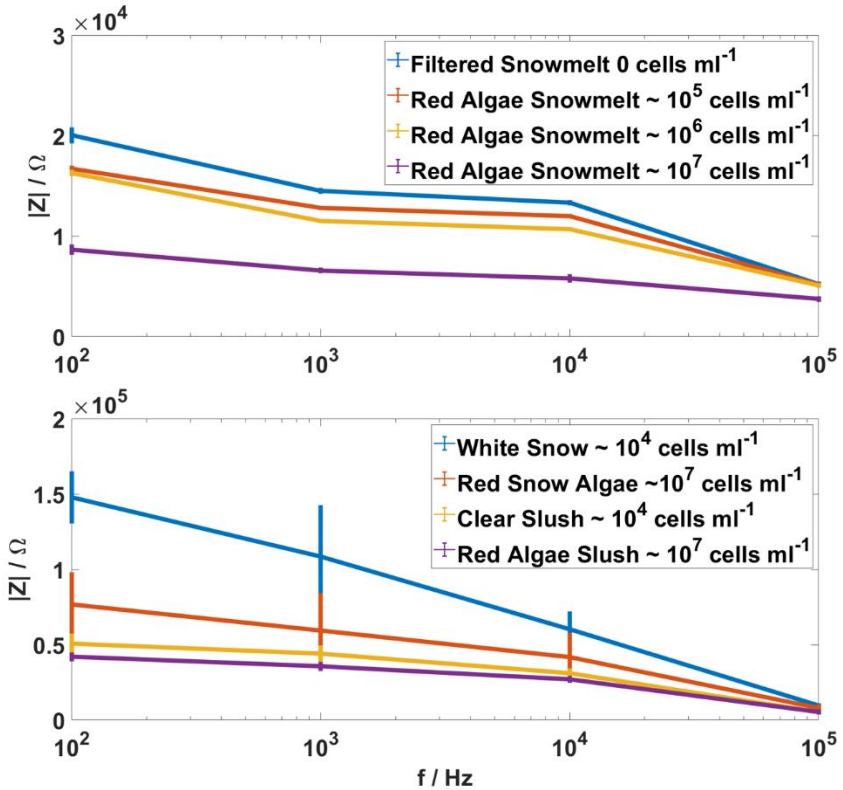

Figure 5.8: Bode plot comparing the measured samples in the field. (Top) *In vitro* measurements on melted snow. (Bottom) Impedance *in situ* measurements. Error bars = σ. Note difference in scaling of y-axis between top and bottom.

For in situ impedance measurements, sensors were directly deployed inside slush and snow (Figure 5.2A and 5.2B). While a detailed biological physicochemical characterization of these

environments was beyond the scope of this study, distinct impedance spectra were observed for the different sample types. Measurements on snow samples showed a higher degree of variability, likely associated with differences in the contact between snow crystals and the sensor surface. Similar to in vitro measurements, changes in impedance signals reflected lower and higher cell concentrations. Statistically significant differences were observed between snow covered with red algae and white snow at 100 Hz and 100 kHz (unpaired T-test, P-value$\leq$0.01). Slush streaked with red snow algae was significantly different from clear slush at all measured frequencies (unpaired T-test, P-value$\leq$0.02) with the exception of 100 kHz. Further analysis and development is needed for future field investigations, as our measurements also indicated that the way a sensor is positioned within an icy matrix affects impedance spectroscopy.

Conclusion

Impedance spectroscopy microsensors enable the study of diverse microbial environments both inside and outside of the laboratory. Here, we present laboratory based experiments and field measurements in icy habitats that measured impedance spectra of different microbial cell concentrations in both aqueous and frozen states. Laboratory and field measurements highlighted distinct impedance spectra based on cell concentration, sample matrix, and sample type, respectively.

Our laboratory data provided insights to the electrochemical mechanisms occurring at the interface of EIS microsensors, and models can be created that closely mimic these mechanisms. These models may be used to understand basic phenomena in the field, where complex microbial environmental interactions take place. Impedance spectroscopy measurements in the field are complex, and further analysis is required prior to generalizing the data. Additionally, given the

potentially lower microbial cell concentration and activity levels in many oligotrophic environments, high sensitivity field impedance sensors are required.

Both the lab and field data revealed useful information in response to icy-microbial environments. Data presented herein have shown that microbial concentrations in icy environments can be differentiated, indicating that impedance spectroscopy could be a viable tool to measure microbial activities in icy environments. Future work will involve the integration of impedance spectroscopy sensors into laboratory simulated icy environments to measure the correlation between microbial activity and changing environmental conditions such as temperature. The sensors will also be optimized to further detect lower cell concentrations/levels of activity, minimize noise, and operate reliably for extended deployments in the field. New designs could integrate additional sensing arrays such as temperature, pH, and conductivity in the same miniaturized platform. Multi-parametric measurements would ultimately allow for a more in-depth investigation of the complex behaviors of microbes in natural and engineered environments.

CONCLUSIONS AND FUTURE OUTLOOK

This study focuses on enhancing and broadening the functionality of microfabricated EIS sensors for *in situ* monitoring of biofilm, and to facilitate large-scale real-time sensing investigations. Each of the following conclusions outlined below correlate with the objectives stated in chapter 1. These conclusions describe how this work contributes to a better overall understanding of the capabilities and limitations of EIS biosensors.

1. Insights into the degree of corrosion induced by biofilms is studied. This is accomplished by analyzing various commonly used thin film materials incorporated in sensor fabrication to determine the physical impacts after extended exposures to biofilm. Testing includes evaluating sheet resistance and stoichiometric alterations of sensor materials. The work informs future design considerations in the development of microfabricated aqueous biosensors. It is concluded that to mitigate the negative effects of biofilm induced corrosion on sensors, an encapsulation material such as a-Si_xN_y:H can be utilized to protect the underlying conductive sensor material, and thus improve sensor durability.
2. A known limitation of EIS biosensors is their propensity for signal drift, even in the absence of biological material. To overcome this limitation, and stabilize sensor signals over extended periods of time, an electrically conductive polymer coating, polypyrrole doped with polystyrene sulfonate (PPy:PSS), is show to minimize sensor signal drift and improve the consistency of μIDE sensor responses compared to bare gold electrode sensors. This coating feature is a key advancement in the integrity of our data sets and is implemented in future sensor designs.

3. The integration of EIS biosensors into a 3D printable flow cell platform allows for simultaneous EIS measurements with standard biofilm microscopy. Biofilm under continuous flow conditions mimics many naturally occurring biofilms. This novel platform had the following advantages: (*i*) can be produced at a low cost and utilizes small fluid volumes, (*ii*) integrates seamlessly with a modern CLSM microscope, and (*iii*) features reliable electrical connection to integrated sensors. Simultaneous EIS and CLSM were collected during biofilm growth from planktonic cell attachment through maturation. *Pseudomonas aeruginosa* PA01 served as the model biofilm-forming bacteria. EIS measurements of biofilm grown in the flow system reproducibly decrease over time in a sigmoidal pattern and indicate biofilm proliferation. It is concluded that using this platform, EIS microsensor data collection, in parallel with CLSM visualization, can reproducibly detect increasing levels of biofilm development.
4. In addition to successfully growing biofilm in the flow cell platform, biofilm dispersal from antimicrobial treatments is successfully detected with EIS biosensors. Maneuvers to deliberately disperse biofilm yield impedance signals returning toward abiotic impedance levels. CLSM imaging reveals reductions in biofilm biomass, in agreement with impedance data. When cell-signaling interference is applied via the application of a quorum sensing inhibitor (QSI), impedance levels remain stable, indicative of successful sensing of delayed or suppressed biofilm formation. CLSM imaging reveals thinner biofilm development in the presence of QSI, in agreement with impedance data. It is concluded that EIS microsensor data collection, in parallel with CLSM visualization, can reproducibly detect biofilm dispersal and suppression of cell signaling.

5. To expand the utility of the sensors outside of the laboratory, the performance of microfabricated EIS sensors in a simulated industrial and real environmental setting are evaluated. When sensors are deployed in an opaque, oil-water emulsion (metalworking fluid (MWF)), decreases in impedance suggest successful detection of biofilm growth, analogous to impedance decreases occurring when biofilm is grown in broth. Likewise, in MWF, anti-biofilm treatment maneuvers result in impedance increases suggesting successful sensing of biofilm dispersal, analogous to impedance increases when biofilm is dispersed in broth. When cell-signaling interference is applied via QSI in MWF, impedance levels remain stable, indicative of suppressed biofilm formation. To further expand the utility of EIS biosensors, a field-test is conducted in an icy environment. EIS sensors successfully detect varying concentrations of both planktonic and surface-bound microbes in liquid (*i.e.*, pond water), solid (solid ice), and semi-solid (snow and slush) conditions.

A review of reports utilizing EIS μIDE sensors for detecting biofilm is included in Table 1.1. As is evident, a variety of biofilm forming microorganisms have been evaluated with a range of experimental formats, conditions, and analyses which limits the comparability of results. Also, a variety of methods for correlating impedance data to standard biofilm techniques were inconsistently reported.

The platform developed herein consists of EIS biosensors integrated in a microfluidic flow environment allowing for impedance measurements that reflect naturally proliferating biofilm conditions. This platform is comprised entirely of commonly available or 3D printable parts that can be inexpensively constructed and easily customized, such as expanding the number of flow

chambers, altering the opening size to accommodate new sensor designs, or varying flow parameters.

The use of μIDEs in combination with PPy:PSS electrode coatings results in highly sensitive biofilm detection, and enhances measurement integrity and repeatability. As shown in Table 1.1, reported μIDEs biosensor applications have relied on unmodified gold electrodes. Bare gold electrodes suffer from low reproducibility and signal drift. A unique feature of our sensor is the coating with PPy:PSS which results in reduced interfacial impedances and more consistent impedance measurements. Lastly, live-cell imaging from CLSM supplemented impedance data. As a non-destructive visual confirmation, CLSM allows in-depth analysis of adherent biofilm structures in 3 dimensions. Our flow system allowed continuous, non-destructive visualization of biofilm throughout the entire duration of each experiment, and biomass could be calculated at any desired timepoint. This feature of the flow cell system is an advantage when compared to other μIDEs biosensor reports which have not been routinely integrated with CLSM imaging (Table 1.1). The marriage of coated μIDE sensors, integration into a flow cell system, and the concurrent CLSM imaging analysis in the present investigation builds on similar reports that incorporated some, but not all, of these elements. Additionally, this work expands on the potential applications of the sensors outside of the laboratory to a real-world problematic fluid.

Building on the proven capability of this impedance sensor system, future investigations should be undertaken. Future work should focus on assessing the performance of these sensors over longer periods of time, in other types of supporting fluids (e.g., opaque, complex formulations, or different ionic concentrations), and under varying environmental conditions (*e.g.*, fluctuations in temperature, oxygenation, or pH). This technology should be expanded to study

other biofilm-forming species and mixed microbial compositions. These data will expand the understanding of EIS biosensing and lead to an integration of EIS biosensors into mainstream biofilm analysis.

Although in this work, *Pseudomonas aeruginosa* was selected as a model organism to study biofilm formation, the sensor is agnostic to the biofilm-forming organism under test. Being able to discern *P. aeruginosa* from other organisms with high degree of selectivity and specificity would be desirable. One approach to achieve this goal could be by functionalizing the sensors with DNA, RNA, or peptide aptamers selective to *P. aeruginosa*, or other *Pseudomonas* specific molecules which could improve selectivity and potentially provide earlier detection of the presence of this pathogen (Khatami et al. 2022).

The technology presented in this dissertation could be modified to study other aqueous environments, where biofilms are prevalent and require early detection. One such application is the study of biofilm growth in the water recirculation system on the International Space Station (ISS; Valez et al., 2023). These sensors also could be integrated into water monitoring platforms to measure harmful biofilm growth in rivers, lakes, and streams, or other industrial applications. In the field of medicine, persistent infections are often associated with biofilm, and are a leading cause of morbidity and mortality (Assefa and Amare, 2022). For example, biosensors could be deployed on the skin to detect the development of methicillin resistant *Staphylococcus aureus* or integrated into a catheter to monitor catheter associated urinary tract infections (CAUTIs) from *Escherichia coli* (Werneburg, 2022). Water cooling towers, and air conditioning units can become contaminated with *Legionella pneumophila*, which when inhaled, can lead to Legionnaire's

disease (Di Pippo et al., 2018). A functionalized biosensor deployed in the cooling tower could alert to the presence of this contaminant, and decontamination measures could be taken.

These investigations will generate large amounts of complex data, which will be difficult to analyze manually. Artificial intelligence (A.I.) algorithms, such as machine learning, would help automate the data collection and analysis, identify sensor malfunctions such as fouling or drift, and facilitate decisions regarding treatment (Jin et al. 2020; Giordano et al. 2022), thus advancing the technology towards real-world applications.

In conclusion, the present study has shown that EIS biosensors can be effectively utilized in the analysis of microorganisms and the biofilms they produce. Furthermore, the ease of use, rapid response time, and cost-effectiveness of EIS biosensors make them a promising alternative to traditional biofilm analytical techniques. EIS biosensors should be integrated into mainstream biofilm analytical techniques, thus providing researchers and clinicians with a novel tool for understanding and combating biofilm-associated problems.

REFERENCES CITED

Abdelrasoul, G.N., Anwar, A., MacKay, S., Tamura, M., Shah, M.A., Khasa, D.P., Montgomery, R.R., Ko, A.I., Chen, J., 2020. DNA aptamer-based non-faradaic impedance biosensor for detecting E. coli. Analytica Chimica Acta.

Abrantes, P., Africa, C.W.J., 2020. Measuring Streptococcus mutans, Streptococcus sanguinis and Candida albicans biofilm formation using a real-time impedance-based system. Journal of Microbiological Methods 169, 5.

Anesio, A.M., Lutz, S., Chrismas, N.A.M., Benning, L.G., 2017. The microbiome of glaciers and ice sheets. NPJ Biofilms Microbiomes 3, 10.

Araujo, P.A., Malheiro, J., Machado, I., Mergulhao, F., Melo, L., Simoes, M., 2016. Influence of Flow Velocity on the Characteristics of Pseudomonas fluorescens Biofilms. J. Environ. Eng.-ASCE 142(7), 8.

Ashton, S.A., Miller, J.D.A., King, R.A., 1973. Corrosion of Ferrous metals in Batch Cultures of Nitrate-Reducingu Bacteria. British Corrosion Journal 8(4), 185-189.

Assefa, M., Amare, A., 2022. Biofilm-Associated Multi-Drug Resistance in Hospital-Acquired Infections: A Review. Infect Drug Resist 15, 5061-5068.

Assenhaimer, C., Domingos, A.S., Glasse, B., Fritsching, U., Guardani, R., 2017. LONG-TERM MONITORING OF METALWORKING FLUID EMULSION AGING USING A SPECTROSCOPIC SENSOR. Can. J. Chem. Eng. 95(12), 2341-2349.

Azeredo, J., Azevedo, N., Briandet, R., Cerca, N., Coenye, T., Costa, A.R., Desvaux, M., Bonaventura, G., Hébraud, M., Jaglic, Z., Kacaniova, M., Knöchel, S., Lourenco, A., Mergulhão, F., Meyer, R., Nychas, G.-J., Simões, M., Tresse, O., Sternberg, C., 2016. Critical review on biofilm methods. Critical reviews in microbiology 43, 313-351.

Azeredo, J., Azevedo, N.F., Briandet, R., Cerca, N., Coenye, T., Costa, A.R., Desvaux, M., Di Bonaventura, G., Hebraud, M., Jaglic, Z., Kacaniova, M., Knochel, S., Lourenco, A., Mergulhao, F., Meyer, R.L., Nychas, G., Simoes, M., Tresse, O., Sternberg, C., 2017. Critical review on biofilm methods. Crit Rev Microbiol 43(3), 313-351.

Bahadır, E.B., Sezgintürk, M.K., 2016. A review on impedimetric biosensors. Artificial Cells, Nanomedicine, and Biotechnology 44(1), 248-262.

Bar-On, Y.M., Milo, R., 2019. Towards a quantitative view of the global ubiquity of biofilms. Nat. Rev. Microbiol. 17(4), 199-200.

Baracu, A.M., Dinu Gugoasa, L.A., 2021. Review—Recent Advances in Microfabrication, Design and Applications of Amperometric Sensors and Biosensors. Journal of The Electrochemical Society 168(3), 037503.

Barsoukov, E., 2005. Impedance Spectroscopy: Theory, Experiment, and Applications, 2nd Edition. Blackwell Science Publ, Oxford.

Becerro, S., Paredes, J., Mujika, M., Lorenzo, E.P., Arana, S., 2016. Electrochemical Real-Time Analysis of Bacterial Biofilm Adhesion and Development by Means of Thin-Film Biosensors. IEEE Sensors Journal 16(7), 1856-1864.

Beech, I.B., Sunner, J., 2004. Biocorrosion: towards understanding interactions between biofilms and metals. Curr Opin Biotechnol 15(3), 181-186.

Bellin, D.L., Sakhtah, H., Rosenstein, J.K., Levine, P.M., Thimot, J., Emmett, K., Dietrich, L.E.P., Shepard, K.L., 2014. Integrated circuit-based electrochemical sensor for spatially resolved detection of redox-active metabolites in biofilms. Nature Communications 5(1), 3256.

Bellin, D.L., Sakhtah, H., Zhang, Y., Price-Whelan, A., Dietrich, L.E.P., Shepard, K.L., 2016. Electrochemical camera chip for simultaneous imaging of multiple metabolites in biofilms. Nature Communications 7(1), 10535.

Blanco-Cabra, N., Lopez-Martinez, M.J., Arevalo-Jaimes, B.V., Martin-Gomez, M.T., Samitier, J., Torrents, E., 2021. A new BiofilmChip device for testing biofilm formation and antibiotic susceptibility. npj Biofilms Microbomes 7(1), 9.

Bordo, K., Rubahn, H.-G., 2012. Effect of Deposition Rate on Structure and Surface Morphology of Thin Evaporated Al Films on Dielectrics and Semiconductors. Materials Science 18(4).

Bosire, E.M., Blank, L.M., Rosenbaum, M.A., 2016. Strain- and Substrate-Dependent Redox Mediator and Electricity Production by Pseudomonas aeruginosa. Appl Environ Microbiol 82(16), 5026-5038.

Bott, T.R., 2009. Biofouling Control in Cooling Water. International Journal of Chemical Engineering 2009, 619873.

Bratov, A., Brosel-Oliu, S., Abramova, N., 2018. Label-Free Impedimetric Biosensing Using 3D Interdigitated Electrodes, in: Schöning, M.J., Poghossian, A. (Eds.), Label-Free Biosensing: Advanced Materials, Devices and Applications. Springer International Publishing, Cham, pp. 179-198.

Breathnach, A.S., Cubbon, M.D., Karunaharan, R.N., Pope, C.F., Planche, T.D., 2012. Multidrug-resistant Pseudomonas aeruginosa outbreaks in two hospitals: association with contaminated hospital waste-water systems. Journal of Hospital Infection 82(1), 19-24.

Brosel-Oliu, S., Abramova, N., Uria, N., Bratov, A., 2019a. Impedimetric transducers based on interdigitated electrode arrays for bacterial detection - A review. Analytica Chimica Acta 1088, 1-19.

Brosel-Oliu, S., Ferreira, R., Uria, N., Abramova, N., Gargallo, R., Munoz-Pascual, F.X., Bratov, A., 2018. Novel impedimetric aptasensor for label-free detection of Escherichia coil O157:H7. Sens. Actuator B-Chem. 255, 2988-2995.

Brosel-Oliu, S., Mergel, O., Uria, N., Abramova, N., van Rijn, P., Bratov, A., 2019b. 3D impedimetric sensors as a tool for monitoring bacterial response to antibiotics. Lab on a Chip 19(8), 1436-1447.

Brown, G.E., Henrich, V.E., Casey, W.H., Clark, D.L., Eggleston, C., Felmy, A., Goodman, D.W., Grätzel, M., Maciel, G., McCarthy, M.I., Nealson, K.H., Sverjensky, D.A., Toney, M.F., Zachara, J.M., 1999. Metal Oxide Surfaces and Their Interactions with Aqueous Solutions and Microbial Organisms. Chemical Reviews 99(1), 77-174.

Brox, T.I., Skidmore, M.L., Brown, J.R., 2015. Characterizing the internal structure of laboratory ice samples with nuclear magnetic resonance. J. Glaciol. 61(225), 55-64.

Bruchmann, J., Sachsenheimer, K., Rapp, B.E., Schwartz, T., 2015. Multi-Channel Microfluidic Biosensor Platform Applied for Online Monitoring and Screening of Biofilm Formation and Activity. PLoS One 10(2), 19.

Cámara, M., Green, W., MacPhee, C.E., Rakowska, P.D., Raval, R., Richardson, M.C., Slater-Jefferies, J., Steventon, K., Webb, J.S., 2022. Economic significance of biofilms: a multidisciplinary and cross-sectoral challenge. npj Biofilms Microbomes 8(1), 42.

Carniello, V., Peterson, B.W., van der Mei, H.C., Busscher, H.J., 2018. Physico-chemistry from initial bacterial adhesion to surface-programmed biofilm growth. Adv Colloid Interface Sci 261, 1-14.

Cesewski, E., Johnson, B.N., 2020. Electrochemical biosensors for pathogen detection. Biosensors and Bioelectronics 159, 112214.

Chabowski, K., Junka, A.F., Piasecki, T., Nowak, D., Nitsch, K., Smutnicka, D., Bartoszewicz, M., Moczala, M., Szymczyk, P., 2017. IMPEDANCE SENSORS MADE IN PCB AND LTCC TECHNOLOGIES FOR MONITORING GROWTH AND DEGRADATION OF PSEUDOMONAL BIOFILM. Metrol. Meas. Syst. 24(2), 369-380.

Chalklen, T., Jing, Q., Kar-Narayan, S., 2020. Biosensors Based on Mechanical and Electrical Detection Techniques. Sensors 20(19), 5605.

Chen, C., Mehl, B.T., Munshi, A.S., Townsend, A.D., Spence, D.M., Martin, R.S., 2016. 3D-printed microfluidic devices: fabrication, advantages and limitations—a mini review. Anal. Methods 8(31), 6005-6012.

Christensen, G.D., Simpson, W.A., Bisno, A.L., Beachey, E.H., 1982. Adherence of slime-producing strains of Staphylococcus epidermidis to smooth surfaces. Infect Immun 37(1), 318-326.

Cook, J.M., Tedstone, A.J., Williamson, C., McCutcheon, J., Hodson, A.J., Dayal, A., Skiles, M., Hofer, S., Bryant, R., McAree, O., McGonigle, A., Ryan, J., Anesio, A.M., Irvine-Fynn, T.D.L., Hubbard, A., Hanna, E., Flanner, M., Mayanna, S., Benning, L.G., van As, D., Yallop, M., McQuaid, J.B., Gribbin, T., Tranter, M., 2020. Glacier algae accelerate melt rates on the south-western Greenland Ice Sheet. Cryosphere 14(1), 309-330.

Costerton, J.W., Stewart, P.S., Greenberg, E.P., 1999. Bacterial biofilms: A common cause of persistent infections. Science 284(5418), 1318-1322.

Couniot, N., Flandre, D., Francis, L.A., Afzalian, A., 2012. Bacteria Detection with Interdigitated Microelectrodes: Noise Consideration and Design Optimization. Procedia Engineering 47, 188-191.

Dani, K.G.S., Mader, H.M., Wolff, E.W., Wadham, J.L., 2012. Modelling the liquid-water vein system within polar ice sheets as a potential microbial habitat. Earth Planet. Sci. Lett. 333, 238-249.

Davey, M.E., Caiazza, N.C., O'Toole, G.A., 2003. Rhamnolipid surfactant production affects biofilm architecture in Pseudomonas aeruginosa PAO1. J Bacteriol 185(3), 1027-1036.

Davies, D., 2003. Understanding biofilm resistance to antibacterial agents. Nat. Rev. Drug Discov. 2(2), 114-122.

Davies, D.G., Parsek, M.R., Pearson, J.P., Iglewski, B.H., Costerton, J.W., Greenberg, E.P., 1998. The involvement of cell-to-cell signals in the development of a bacterial biofilm. Science 280(5361), 295-298.

Davison, W.M., Pitts, B., Stewart, P.S., 2010. Spatial and temporal patterns of biocide action against Staphylococcus epidermidis biofilms. Antimicrob Agents Chemother 54(7), 2920-2927.

Dhillon, S., Kant, R., 2017. Theory for electrochemical impedance spectroscopy of heterogeneous electrode with distributed capacitance and charge transfer resistance. Journal of Chemical Sciences 129(8), 1277-1292.

Di Maiuta, N., Rüfenacht, A., Küenzi, P., 2017. Assessment of bacteria and archaea in metalworking fluids using massive parallel 16S rRNA gene tag sequencing. Lett Appl Microbiol 65(4), 266-273.

Di Pippo, F., Di Gregorio, L., Congestri, R., Tandoi, V., Rossetti, S., 2018. Biofilm growth and control in cooling water industrial systems. FEMS Microbiol Ecol 94(5).

Dieser, M., Greenwood, M., Foreman, C.M., 2010. Carotenoid Pigmentation in Antarctic Heterotrophic Bacteria as a Strategy to Withstand Environmental Stresses. Arct. Antarct. Alp. Res. 42(4), 396-405.

Ding, Y., Weindl, P., Lenz, A.G., Mayer, P., Krebs, T., Schmid, O., 2020. Quartz crystal microbalances (QCM) are suitable for real-time dosimetry in nanotoxicological studies using VITROCELL®Cloud cell exposure systems. Part Fibre Toxicol 17(1), 44.

Dizon, A., Orazem, M.E., 2020. On experimental determination of cell constants for interdigitated electrodes. Electrochimica Acta 337, 12.

Dominguez-Benetton, X., Sevda, S., Vanbroekhoven, K., Pant, D., 2012. The accurate use of impedance analysis for the study of microbial electrochemical systems. Chem. Soc. Rev. 41(21), 7228-7246.

Dorledo de Faria, R.A., Dias Heneine, L.G., Matencio, T., Messaddeq, Y., 2019. Faradaic and non-faradaic electrochemical impedance spectroscopy as transduction techniques for sensing applications. International Journal of Biosensors & Bioelectronics 5(1).

Dunwell, M., Yan, Y., Xu, B., 2018. Understanding the influence of the electrochemical double-layer on heterogeneous electrochemical reactions. Current Opinion in Chemical Engineering 20, 151-158.

El Hasni, A., Schmitz, C., Bui-Göbbels, K., Bräunig, P., Jahnen-Dechent, W., Schnakenberg, U., 2017. Electrical impedance spectroscopy of single cells in hydrodynamic traps. Sensors and Actuators B: Chemical 248, 419-429.

Estrada-Leypon, O., Moya, A., Guimera, A., Gabriel, G., Agut, M., Sanchez, B., Borros, S., 2015. Simultaneous monitoring of Staphylococcus aureus growth in a multi-parametric microfluidic platform using microscopy and impedance spectroscopy. Bioelectrochemistry 105, 56-64.

Fukazawa, H., Suzuki, D., Ikeda, T., Mae, S., Hondoh, T., 1997. Raman spectra of translational lattice vibrations in polar ice. J. Phys. Chem. B 101(32), 6184-6187.

Funari, R., Shen, A.Q., 2022. Detection and Characterization of Bacterial Biofilms and Biofilm-Based Sensors. ACS Sensors 7(2), 347-357.

Furst, A.L., Francis, M.B., 2019. Impedance-Based Detection of Bacteria. Chemical Reviews 119(1), 700-726.

Giordano, G.F., Ferreira, L.F., Bezerra, Í.R.S., Barbosa, J.A., Costa, J.N.Y., Pimentel, G.J.C., Lima, R.S., 2023. Machine learning toward high-performance electrochemical sensors. Anal. Bioanal. Chem.

Goeres, D.M., Loetterle, L.R., Hamilton, M.A., Murga, R., Kirby, D.W., Donlan, R.M., 2005. Statistical assessment of a laboratory method for growing biofilms. Microbiology 151(Pt 3), 757-762.

Goikoetxea, E., Routkevitch, D., de Weerdt, A., Green, J.J., Steenackers, H., Braeken, D., 2018. Impedimetric fingerprinting and structural analysis of isogenic E. coli biofilms using multielectrode arrays. Sens. Actuator B-Chem. 263, 319-326.

Gomez, R., Bashir, R., Bhunia, A.K., 2002. Microscale electronic detection of bacterial metabolism. Sens. Actuator B-Chem. 86(2-3), 198-208.

Green, A.E., Amézquita, A., Le Marc, Y., Bull, M.J., Connor, T.R., Mahenthiralingam, E., 2018. The consistent differential expression of genetic pathways following exposure of an industrial Pseudomonas aeruginosa strain to preservatives and a laundry detergent formulation. FEMS Microbiol Lett 365(9).

Grieshaber, D., MacKenzie, R., Vörös, J., Reimhult, E., 2008. Electrochemical Biosensors - Sensor Principles and Architectures. Sensors (Basel) 8(3), 1400-1458.

Gu, H., Lee, S.W., Carnicelli, J., Jiang, Z., Ren, D., 2019. Antibiotic Susceptibility of Escherichia coli Cells during Early-Stage Biofilm Formation. J Bacteriol 201(18).

Gula, G., Szymanowska, P., Piasecki, T., Goras, S., Gotszalk, T., Drulis-Kawa, Z., 2020. The Application of Impedance Spectroscopy for Pseudomonas Biofilm Monitoring during Phage Infection. Viruses-Basel 12(4), 19.

Gutierrez, D., Hidalgo-Cantabrana, C., Rodriguez, A., Garcia, P., Ruas-Madiedo, P., 2016. Monitoring in Real Time the Formation and Removal of Biofilms from Clinical Related Pathogens Using an Impedance-Based Technology. PLoS One 11(10), 17.

Hall-Stoodley, L., Costerton, J.W., Stoodley, P., 2004. Bacterial biofilms: From the natural environment to infectious diseases. Nat. Rev. Microbiol. 2(2), 95-108.

Hassan, A., Usman, J., Kaleem, F., Omair, M., Khalid, A., Iqbal, M., 2011. Evaluation of different detection methods of biofilm formation in the clinical isolates. Braz J Infect Dis 15(4), 305-311.

He, Z., Wang, Q., Hu, Y., Liang, J., Jiang, Y., Ma, R., Tang, Z., Huang, Z., 2012. Use of the quorum sensing inhibitor furanone C-30 to interfere with biofilm formation by Streptococcus mutans and its luxS mutant strain. Int J Antimicrob Agents 40(1), 30-35.

Hentzer, M., Wu, H., Andersen, J.B., Riedel, K., Rasmussen, T.B., Bagge, N., Kumar, N., Schembri, M.A., Song, Z., Kristoffersen, P., Manefield, M., Costerton, J.W., Molin, S., Eberl, L., Steinberg, P., Kjelleberg, S., Høiby, N., Givskov, M., 2003. Attenuation of Pseudomonas aeruginosa virulence by quorum sensing inhibitors. Embo j 22(15), 3803-3815.

Ho, L.S.J., Limson, J.L., Fogel, R., 2019. Certain Methods of Electrode Pretreatment Create Misleading Responses in Impedimetric Aptamer Biosensors. ACS Omega 4(3), 5839-5847.

Hoogvliet, J.C., van Bennekom, W.P., 2001. Gold thin-film electrodes: an EQCM study of the influence of chromium and titanium adhesion layers on the response. Electrochimica Acta 47(4), 599-611.

Huiszoon, R.C., Han, J.J., Chu, S., Stine, J.M., Beardslee, L.A., Ghodssi, R., 2021. Integrated System for Bacterial Detection and Biofilm Treatment on Indwelling Urinary Catheters. Ieee Transactions on Biomedical Engineering 68(11), 3241-3249.

Huiszoon, R.C., Subramanian, S., Ramiah Rajasekaran, P., Beardslee, L.A., Bentley, W.E., Ghodssi, R., 2019. Flexible Platform for In Situ Impedimetric Detection and Bioelectric Effect Treatment of Escherichia Coli Biofilms. IEEE Trans Biomed Eng 66(5), 1337-1345.

Ibrahim, M., Claudel, J., Kourtiche, D., Nadi, M., 2013. Geometric parameters optimization of planar interdigitated electrodes for bioimpedance spectroscopy. Journal of Electrical Bioimpedance 4(1).

Jin, X., Liu, C., Xu, T., Su, L., Zhang, X., 2020. Artificial intelligence biosensors: Challenges and prospects. Biosensors and Bioelectronics 165, 112412.

Jun, L.Q., Djaswadi, G.W.b., Hawari, H.F.b., Zakariya, M.A.B., 2018. Simulation of Interdigitated Electrodes (IDEs) Geometry Using COMSOL Multiphysics, 2018 International Conference on Intelligent and Advanced System (ICIAS). pp. 1-6.

Kang, S.-K., Hwang, S.-W., Cheng, H., Yu, S., Kim, B.H., Kim, J.-H., Huang, Y., Rogers, J.A., 2014. Dissolution Behaviors and Applications of Silicon Oxides and Nitrides in Transient Electronics. Advanced Functional Materials 24(28), 4427-4434.

Khatami, S.H., Karami, S., Siahkouhi, H.R., Taheri-Anganeh, M., Fathi, J., Aghazadeh Ghadim, M.B., Taghvimi, S., Shabaninejad, Z., Tondro, G., Karami, N., Dolatshah, L., Soltani Fard, E., Movahedpour, A., Darvishi, M.H., 2022. Aptamer-based biosensors for Pseudomonas aeruginosa detection. Mol Cell Probes 66, 101865.

Kiefer, J., Seidel, B., Meyer, D., 2018. Optical Spectroscopy for Analysis and Monitoring of Metalworking Fluids. Appl. Spectrosc. 72(12), 1790-1797.

Kılıc, Y., 2020. Brief Fine Polishing of Thin-film Gold Electrode Sensors Leads to Better Reproducibility than Electrochemical Pretreatment. Int. J. Electrochem. Sci., 5067-5075.

Killough, M., Rodgers, A.M., Ingram, R.J., 2022. Pseudomonas aeruginosa: Recent Advances in Vaccine Development. Vaccines (Basel) 10(7).

Kim, D.J., Pitchimani, R., Snow, D.E., Hope-Weeks, L.J., 2008. A simple method for the removal of thiols on gold surfaces using an NH4OH-H2O2-H2O solution. Scanning 30(2), 118-122.

Kim, S., Yu, G., Kim, T., Shin, K., Yoon, J., 2012. Rapid bacterial detection with an interdigitated array electrode by electrochemical impedance spectroscopy. Electrochimica Acta 82, 126-131.

Koch, T., 2023. Microbiology of Metalworking Fluids: What We Know and Lessons to be Learnt. Acta Mechanica et Automatica 17(2), 166-172.

Kosri, E., Ibrahim, F., Thiha, A., Madou, M., 2022. Micro and Nano Interdigitated Electrode Array (IDEA)-Based MEMS/NEMS as Electrochemical Transducers: A Review, Nanomaterials.

Kremers, T., Tintelott, M., Pachauri, V., Vu, X.T., Ingebrandt, S., Schnakenberg, U., 2021. Microelectrode Combinations of Gold and Polypyrrole Enable Highly Stable Two-electrode Electrochemical Impedance Spectroscopy Measurements under Turbulent Flow Conditions. Electroanalysis 33(1), 197-207.

Kumar, S., Nguyen, A.T., Goswami, S., Ferracane, J., Koley, D., 2023. Real-time monitoring of biofilm formation using a noninvasive impedance-based method. Sensors and Actuators B: Chemical 376, 133034.

Lappin-Scott, H.M., Costerton, J.W., 1989. Bacterial biofilms and surface fouling. Biofouling 1(4), 323-342.

Lasia, A., 2014. Electrochemical Impedance Spectroscopy and its Applications, 2014 ed. New York, NY: Springer New York, New York, NY.

Lazar, J., Schnelting, C., Slavcheva, E., Schnakenberg, U., 2016. Hampering of the Stability of Gold Electrodes by Ferri-/Ferrocyanide Redox Couple Electrolytes during Electrochemical Impedance Spectroscopy. Analytical Chemistry 88(1), 682-687.

Lebeaux, D., Ghigo, J.-M., Beloin, C., 2014. Biofilm-Related Infections: Bridging the Gap between Clinical Management and Fundamental Aspects of Recalcitrance toward Antibiotics. Microbiology and Molecular Biology Reviews 78(3), 510-543.

Li, H., Zhou, E., Ren, Y., Zhang, D., Xu, D., Yang, C., Feng, H., Jiang, Z., Li, X., Gu, T., Yang, K., 2016. Investigation of microbiologically influenced corrosion of high nitrogen nickel-free stainless steel by Pseudomonas aeruginosa. Corrosion Sci. 111, 811-821.

Li, S.-W., Sheng, G.-P., Cheng, Y.-Y., Yu, H.-Q., 2016. Redox properties of extracellular polymeric substances (EPS) from electroactive bacteria. Scientific Reports 6(1), 39098.

Lim, C.P., Mai, P.N.Q., Roizman Sade, D., Lam, Y.C., Cohen, Y., 2016. Biofilm development of an opportunistic model bacterium analysed at high spatiotemporal resolution in the framework of a precise flow cell. NPJ Biofilms Microbiomes 2, 16023.

Lisoń, J., Taratuta, A., Paszenda, Z., Szindler, M., Basiaga, M., 2022. Perspectives in Prevention of Biofilm for Medical Applications, Coatings.

Liu, L., Xu, Y., Cui, F., Xia, Y., Chen, L., Mou, X., Lv, J., 2018. Monitoring of bacteria biofilms forming process by in-situ impedimetric biosensor chip. Biosens Bioelectron 112, 86-92.

Lu, L., Hu, W., Tian, Z.R., Yuan, D.D., Yi, G.J., Zhou, Y.Y., Cheng, Q., Zhu, J., Li, M.X., 2019. Developing natural products as potential anti-biofilm agents. Chin. Med. 14, 17.

Lvovich, V.F., 2012. Impedance Spectroscopy: Applications to Electrochemical and Dielectric Phenomena. Wiley.

MacDonald, M.A., Andreas, H.A., 2014. Method for equivalent circuit determination for electrochemical impedance spectroscopy data of protein adsorption on solid surfaces. Electrochimica Acta 129, 290-299.

Maduraiveeran, G., Sasidharan, M., Ganesan, V., 2018. Electrochemical sensor and biosensor platforms based on advanced nanomaterials for biological and biomedical applications. Biosens. Bioelectron. 103, 113-129.

Magar, H.S., Hassan, R.Y.A., Mulchandani, A., 2021. Electrochemical Impedance Spectroscopy (EIS): Principles, Construction, and Biosensing Applications. Sensors (Basel) 21(19).

Mallén-Alberdi, M., Vigués, N., Mas, J., Fernández-Sánchez, C., Baldi, A., 2016. Impedance spectral fingerprint of E. coli cells on interdigitated electrodes: A new approach for label free and selective detection. Sensing and Bio-Sensing Research 7, 100-106.

Malvankar, N.S., Lovley, D.R., 2014. Microbial nanowires for bioenergy applications. Current Opinion in Biotechnology 27, 88-95.

Malvankar, N.S., Vargas, M., Nevin, K.P., Franks, A.E., Leang, C., Kim, B.-C., Inoue, K., Mester, T., Covalla, S.F., Johnson, J.P., Rotello, V.M., Tuominen, M.T., Lovley, D.R., 2011. Tunable metallic-like conductivity in microbial nanowire networks. Nature Nanotechnology 6(9), 573-579.

Markovic, N.M., 2013. Interfacing electrochemistry. Nature Materials 12(2), 101-102.

Markus, V., Golberg, K., Teralı, K., Ozer, N., Kramarsky-Winter, E., Marks, R.S., Kushmaro, A., 2021. Assessing the Molecular Targets and Mode of Action of Furanone C-30 on Pseudomonas aeruginosa Quorum Sensing. Molecules 26(6).

Marsili, E., Sun, J., Bond, D.R., 2010. Voltammetry and Growth Physiology of Geobacter sulfurreducens Biofilms as a Function of Growth Stage and Imposed Electrode Potential. Electroanalysis 22(7-8), 865-874.

Maruthupandy, M., Anand, M., Maduraiveeran, G., Beevi, A.S.H., Priya, R.J., 2015. Electrical conductivity measurements of bacterial nanowires from Pseudomonas aeruginosa. Advances in Natural Sciences: Nanoscience and Nanotechnology 6(4), 045007.

Mazza, M.G., 2016. The physics of biofilms-an introduction. J. Phys. D-Appl. Phys. 49(20), 24.

Mazzaracchio, V., Neagu, D., Porchetta, A., Marcoccio, E., Pomponi, A., Faggioni, G., D'Amore, N., Notargiacomo, A., Pea, M., Moscone, D., Palleschi, G., Lista, F., Arduini, F., 2019. A label-free impedimetric aptasensor for the detection of Bacillus anthracis spore simulant. Biosensors and Bioelectronics 126, 640-646.

McGlennen, M., Dieser, M., Foreman, C., Warnat, S., 2019. Effects of Escherichia coli K12 Biofilm on Sensor Thin Film Materials, 2019 IEEE SENSORS. pp. 1-4. © 2019 IEEE.

McGlennen, M., Dieser, M., Foreman, C.M., Warnat, S., 2023. Using electrochemical impedance spectroscopy to study biofilm growth in a 3D-printed flow cell system. Biosensors and Bioelectronics: X 14, 100326.

McGlennen, M., Neubauer, M., Driesler, M., Dieser, M., Foreman, C.M., Warnat, S., 2020. Microsensors in Icy Environments to Detect Microbial Activities. Journal of Microelectromechanical Systems 29(5), 853-859. © 2020 IEEE.

Miller, M.B., Bassler, B.L., 2001. Quorum sensing in bacteria. Annu Rev Microbiol 55, 165-199.

Moradali, M.F., Ghods, S., Rehm, B.H., 2017. Pseudomonas aeruginosa Lifestyle: A Paradigm for Adaptation, Survival, and Persistence. Front Cell Infect Microbiol 7, 39.

Mukherjee, S., Bassler, B.L., 2019. Bacterial quorum sensing in complex and dynamically changing environments. Nat. Rev. Microbiol. 17(6), 371-382.

Neubauer, M., McGlennen, M., Thomas, S., Warnat, S., 2019. 3D printing on glass for direct sensor integration. Engineering Research Express 1(2), 025051.

Nivens, D.E., Ohman, D.E., Williams, J., Franklin, M.J., 2001. Role of alginate and its O acetylation in formation of Pseudomonas aeruginosa microcolonies and biofilms. J Bacteriol 183(3), 1047-1057.

Ozcan, S.S., Dieser, M., Parker, A.E., Balasubramanian, N., Foreman, C.M., 2019. Quorum sensing inhibition as a promising method to control biofilm growth in metalworking fluids. J. Ind. Microbiol. Biotechnol. 46(8), 1103-1111.

Oziat, J., Cohu, T., Elsen, S., Gougis, M., Malliaras, G.G., Mailley, P., 2021. Electrochemical detection of redox molecules secreted by Pseudomonas aeruginosa – Part 1: Electrochemical signatures of different strains. Bioelectrochemistry 140, 107747.

Oziat, J., Elsen, S., Owens, R.M., Malliaras, G.G., Mailley, P., 2015. Electrochemistry provides a simple way to monitor Pseudomonas aeruginosa metabolites, 2015 37th Annual International Conference of the IEEE Engineering in Medicine and Biology Society (EMBC). pp. 7522-7525.

Pantanella, F., Valenti, P., Natalizi, T., Passeri, D., Berlutti, F., 2013. Analytical techniques to study microbial biofilm on abiotic surfaces: pros and cons of the main techniques currently in use. Ann Ig 25(1), 31-42.

Paredes, J., Becerro, S., Arana, S., 2014. Comparison of real time impedance monitoring of bacterial biofilm cultures in different experimental setups mimicking real field environments. Sensors and Actuators B: Chemical 195, 667-676.

Paredes, J., Becerro, S., Arana, S., 2014. Label-free interdigitated microelectrode based biosensors for bacterial biofilm growth monitoring using Petri dishes. Journal of Microbiological Methods 100, 77-83.

Paredes, J., Becerro, S., Arizti, F., Aguinaga, A., Del Pozo, J.L., Arana, S., 2012. Real time monitoring of the impedance characteristics of Staphylococcal bacterial biofilm cultures with a modified CDC reactor system. Biosensors and Bioelectronics 38(1), 226-232.

Paredes, J., Becerro, S., Arizti, F., Aguinaga, A., Del Pozo, J.L., Arana, S., 2013. Interdigitated microelectrode biosensor for bacterial biofilm growth monitoring by impedance spectroscopy technique in 96-well microtiter plates. Sensors and Actuators B: Chemical 178, 663-670.

Park, J.S., Kim, H.J., Lee, J.H., Park, J.H., Kim, J., Hwang, K.S., Lee, B.C., 2018. Amyloid Beta Detection by Faradaic Electrochemical Impedance Spectroscopy Using Interdigitated Microelectrodes. Sensors (Basel) 18(2).

Passman, F.J., Küenzi, P., 2020. Microbiology in Water-Miscible Metalworking Fluids. Tribology Transactions, 1-25.

Peeters, E., Nelis, H.J., Coenye, T., 2008. Comparison of multiple methods for quantification of microbial biofilms grown in microtiter plates. Journal of Microbiological Methods 72(2), 157-165.

Perini, N., Prado, A.R., Sad, C.M.S., Castro, E.V.R., Freitas, M.B.J.G., 2012. Electrochemical impedance spectroscopy for in situ petroleum analysis and water-in-oil emulsion characterization. Fuel 91(1), 224-228.

Peterson, B.W., He, Y., Ren, Y., Zerdoum, A., Libera, M.R., Sharma, P.K., van Winkelhoff, A.-J., Neut, D., Stoodley, P., van der Mei, H.C., Busscher, H.J., 2015. Viscoelasticity of biofilms and their recalcitrance to mechanical and chemical challenges. FEMS Microbiology Reviews 39(2), 234-245.

Pitts, B., Hamilton, M.A., Zelver, N., Stewart, P.S., 2003. A microtiter-plate screening method for biofilm disinfection and removal. Journal of Microbiological Methods 54(2), 269-276.

Poma, N., Vivaldi, F., Bonini, A., Salvo, P., Kirchhain, A., Melai, B., Bottai, D., Tavanti, A., Di Francesco, F., 2020. A graphenic and potentiometric sensor for monitoring the growth of bacterial biofilms. Sens. Actuator B-Chem. 323, 10.

Pousti, M., Zarabadi, M.P., Abbaszadeh Amirdehi, M., Paquet-Mercier, F., Greener, J., 2018. Microfluidic bioanalytical flow cells for biofilm studies: a review. Analyst 144(1), 68-86.

Pratikno, H., Titah, H.S., 2017. Bio-corrosion on Aluminum 6063 by Escherichia coli in Marine Environment. The Journal for Technology and Science 28(2).

Proctor, C.R., McCarron, P.A., Ternan, N.G., 2020. Furanone quorum-sensing inhibitors with potential as novel therapeutics against Pseudomonas aeruginosa. J. Med. Microbiol. 69(2), 195-206.

Qiao, Y., Qiao, Y.-J., Zou, L., Ma, C.-X., Liu, J.-H., 2015. Real-time monitoring of phenazines excretion in Pseudomonas aeruginosa microbial fuel cell anode using cavity microelectrodes. Bioresource Technology 198, 1-6.

Queiros, R.B., de-los-santos-Alvarez, N., Noronha, J.P., Sales, M.G.F., 2013. A label-free DNA aptamer-based impedance biosensor for the detection of E. coli outer membrane proteins. Sens. Actuator B-Chem. 181, 766-772.

Radke, S.M., Alocilja, E.C., 2004. Design and fabrication of a microimpedance biosensor for bacterial detection. Ieee Sensors Journal 4(4), 434-440.

Randviir, E.P., Banks, C.E., 2013. Electrochemical impedance spectroscopy: an overview of bioanalytical applications. Anal. Methods 5(5), 1098-1115.

Rather, M.A., Gupta, K., Mandal, M., 2021. Microbial biofilm: formation, architecture, antibiotic resistance, and control strategies. Braz J Microbiol 52(4), 1701-1718.

Reasoner, D.J., Geldreich, E.E., 1985. A new medium for the enumeration and subculture of bacteria from potable water. Applied and environmental microbiology 49(1), 1-7.

Ripa, R., Shen, A.Q., Funari, R., 2020. Detecting Escherichia coli Biofilm Development Stages on Gold and Titanium by Quartz Crystal Microbalance. ACS Omega 5(5), 2295-2302.

Robb, A.J., Vinogradov, S., Danell, A.S., Anderson, E., Blackledge, M.S., Melander, C., Hvastkovs, E.G., 2018. Electrochemical detection of small molecule induced Pseudomonas aeruginosa biofilm dispersion. Electrochimica Acta 268, 276-282.

Roberts, J.G., Sombers, L.A., 2018. Fast-Scan Cyclic Voltammetry: Chemical Sensing in the Brain and Beyond. Analytical Chemistry 90(1), 490-504.

Roy, R., Tiwari, M., Donelli, G., Tiwari, V., 2018. Strategies for combating bacterial biofilms: A focus on anti-biofilm agents and their mechanisms of action. Virulence 9(1), 522-554.

Saccomano, S.C., Jewell, M.P., Cash, K.J., 2021. A review of chemosensors and biosensors for monitoring biofilm dynamics. Sensors and Actuators Reports 3, 100043.

Sadekuzzaman, M., Yang, S., Mizan, M.F.R., Ha, S.D., 2015. Current and Recent Advanced Strategies for Combating Biofilms. Comprehensive Reviews in Food Science and Food Safety 14(4), 491-509.

Saha, R., Donofrio, R.S., 2012. The microbiology of metalworking fluids. Appl. Microbiol. Biotechnol. 94(5), 1119-1130.

Saha, R., Donofrio, R.S., Goeres, D.M., Bagley, S.T., 2012. Rapid detection of rRNA group I pseudomonads in contaminated metalworking fluids and biofilm formation by fluorescent in situ hybridization. Appl. Microbiol. Biotechnol. 94(3), 799-808.

San, N.O., Nazır, H., Dönmez, G., 2014. Microbially influenced corrosion and inhibition of nickel–zinc and nickel–copper coatings by Pseudomonas aeruginosa. Corrosion Sci. 79, 177-183.

Sedky, S., Witvrouw, A., Bender, H., Baert, K., 2001. Experimental determination of the maximum post-process annealing temperature for standard CMOS wafers. IEEE Transactions on Electron Devices 48(2), 377-385.

Sezonov, G., Joseleau-Petit, D., D'Ari, R., 2007. Escherichia coli physiology in Luria-Bertani broth. J Bacteriol 189(23), 8746-8749.

Shi, L., Dong, H., Reguera, G., Beyenal, H., Lu, A., Liu, J., Yu, H.Q., Fredrickson, J.K., 2016. Extracellular electron transfer mechanisms between microorganisms and minerals. Nat Rev Microbiol 14(10), 651-662.

Sidhu, R.K., Cavallaro, N.D., Pola, C.C., Danyluk, M.D., McLamore, E.S., Gomes, C.L., 2020. Planar Interdigitated Aptasensor for Flow-Through Detection of Listeria spp. in Hydroponic Lettuce Growth Media. Sensors (Basel) 20(20).

Silva, V., Silva, C., Soares, P., Garrido, E.M., Borges, F., Garrido, J., 2020. Isothiazolinone Biocides: Chemistry, Biological, and Toxicity Profiles. Molecules 25(4).

Simic, M., Kojic, T., Radovanovic, M., Stojanovic, G.M., Al-Salami, H., 2020. Impedance Spectroscopic Analysis of the Interidigitated Flexible Sensor for Bacteria Detection. Ieee Sensors Journal 20(21), 12791-12798.

Simpson, A.T., Stear, M., Groves, J.A., Piney, M., Bradley, S.D., Stagg, S., Crook, B., 2003. Occupational Exposure to Metalworking Fluid Mist and Sump Fluid Contaminants. The Annals of Occupational Hygiene 47(1), 17-30.

Skindersoe, M.E., Alhede, M., Phipps, R., Yang, L., Jensen, P.O., Rasmussen, T.B., Bjarnsholt, T., Tolker-Nielsen, T., Høiby, N., Givskov, M., 2008. Effects of antibiotics on quorum sensing in Pseudomonas aeruginosa. Antimicrob Agents Chemother 52(10), 3648-3663.

Sopoušek, J., Věžník, J., Houser, J., Skládal, P., Lacina, K., 2021. Crucial factors governing the electrochemical impedance on protein-modified surfaces. Electrochimica Acta 388, 138616.

Stewart, P.S., 2003. Diffusion in biofilms. J. Bacteriol. 185(5), 1485-1491.

Stewart, P.S., White, B., Boegli, L., Hamerly, T., Williamson, K.S., Franklin, M.J., Bothner, B., James, G.A., Fisher, S., Vital-Lopez, F.G., Wallqvist, A., 2019. Conceptual Model of Biofilm Antibiotic Tolerance That Integrates Phenomena of Diffusion, Metabolism, Gene Expression, and Physiology. J Bacteriol 201(22).

Straub, H., Eberl, L., Zinn, M., Rossi, R.M., Maniura-Weber, K., Ren, Q., 2020. A microfluidic platform for in situ investigation of biofilm formation and its treatment under controlled conditions. J. Nanobiotechnol. 18(1), 12.

Subramanian, S., Huiszoon, R.C., Chu, S., Bentley, W.E., Ghodssi, R., 2019. Microsystems for Biofilm Characterization and Sensing – A Review. Biofilm, 100015.

Subramanian, S., Tolstaya, E.I., Winkler, T.E., Bentley, W.E., Ghodssi, R., 2017. An Integrated Microsystem for Real-Time Detection and Threshold-Activated Treatment of Bacterial Biofilms. ACS Appl Mater Interfaces 9(37), 31362-31371.

Tan, B., Zhou, S., Wang, Y., Zhang, B., Zhou, L., Yuan, Y., 2019. Molecular insight into electron transfer properties of extracellular polymeric substances of electroactive bacteria by surface-enhanced Raman spectroscopy. Science China Technological Sciences 62(10), 1679-1687.

Tang, X., Flandre, D., Raskin, J.-P., Nizet, Y., Moreno-Hagelsieb, L., Pampin, R., Francis, L.A., 2011. A new interdigitated array microelectrode-oxide-silicon sensor with label-free, high sensitivity and specificity for fast bacteria detection. Sensors and Actuators B: Chemical 156(2), 578-587.

Thurnheer, T., Gmür, R., Guggenheim, B., 2004. Multiplex FISH analysis of a six-species bacterial biofilm. J Microbiol Methods 56(1), 37-47.

Tiozzo-Lyon, P., Andrade, M., Leiva-Sabadini, C., Morales, J., Olivares, A., Ravasio, A., Aguayo, S., 2023. Microfabrication approaches for oral research and clinical dentistry. Frontiers in Dental Medicine 4.

Trafny, E.A., 2013. MICROORGANISMS IN METALWORKING FLUIDS: CURRENT ISSUES IN RESEARCH AND MANAGEMENT. Int. J. Occup. Med. Environ. Health 26(1), 4-15.

Trunzo, N.E., Hong, K.L., 2020. Recent Progress in the Identification of Aptamers Against Bacterial Origins and Their Diagnostic Applications. Int. J. Mol. Sci. 21(14), 25.

Tuon, F.F., Dantas, L.R., Suss, P.H., Tasca Ribeiro, V.S., 2022. Pathogenesis of the Pseudomonas aeruginosa Biofilm: A Review. Pathogens 11(3).

Turick, C.E., Shimpalee, S., Satjaritanun, P., Weidner, J., Greenway, S., 2019. Convenient non-invasive electrochemical techniques to monitor microbial processes: current state and perspectives. Appl. Microbiol. Biotechnol. 103(20), 8327-8338.

Vadhva, P., Hu, J., Johnson, M.J., Stocker, R., Braglia, M., Brett, D.J.L., Rettie, A.J.E., 2021. Electrochemical Impedance Spectroscopy for All-Solid-State Batteries: Theory, Methods and Future Outlook. ChemElectroChem 8(11), 1930-1947.

van Duuren, J., Musken, M., Karge, B., Tomasch, J., Wittmann, C., Haussler, S., Bronstrup, M., 2017. Use of Single-Frequency Impedance Spectroscopy to Characterize the Growth Dynamics of Biofilm Formation in Pseudomonas aeruginosa. Sci Rep 7(1), 5223.

Van Gerwen, P., Laureyn, W., Laureys, W., Huyberechts, G., De Beeck, M.O., Baert, K., Suls, J., Sansen, W., Jacobs, P., Hermans, L., Mertens, R., 1998. Nanoscaled interdigitated electrode arrays for biochemical sensors. Sens. Actuator B-Chem. 49(1-2), 73-80.

Varshney, M., Li, Y.B., 2009. Interdigitated array microelectrodes based impedance biosensors for detection of bacterial cells. Biosens. Bioelectron. 24(10), 2951-2960.

Vélez Justiniano, Y.-A., Goeres, D.M., Sandvik, E.L., Kjellerup, B.V., Sysoeva, T.A., Harris, J.S., Warnat, S., McGlennen, M., Foreman, C.M., Yang, J., Li, W., Cassilly, C.D., Lott, K., HerrNeckar, L.E., 2023. Mitigation and use of biofilms in space for the benefit of human space exploration. Biofilm 5, 100102.

Videla, H.A., Herrera, L.K., 2005. Microbiologically influenced corrosion: looking to the future. Int Microbiol 8(3), 169-180.

Vivier, V., Orazem, M.E., 2022. Impedance Analysis of Electrochemical Systems. Chem Rev 122(12), 11131-11168.

Wang, S., Zhang, J., Gharbi, O., Vivier, V., Gao, M., Orazem, M.E., 2021. Electrochemical impedance spectroscopy. Nature Reviews Methods Primers 1(1), 41.

Wang, W., Zhang, X., Wang, J., 2009. Heterogeneous electrochemical characteristics of biofilm/metal interface and local electrochemical techniques used for this purpose. Materials and Corrosion 60(12), 957-962.

Wang, Y., Zhang, R., Duan, J., Shi, X., Zhang, Y., Guan, F., Sand, W., Hou, B., 2022. Extracellular Polymeric Substances and Biocorrosion/Biofouling: Recent Advances and Future Perspectives, Int. J. Mol. Sci. pp. 5566–.

Ward, A.C., Connolly, P., Tucker, N.P., 2014. Pseudomonas aeruginosa Can Be Detected in a Polymicrobial Competition Model Using Impedance Spectroscopy with a Novel Biosensor. PLoS One 9(3), 13.

Ward, A.C., Hannah, A.J., Kendrick, S.L., Tucker, N.P., MacGregor, G., Connolly, P., 2018. Identification and characterisation of Staphylococcus aureus on low cost screen printed carbon electrodes using impedance spectroscopy. Biosens. Bioelectron. 110, 65-70.

Warnat, S., Forbrigger, C., Hubbard, T., Bertuch, A., Sundaram, G., 2015. Thermal MEMS actuator operation in aqueous media/seawater: Performance enhancement through atomic layer deposition post processing of PolyMUMPs devices. Journal of Vacuum Science & Technology A: Vacuum, Surfaces, and Films 33(1).

Werneburg, G.T., 2022. Catheter-Associated Urinary Tract Infections: Current Challenges and Future Prospects. Res Rep Urol 14, 109-133.

Wimpenny, J., Manz, W., Szewzyk, U., 2000. Heterogeneity in biofilms. FEMS Microbiology Reviews 24(5), 661-671.

Wingender, J., Flemming, H.-C., 2011. Biofilms in drinking water and their role as reservoir for pathogens. International Journal of Hygiene and Environmental Health 214(6), 417-423.

World Health, O., 2017. Guidelines for the prevention and control of carbapenem-resistant Enterobacteriaceae, Acinetobacter baumannii and Pseudomonas aeruginosa in health care facilities. World Health Organization, Geneva.

Wu, H., Song, Z., Hentzer, M., Andersen, J.B., Molin, S., Givskov, M., Høiby, N., 2004. Synthetic furanones inhibit quorum-sensing and enhance bacterial clearance in Pseudomonas aeruginosa lung infection in mice. J Antimicrob Chemother 53(6), 1054-1061.

Wu, J., 2022. Understanding the Electric Double-Layer Structure, Capacitance, and Charging Dynamics. Chemical Reviews 122(12), 10821-10859.

Xu, Y., Li, C., Jiang, Y., Guo, M., Yang, Y., Yang, Y., Yu, H., 2020. Electrochemical Impedance Spectroscopic Detection of E.coli with Machine Learning. Journal of The Electrochemical Society 167(4).

Yang, L., 2008. Electrical impedance spectroscopy for detection of bacterial cells in suspensions using interdigitated microelectrodes. Talanta 74(5), 1621-1629.

Yang, L., Bashir, R., 2008. Electrical/electrochemical impedance for rapid detection of foodborne pathogenic bacteria. Biotechnol Adv 26(2), 135-150.

Yang, L., Li, Y., Griffis, C.L., Johnson, M.G., 2004. Interdigitated microelectrode (IME) impedance sensor for the detection of viable Salmonella typhimurium. Biosensors and Bioelectronics 19(10), 1139-1147.

Zdrachek, E., Bakker, E., 2019. Potentiometric Sensing. Analytical Chemistry 91(1), 2-26.

Zhang, D., Men, L., Chen, Q., 2011. Microfabrication and Applications of Opto-Microfluidic Sensors. Sensors 11(5), 5360-5382.

Zhang, T., Chen, Q., Li, X., Liu, J., Zhou, W., Wang, B., Zhao, Z., Li, W., Chao, D., Zhao, D., 2022. Redox Mediator Chemistry Regulated Aqueous Batteries: Insights into Mechanisms and Prospects. CCS Chemistry 4(9), 2874-2887.

Zhang, W., Seminara, A., Suaris, M., Brenner, M.P., Weitz, D.A., Angelini, T.E., 2014. Nutrient depletion in Bacillus subtilis biofilms triggers matrix production. New Journal of Physics 16(1), 015028.

Zhao, J., Cheng, W., He, X., Liu, Y., Li, J., Sun, J., Li, J., Wang, F., Gao, Y., 2018. Association of furanone C-30 with biofilm formation & antibiotic resistance in Pseudomonas aeruginosa. Indian J Med Res 147(4), 400-406.

Zheng, L.Y., Congdon, R.B., Sadik, O.A., Marques, C.N.H., Davies, D.G., Sammakia, B.G., Lesperance, L.M., Turner, J.N., 2013. Electrochemical measurements of biofilm development using polypyrrole enhanced flexible sensors. Sensors and Actuators B: Chemical 182, 725-732.

APPENDICES

APPENDIX A

SUPPLEMENTAL MATERIAL FOR: USING ELECTROCHEMICAL IMPEDANCE SPECTROSCOPY TO STUDY BIOFILM GROWTH IN A 3D PRINTED FLOW CELL SYSTEM

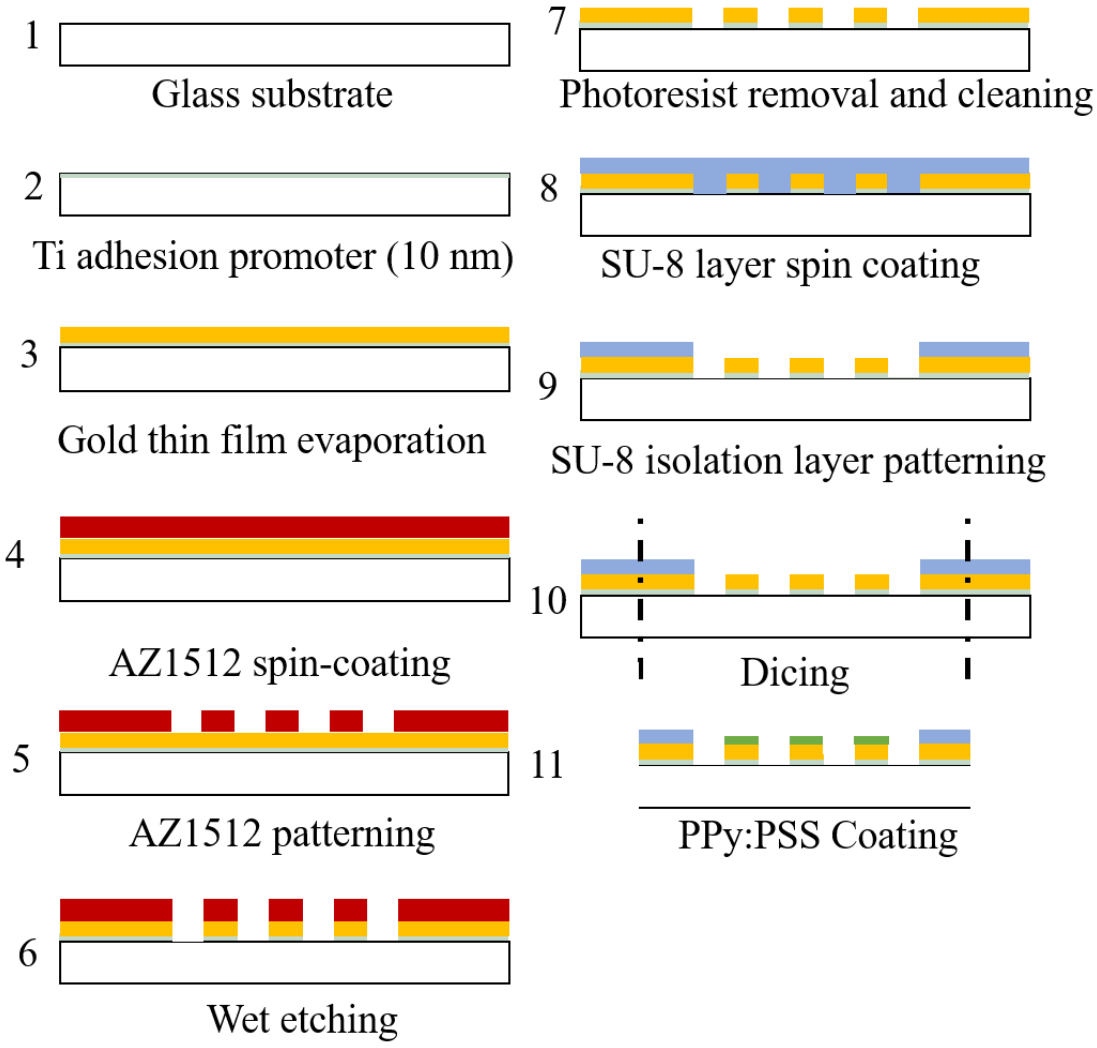

Figure A.1: Sensor design and fabrication flow. (A) Electron beam physical vapor deposition thin film, lithography, wet etching, and dicing processes used in the fabrication.

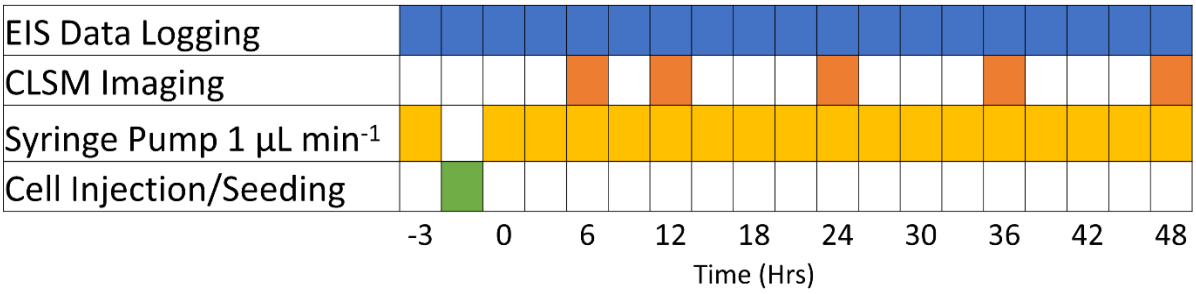

Figure A.2: Summary of experimental procedure for operating flow-cell for biofilm growth.

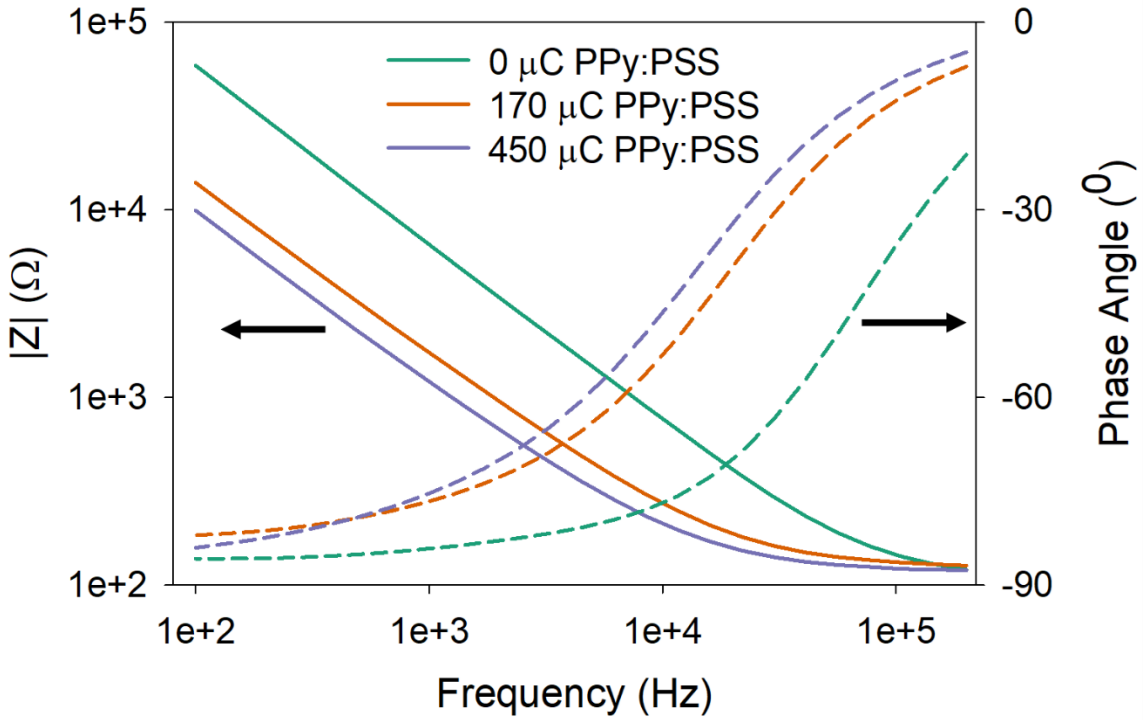

Figure A.3: Bode plot of impedance and phase angle for different electropolymerization coatings. Solid lines represent impedance, and dashed lines represent phase angle.

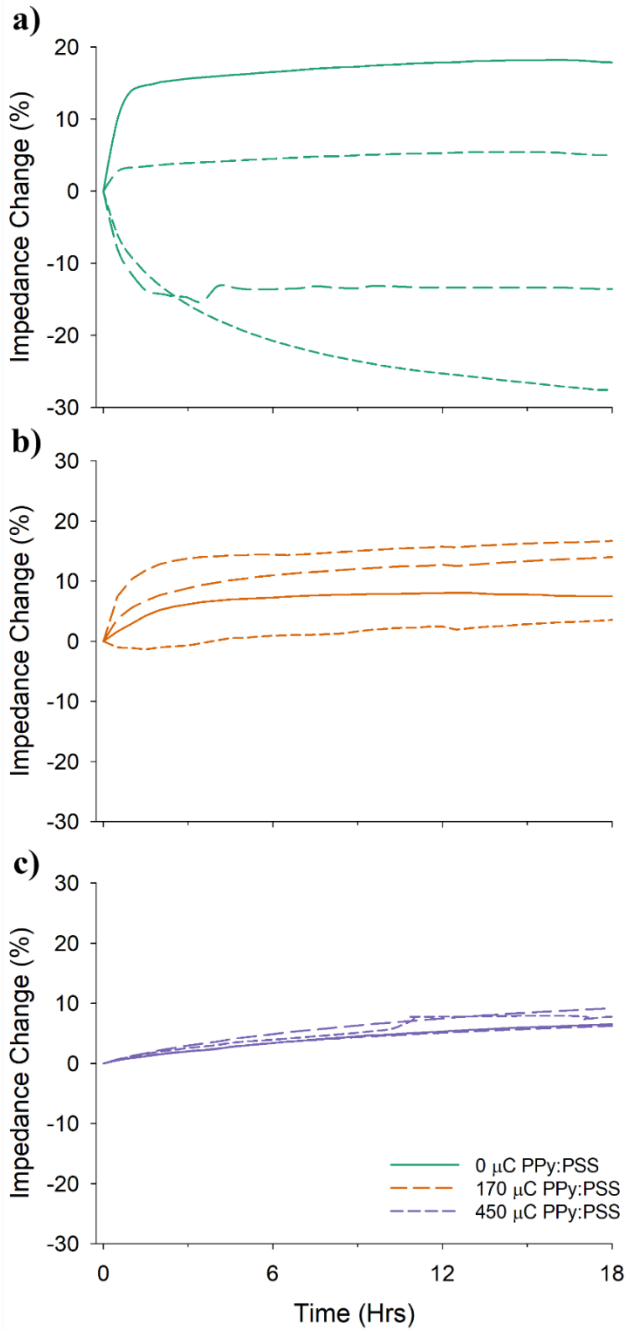

Figure A.4: Evaluation of sensor drift from EIS in sterile 1:10X TSB from sensors coated with electrically conductive polymer, PPy:PSS, with coatings deposition charges ranging from 0 to 450 µC. Transient behavior of the impedance during exposure to 1:10X TSB measured at 100 Hz for 18 hours for (a) uncoated sensors, (b) 170 µC PPy:PSS coated sensors, and (c) 450 µC PPy:PSS coated sensors.

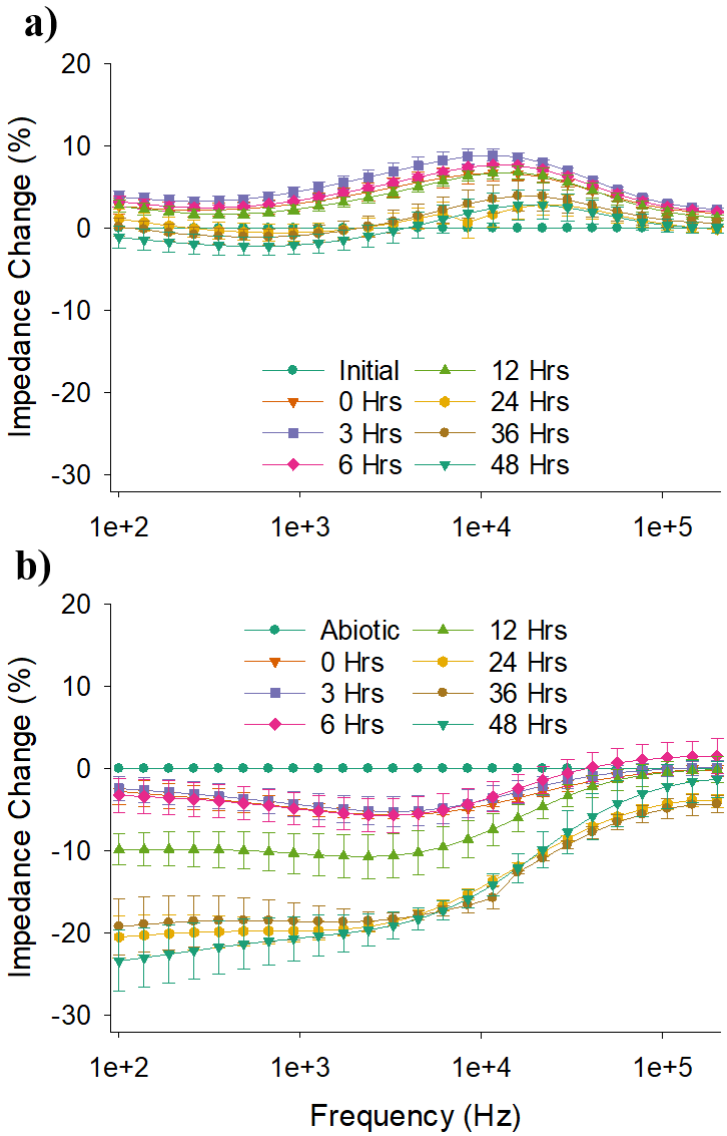

Figure A.5: Relative impedance response of entire measured frequency range at selected timepoints of 0, 6, 12, 17, and 24 hrs of media flow in flow-cell. (a) Relative impedance changes of abiotic, and (b) relative impedance change of sensors exposed to *P. aeruginosa* biofilm.

APPENDIX B

SUPPLEMENTAL MATERIAL FOR: APPLICATION OF IMPEDANCE SPECTROSCOPY SENSORS FOR ASSESSING BIOFILM CONTROL IN REAL TIME

Compared to TSB, MWF has properties that effected biosensor responses. We postulate that the thick, oily layer created by MWF constituents reduced sensitivity at the electrochemical interface, thus masking measurable interactions between biofilm and the electrodes. To determine the optimal frequency range that best captured biofilm growth in 5% MWF, abiotic and biofilm growth experiments were carried out in the flow cell system. Impedance changes at timepoints t=initial, 0, 6, 12, 18, 24, 30, and 36 hrs under flowing conditions were measured (Fig B.1). Frequency ranges of interest were defined at low (100≤f≤1 kHz), medium (1 kHz≤f≤10 kHz), or high frequency (10 kHz≤f≤200 kHz). Under abiotic conditions in 5% MWF, impedance changes across the entire frequency range (100 Hz≤f≤200 kHz) fluctuated less than 10% without a trend for 36 hrs (Fig B.1a).

However, in the presence of biofilm, impedance in the high-frequency range was most pronounced (≤25%) and consistently decreased with respect to time (Fig B.1b). Unlike TSB, biofilm in 5% MWF impedance in the low and middle frequency ranges fluctuated with no trend (≤10%). The high-frequency range (10 kHz≤f≤200 kHz) was identified as the most suitable frequency range to measure biofilm in 5% MWF due to better sensitivity. Therefore, 200 kHz was chosen as the single representative frequency to measure biofilm in 5% MWF.

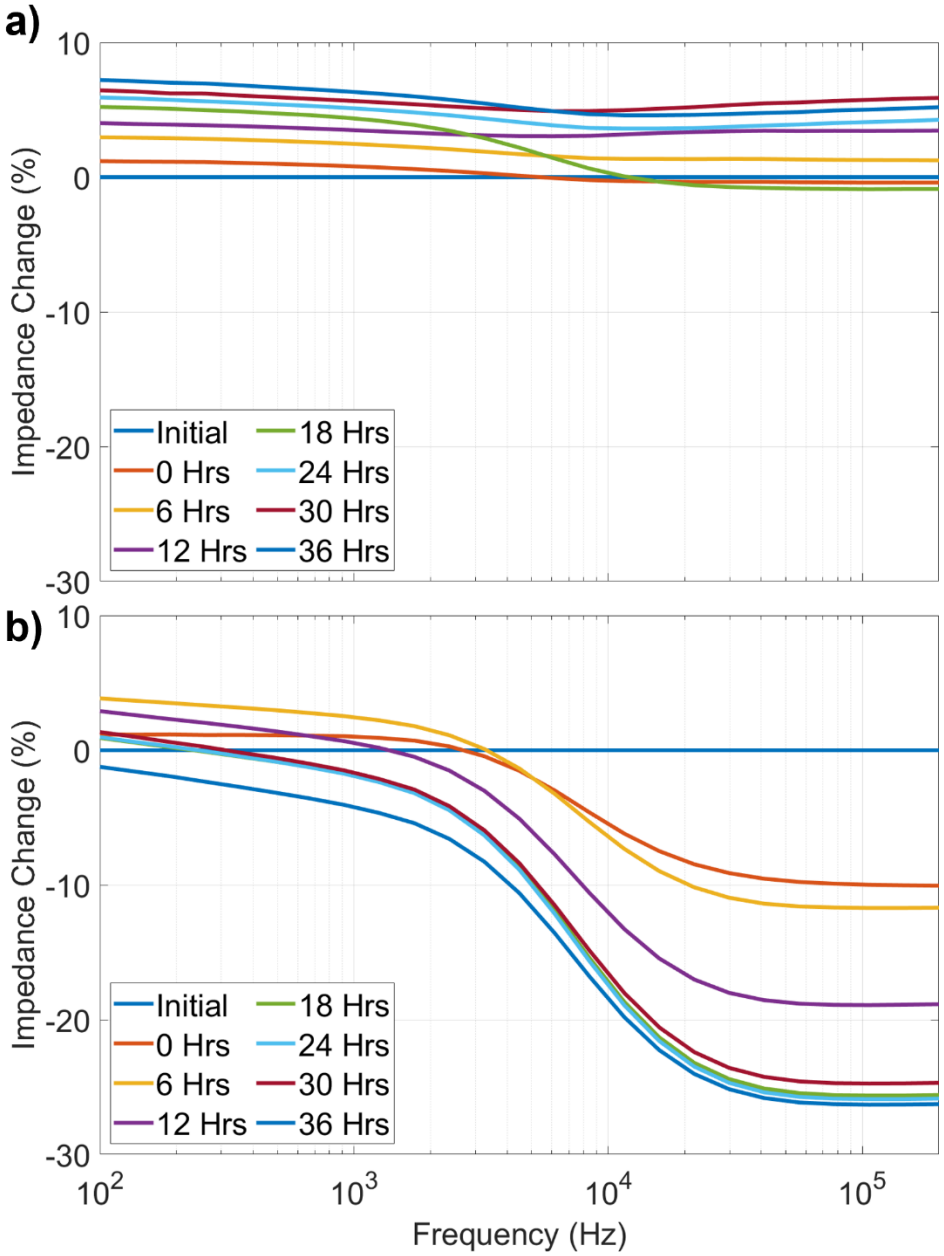

Figure B.1: a) Relative impedance response of entire measured frequency range at selected timepoints of 0, 6, 12, 18, 24 hrs of 5% MWF flow in flow-cell under abiotic conditions. b) Relative impedance response of entire measured frequency range at selected timepoints of 0, 6, 12, 18, 24 hrs of 5% MWF flow in flow-cell under biofilm growth conditions.